

University of Rhode Island

DigitalCommons@URI

Open Access Dissertations

2018

UNDERSTANDING THE CONNECTION BETWEEN THE HYDRO-CLIMATIC EXTREMES AND DIARRHEAL DISEASES OVER BENGAL DELTA: THE VULNERABILITY ASSESSMENT OF PAST, PRESENT AND FUTURE

Mohammad Alfi Hasan

University of Rhode Island, mdalfihasan19@gmail.com

Follow this and additional works at: https://digitalcommons.uri.edu/oa_diss

Recommended Citation

Hasan, Mohammad Alfi, "UNDERSTANDING THE CONNECTION BETWEEN THE HYDRO-CLIMATIC EXTREMES AND DIARRHEAL DISEASES OVER BENGAL DELTA: THE VULNERABILITY ASSESSMENT OF PAST, PRESENT AND FUTURE" (2018). *Open Access Dissertations*. Paper 772.
https://digitalcommons.uri.edu/oa_diss/772

This Dissertation is brought to you by the University of Rhode Island. It has been accepted for inclusion in Open Access Dissertations by an authorized administrator of DigitalCommons@URI. For more information, please contact digitalcommons-group@uri.edu. For permission to reuse copyrighted content, contact the author directly.

UNDERSTANDING THE CONNECTION BETWEEN THE HYDRO-CLIMATIC
EXTREMES AND DIARRHEAL DISEASES OVER BENGAL DELTA: THE
VULNERABILITY ASSESSMENT OF PAST, PRESENT AND FUTURE

BY

MOHAMMAD ALFI HASAN

A DISSERTATION SUBMITTED IN PARTIAL FULFILLMENT OF THE
REQUIREMENTS FOR THE DEGREE OF DOCTOR OF PHILOSOPHY

IN

CIVIL AND ENVIRONMENTAL ENGINEERING

UNIVERSITY OF RHODE ISLAND

2018

DOCTOR OF PHILOSOPHY DISSERTATION
OF
MOHAMMAD ALFI HASAN

APPROVED:

Dissertation Committee

Major Professor: Ali S Akanda

Vinka Oyanedel-Craver

Soni M. Pradhanang

Antar Jutla

Nasser H. Zawia

UNIVERSITY OF RHODE ISLAND

2018

ABSTRACT

Living in the age of space exploration and nanotechnology, the significant portion of human population still have threatened by diarrheal diseases throughout the globe. Being a major contributor of the global mortality, the diarrheal diseases account for an estimated 3.1% of the total burden of disease in terms of Disability-Adjusted Life Year (DALY) where cholera and rotavirus diarrhea comprise more than two-thirds of the diarrheal morbidity in developing countries of South Asia.

Alongside with many more challenges like climate change or civil war, the capability to resolve the diarrheal disease burden in developing countries remains questionable. As the primary reasons for the disease transmission in epidemic scale are due to the exposure of contaminating pathogens via unsafe drinking water sources, lack of sanitation, deficient hygiene, insufficient drainage infrastructures and poor access to health care, ensuring clean water sources and improved sanitation may seem to untangle the problem. However, it will take a longer time to achieve such improvement by the developing countries as many of them are already missed the Millennium Development Goals (WHO/UNICEF 2015). Moreover, ongoing global climatic change also leads the disease vulnerability in much degrading state (Woodward et al. 2014). In this context, the Bengal delta of South Asia, exhibits the highest population density of globe and is one of the most vulnerable region of the world in terms of both climate change and diarrheal diseases (Bowen and Friel 2012). Therefore, the challenges to tackle the vulnerability of diarrheal disease under ongoing global warming is paramount in this region.

Previous studies found that the diarrhoeal diseases like cholera and rotavirus are significantly influenced by environmental factors in the developing countries of Asia and Sub Saharan Africa. The outbreaks of the diseases can occur in the wake of climatic extremes like heavy rainfall, flooding, cyclone, drought, extreme temperature and El-Nino (Bradley et al. 1996; Corwin et al. 1996; Patz et al. 2000; Vanasco et al. 2001; Chhotray et al. 2002; Kalashnikov et al. 2002; Qadri et al. 2005; Yang et al. 2005; Harmeling 2012). However, most studies have explored the influence on disease transmission for particular climatic extremes or related natural disasters, but the integration of multiple variables along with disease cases is infrequently done. Moreover, a deterministic quantification of the diseases epidemic based on the hydro-climatic factors is absent in existing literatures.

In terms of diarrheal disease epidemic as well as climate vulnerability, the Bengal delta is frequently considered as one of the high-risk region of the globe (IPCC, 2014). The policy makers of the region not only need to tackle the burden of diarrheal disease but also need to understand the future impact of these diseases under ongoing climate change. However, not only the future assessment of the disease is challenging but also, the meaningfully quantification of climatic extremes under future climate change scenarios require robust assessment due to the absence of such kind of studies.

Therefore, the objective of this dissertation is to develop the deterministic models that can project the future risk of diarrheal diseases, primarily rotavirus and cholera, driven by hydro-climatic extremes over the climate vulnerable region of Bengal delta. In order to

achieve this objective, I developed a bias-correction method for the high-resolution regional climate models, generated an observed data set over the Bengal delta, formulated a deterministic epidemic model for rotavirus that accounts intra-annual variability, proposed a spatial risk model of rotavirus and cholera and projected the future of the diarrheal disease for 21st century. The work has been described in the following three manuscripts, as per the Graduate School Manual guidelines:

Chapter 1. MANUSCRIPT I (published in *Climate Dynamics*, 2017).

The objective of this work was to explore the climate and its extremes over a monsoon dominated country like Bangladesh by following the latest RCP (Representative Concentration Pathways) emission scenarios, considering fine scale regional physics, incorporating the uncertainties range, and also by conducting advance bias correction methods to accomplish most reliable future projections. In this relation, the article aimed to investigate (1) the future probabilistic climate of Bengal delta, using five regional climate model projections driven by GCM results, (2) to develop a new spatial gridded observed data that represents historical climate extremes set and (3) to implement the latest QM (Quantile Mapping) bias correction methods over multi-model RCM outputs.

Chapter 2. MANUSCRIPT II (published in *Geo Health*, 2018).

In this manuscript, we investigated the role of climatic extremes on one of the prevalent diarrheal disease, rotavirus. The study aimed (1) to determine the effect of climatic extremes on the rotavirus epidemic over Bangladesh, both in spatially and temporal scale,

(2) to evaluate the rotavirus patterns over the cities of South Asia to understand the relation of the virus to regional hydro climatic processes and (3) to implemented a deterministic multivariate modeling for risk assessment and integrating near real-time satellite products (with GPM for rainfall and MODIS for temperature).

Chapter 3. MANUSCRIPT III (prepared for International Journal of Biometeorology).

The objective of this manuscript was to project the future the diarrheal disease risk based on the epidemic models driven by the bias-corrected regional climate models. To implement the long-term development medical initiatives under ongoing climate change, the policy makers requires comprehensive and meaningfully estimate of the future vulnerability of the diseases. Thus, the manuscript aimed (1) to develop some spatial multivariate models of the rotavirus and cholera epidemic over Bengal delta, (2) to assess the effect of relative humidity on rotavirus cycle, and (3) to project the probable future risk during the rising phase for both the diseases in the early, mid and late 21st Century.

In conclusion, the diarrheal diseases are a recurrent burden in the developing world. Though there are many factors such as population dynamic, poor water sanitation and hygiene can be responsible for diarrhreal outbreak in the region, the climate drivers still can plays a significant role in the diseases epidemic thus essential to pre-epidemic management. As this study proposed a risk based methodology rather than prevalence or incidence based method, the method can overlook the influence of the population infectivity the disease and can be utilize to detect the influence of climatic change. This

will allow the relevant stakeholders to improve the decision-making process. The novel approach and result of this dissertation can be utilized as a guideline for long-term diseases preparedness or vaccination strategy for Bangladesh. High-resolution regional model results will also provide valuable insight to the disease burden estimation which can be implemented in sub-district level with appropriate stakeholder. The findings of this study will be shared with ICDDRB (International Centre for Diarrhoeal Disease Research, Bangladesh) and Bill & Melinda Gates Foundation for further improvement of the vaccination and surveillance strategy over the region.

ACKNOWLEDGMENT

First and foremost, praise and thanks to ALLAH, the almighty, for giving me the strength, knowledge, ability and blessing to undertake this research study and to finish my Ph.D. successfully.

I would like to express my sincere gratitude to my advisor Ali Shafqat Akanda for the continuous support of my Ph.D study and research, for his patience, motivation and enthusiasm. My sincere thanks must also go to the members of my thesis advisory and exam committee: Vinka Oyanedel-Craver, Soni M. Pradhanang, and Antar Jutla, for their encouragement, insightful comments, and support throughout my PhD research.

I would like to give special thanks to Dr. Leon Thiem for his continuous support and providing valuable advice throughout my PhD journey. My gratitude also goes to Kelly Stanzione for making my journey in the civil department easy and enjoyable.

Above all, I would like to thank my wife, Supria for her love and constant support, for all the early mornings, and for keeping me sane through all my travails, my fits of pique and impatience. Thank you for being my advisor, co-worker, proofreader, and editor. But most of all, thank you for being my best friend. Lastly, I thank my parents, brother and friends for their constant encouragement without which this assignment would not be possible.

PREFACE

This dissertation is a final work as a partial fulfillment for the degree of Ph.D. of Environmental Engineering, Rhode Island University of United States of America titled “Understanding the connection between the hydro-climatic extremes and diarrheal diseases over Bengal delta: the vulnerability assessment of past, present and future.” The format of this dissertation formatted as Manuscript format, publication style. The idea is to combine all three papers as a plan to achieve my objectives in this dissertation.

CHAPTER 1: MANUSCRIPT I: Climate Projections and Extremes in dynamically downscaled CMIP5 model outputs over the Bengal Delta: A quartile based bias-correction approach with new gridded data.

This manuscript was published in “Climate Dynamics, 2017”.

CHAPTER 2: MANUSCRIPT II: Quantification of rotavirus diarrheal risk due to hydroclimatic extremes over South Asia: Prospects of satellite-based observations in detecting outbreaks.

This manuscript was published in “Geo Health, 2018”.

CHAPTER 3: MANUSCRIPT III. The future risk of diarrheal disease over Bengal delta based on climatic driven epidemic models: a case study with bias-corrected regional climate model results.

This manuscript is in process. (being prepared for “International Journal of Biometeorology”)

TABLE OF CONTENTS

ABSTRACT..... ii

ACKNOWLEDGMENTv

PREFACE..... vi

TABLE OF CONTENTS ix

LIST OF FIGURESx

LIST OF TABLES xiii

LIST OF ABBREVIATIONS xiv

CHAPTER 1 : MANUSCRIPT I.....1

CHAPTER 2 : MANUSCRIPT II43

CHAPTER 3 : MANUSCRIPT III.....82

APPENDIX A111

LIST OF FIGURES

CHAPTER 1. MANUSCRIPT I

Fig 1. Monthly climatology of rainfall (a), maximum temperature(b) and minimum temperature (c) that found from the five CMIP5 regional models and the observed gridded data over Bangladesh. (d-e) Taylor diagram (after Taylor, 2001) for annual mean rainfall and mean temperature over the period 1981–2000 over Bangladesh in reference to observed BMD data, showing raw RCM results and bias-corrected RCM results generated from CMIP5 models. 54

Fig 2. The temporal mean (1981–2005) of Rx50 (i.e. Number of days greater than 50mm rainfall per year) over Bangladesh derived from observed (a) BMD Grid, from the raw RCM of (b) RCA4-EC-EARTH, (c) REMO-MPI, (d) CSIRO-CCSM4, (e) CSIRO-CCSM4, (f) CSIRO-CCSM4 and from the respective error-corrected RCMs (g-k). 55

Fig. 3 The temporal mean (1981–2005) of Rx1 (i.e. Number of days greater than 1mm rainfall per year) over Bangladesh derived from observed (a) BMD Grid, from the raw RCM of (b) RCA4-EC-EARTH, (c) REMO-MPI, (d) CSIRO-CCSM4, (e) CSIRO-CCSM4, (f) CSIRO-CCSM4 and from the respective error-corrected RCMs (g-k). 56

Fig. 4 Rx10 and Rx50 values from multi-models and observed data over Bangladesh from 1981 to 2005 are presented with shaded time series plot. Blue and yellow region represent the range of model before correction and after correction respectively. 57

Fig. 5 Projected annual precipitation, maximum temperature and minimum temperature over Bangladesh in RCP 4.5 (top) and RCP 8.5 (bottom) scenarios. 58

Fig. 6 Changes of annual precipitation from baseline (1981-2005) to 2050s (2041-2070) and 2080s (2071-2100) observed in RCA4-EC-EARTH, REMO-MPI, CSIRO-CCSM4, CSIRO-CCNRM and CSIRO-CNRM-CM5 RCMs in RCP 4.5 scenario. Similar results, but in RCP 8.5 are also shown in (k-t)..... 59

Fig. 7 Changes of average temperature from baseline to 2050s (2041-2070) and 2080s (2071-2100) derived from RCA4-EC-EARTH, REMO-MPI, CSIRO-CCSM4, CSIRO-CCNRM and CSIRO-CNRM-CM5 RCMs in RCP 4.5 scenario. Similar result but in RCP 8.5 are also shown in (k-t)..... 60

Fig. 9 Projected mean changes of highest summer temperature (TXx) and lowest winter temperature (TNn) from five RCMs for 2050s and 2080s relative to 1981–2005. Changes are showed in annual scale and contour line represents the variability of the five models from its mean values. Bias corrected (top) and bias uncorrected (bottom) regional climate projections have been compared. 62

Fig. 10 Annual probability distribution functions for Rx1, Rx50, TXx and TNn indices for five regional climate model in three time periods of 21st Century. The solid line represents the observed period and dashed line represent mean of the five models in future time slices. 63

CHAPTER 2. MANUSCRIPT II

Figure 1. The location of the rotavirus prevalent cities in South Asia.109

Figure 2. (a) Annual monthly rotavirus outbreaks over South Asian cities. (b) Z-score of rotavirus over Dhaka from 2003 to 2015 (c) Auto-correlation function of rotavirus in the

city of Dhaka from 2003 to 2015.	110
Figure 3. (a) Rotavirus incidence for the month of November with RR1 of September (the y-axis is plotted in reverse order); (b) rotavirus of June-July-August with RR70 of June-July-August; (c) Rotavirus incidence for the month of December with Tmin (left); and (d) Tn1621GE (right) of same month (the y-axis of the indices are plotted in reverse order).	111
Figure 4. (a) Temporal correlation of rotavirus in winter months over Dhaka from January 2003 to May 2015 and (b) Spatial correlation of rotavirus in winter months over six cites of Bangladesh from July 2012 to May 2015. (c) Temporal correlation of rotavirus in monsoon months over Dhaka from January 2003 to May 2015 and (d) Spatial correlation of rotavirus in monsoon months over six cites of Bangladesh from July 2012 to May 2015.	112
Figure 5. The rotavirus cycle in the six selected cities with compared to RR1 and Tn1621GE from June 2012 to May 2015.....	113
Figure 6. Spatial distribution of the observed (left) and model-estimated (right, GPM + MODIS) z-score of rotavirus incidence for (a-b) October and (c-d) November, 2015...	114
Figure 7. Spatial distribution of the observed (left) and model-estimated (right, TRMM + MODIS) z-score of rotavirus incidence for (a-b) October and (c-d) November, 2014.).	115

CHAPTER 3. MANUSCRIPT III

Figure 1: Spatial distribution of (a) Observed and (b) Model z-score* (without relative humidity) of rotavirus outbreak at rising phase of epidemic (November-December) during the respective validation period.	143
Figure 2: Spatial distribution of (a) Observed and (b) Model z-score* (including relative humidity) of rotavirus outbreak at rising phase of epidemic (November-December) during the respective validation period.....	144
Figure 3: Spatial distribution of (a) Observed and (b) Model z-score* (including relative humidity) of cholera outbreak at rising phase of epidemic (August-September) during the respective validation period.....	145
Figure 4: The changes of risk (in percentage) of cholera epidemic from baseline (1981-2005) to 2020s (2006-2040), 2040s (2041-2070) and 2080s (2071-2099) over Bangladesh.....	146
Figure 5: The changes of risk (in percentage) of rotavirus diarrhea epidemic from baseline (1981-2005) to 2020s (2006-2040), 2040s (2041-2070) and 2080s (2071-2099) over Bangladesh.....	147
Figure 6: The changes of risk (in percentage) of diarrhea over Bangladesh from 2006 to 2100. The time series represent 10-year moving average changes.....	148

LIST OF TABLES

CHAPTER 1. MANUSCRIPT I

Table 1: Yearly, monthly and daily statistics of BMD stations, Aphrodite, Era-interim and newly developed BMD gridded datasets over Bangladesh from 1981 to 2000. Bracket values represent the difference between BMD station data and respective gridded data value.64

Table 2. Description of selected regional climate models over Bangladesh.....65

CHAPTER 2. MANUSCRIPT II

Table 1. Description of climate indices parameters.....117

Table 2. The spatial and temporal correlations between climatic indices and the three phases of the winter rotavirus epidemic.....118

CHAPTER 3. MANUSCRIPT III

Table 1. Description of selected regional climate models over Bangladesh.....145

Table 2: The results from the multivariate analysis, temporal analysis and spatial analysis for Rising phase of rotavirus (without considering relative humidity).....146

Table 3: The results from the multivariate analysis, temporal analysis and spatial analysis for Rising phase of rotavirus.....147

Table 4: The results from the multivariate analysis, temporal analysis and spatial analysis

for the rising phase of fall cholera.....148

Table 5: The combined score of the top ten models for the rotavirus and cholera diarrheal epidemic (during the rising phase).....149

LIST OF ABBREVIATIONS

RCM	Regional Climate Model
WHO	World Health Organization
GCM	Global Climate Model
RH	Relative Humidity
PR	Precipitation
GPM	Global Precipitation Measuring Mission
IPCC	Intergovernmental Panel on Climate Change
RCP	Representative Concentration Pathways
CMIP5	Coupled Model Intercomparison Project Phase 5

CHAPTER 1

Manuscript I

Published in *Climate Dynamics*, 2017

Climate Projections and Extremes in dynamically downscaled CMIP5 model outputs over the Bengal Delta: A quartile based bias-correction approach with new gridded data

M. Alfi Hasan¹, A.K.M. Saiful Islam², Ali S. Akanda^{1}*

- 1) Department of Civil and Environmental Engineering, University of Rhode Island, Kingston, Rhode Island 02881.
- 2) Institute of Water and Flood Management (IWFM), Bangladesh University of Engineering and Technology (BUET), Dhaka, Bangladesh.

Abstract

In the era of global warming, the insight of future climate and their changing extremes is critical for climate-vulnerable regions of the world. In this study, we have conducted a robust assessment of Regional Climate Model (RCM) results in a monsoon-dominated region within the new Coupled Model Intercomparison Project Phase 5 (CMIP5) and the latest Representative Concentration Pathways (RCP) scenarios. We have applied an advanced bias correction approach to five RCM simulations in order to project future climate and associated extremes over Bangladesh, a critically climate-vulnerable country with a complex monsoon system. We have also generated a new gridded product that performed better in capturing observed climatic extremes than existing products. The bias-correction approach provided a notable improvement in capturing the precipitation extremes as well as mean climate. The majority of projected multi-model RCMs indicate an increase of rainfall, where one model shows contrary results during the 2080s (2071-2100) era. The multi-model mean shows that nighttime temperatures will increase much faster than daytime temperatures and the average annual temperatures are projected to be as hot as present-day summer temperatures. The expected increase of precipitation and temperature over the hilly areas are higher compared to other parts of the country. Overall, the projected extremities of future rainfall are more variable than temperature. According to the majority of the models, the number of the heavy rainy days will increase in future years. The severity of summer-day temperatures will be alarming, especially over hilly regions, where winters are relatively warm. The projected rise of both precipitation and temperature extremes over the intense rainfall-prone northeastern region of the country creates a possibility of devastating flash floods with harmful impacts on agriculture.

Moreover, the effect of bias-correction, as presented in probable changes of both bias-corrected and uncorrected extremes, can be considered in future policy making.

1. Introduction

Observations show that the global land and ocean temperature has risen by 0.85 °C over the period of 1880 to 2012, and the warming trend has accelerated in the last 60 years (IPCC, 2013). Rising global temperatures have been accompanied by changes in the mean state of the climate as well as their associated extreme events. As climate extremes and weather events have significant impacts on the socio-economic stability and sustainability of any region, the information about their probabilistic future as well as existing understanding has received wide attention in the scientific community (Hartmann et al., 2013; IPCC 2007; IPCC 2013). The 4th Assessment report (AR4) of the Intergovernmental Panel on Climate Change (IPCC) has extensively used the climate models that adopted a set of future emission pathways based on socio-economic condition and also participated in Phase 3 of the Coupled Model Intercomparison Project (CMIP3). In the recent IPCC 5th Assessment report (AR5), next generation climate models from the Phase 5 of Coupled Model Intercomparison Project (CMIP5) have utilized a new suite of gas emission scenarios termed as Representative Concentration Pathways (RCPs) (van Vuuren et al. 2011). Combined with RCP scenarios, the models from CMIP5 have provided more accurate representations of climate processes than CMIP3 models by incorporating key assumptions of climate, which were previously ignored by the model developers (Knutti and Sedláček 2012; Taylor et al. 2012). Therefore, the latest CMIP5 projections have become imperative tools for understanding probabilistic changes of climatic extremes in recent years.

Due to devastating societal impacts of climatic extremes, their projected changes are of

particular relevance to policy makers and planners across the world. A disaster prone geography coupled with high population density has rendered South Asia as one of the most vulnerable regions under the impact of extreme events. Previously, some studies explored South Asian climatic extremes over the northern high mountain areas or Indian parts of the Ganges, Brahmaputra and Meghna (GBM) basin, but climatic conditions of the downstream confluence of the GBM were often left unattended (Revadekar et al. 2011; Rao et al. 2014; Freychet et al. 2015). To have a better understanding of socio-economic and hydrologic impacts, the perception of climate and its associated extremes over both upstream and downstream of the basin are important. Bangladesh, situated at the downstream of the basin, is at the front line of climate change, at-risk due to its flood-prone flat topography, overcrowded population and challenging socio-economic condition (Mirza et al. 2003; Rajib et al. 2011; Schiermeier 2011; Dastagir 2015). In this study, the country has been selected as a case study area of the downstream parts of the GBM basin to analyze the changes of the imminent climate and its associated extremes.

Located on the low-lying deltaic floodplains of the GBM basin, Bangladesh is already experiencing adverse impacts of global warming, disasters related to potential climatic changes and associated mean sea level rise (Mirza et al. 2003; Rajib et al. 2011; Schiermeier 2011; Dastagir 2015). As a consequence of observed increasing trends in the number of wet days, the region is likely to experience more seasonal flooding (Shahid 2010). Researchers have taken a great deal of effort to study the probable climate of the country using climate model simulations. For example, Rahman. et al., (2012b) projected 50% reduction of annual rainfall and 0.9°C to 3.5°C increase of temperature in 2060 using

Regional Climate Model of version 3 (RegCM3) driven by A2 AR4 scenario. Based on the multi-ensemble mean (MME) of 17 model simulations, Nowreen et al. (2014) showed that the annual mean precipitation is expected to increase on average by 20% over northwestern Bangladesh with a 2°C increase in global temperature. Increase of monsoon rainfall, decrease of post-monsoon rainfall and projected rise of winter temperature are suggested in a number of studies (Rahman et al. 2012a; Hasan et al. 2013). However, these analyses are all based on previous IPCC AR4 scenarios, and an update of the literature and studies considering RCP scenarios is in demand.

Monsoon-dominated micro scale climate processes play a strong role in precipitation and related extremes over Bangladesh, understanding which are essential to evaluate and explain the condition of future extremes. Therefore, the assessment of the climatic processes at a regional scale is required to derive consistent and reliable projections of probable future climate. In this context, high-resolution ($0.25^{\circ}\times 0.25^{\circ}$ or $0.5^{\circ}\times 0.5^{\circ}$ resolution) projections are imperative for climate evaluation at a regional level, where results from Global Climate Models (GCMs) are sparsely gridded (typically more than $1^{\circ}\times 1^{\circ}$ resolution) (Dankers et al. 2007; Bhaskaran et al. 2012). The GCMs downscaling are a widely used method for regional climate studies. Although statistical downscaling is a computationally inexpensive tool for simulating climate projections, dynamic downscaling is proven to be more representative of fine scale physical processes (Paul et al. 2008; Hong and Kanamitsu 2014; Kang et al. 2014; Lee et al. 2014; Lee and Hong 2014). Dynamically downscaled data generated by regional climate models (RCMs) such as PRECIS and RegCM have been used to project the future climates of Bangladesh (Rajib

et al. 2011; Rajib and Rahman 2012; Hasan et al. 2013; Hussain et al. 2013; Murshed et al. 2013; Nowreen et al. 2014). However, all these studies are based on the scenarios from AR4. Furthermore, single GCM or RCM projections ignore the uncertainties of the future climate, where such uncertainties can be captured using multi-model RCMs derived from various GCMs (Nowreen et al. 2014). Thus, in this study, projections from multi-model RCMs, driven by the CMIP5 GCMs have been used to meet the requisite of the relevant research community.

Though RCMs are common tools for regionalization of GCMs in a more accurate manner, its historical climatology still deviates from observed climatology in a consistent pattern due to improper model parameterizations, unknown complexity in differential equations, coarse spatial resolution, or inadequacy of data. These differences or ‘biases’ are systematic deviation of RCMs, which can be corrected with various methods (Déqué 2007; Themeßl et al. 2011). The choices of bias-correction are often arguable, when it is applied to RCM climate projections (Ehret et al. 2012). However, the projected extremes from bias-correction compares future changes from closer observed values, where uncorrected results confers it from hindcast results of a particular model (Ho et al. 2012). This can create confusion for future decision makers with a limited number of RCM projections, where the future development initiatives require realistic interferences. Although some studies preferred to project climate extremes using uncorrected GCM projections (Christidis and Stott 2016; Alexander and Arblaster 2017), others have also emphasized the utilization of bias-corrected RCM results in the impact studies (Bennett et al. 2014; Macadam et al. 2016; Kis et al. 2017). As climatic extremes are secondary products of the main variables of the

RCM outputs, the future extremes from bias-corrected results could be useful for policy makers. Therefore, in addition to projecting extremes without bias-correction from RCMs, we have explored the projected extremes from bias-corrected climate, where the derived extremes were considered as an impact model itself. To avoid conflicting argument, we also presented underlying biases and their effects over the study region.

Among commonly used bias correction methods, the quartile mapping (QM) methods are considered to be the most up-to-date and accurate methods for climatic studies (Li et al. 2010; Wilcke et al. 2013; Wilcke 2014). Over the South Asian domain, researchers have used delta-based bias correction in annual scales for various climate studies, but none has used QM in daily scales to examine the extremity of present and future climate yet (Raneesh and Thampi 2013; Shashikanth et al. 2014; Apurv et al. 2015). Climate projection using QM based bias correction in RCM results will thus be an advancement to evaluate the South Asian monsoon climate and its extremes in forthcoming years. Therefore, this study has conducted a quantile based bias correction approach to evaluate future climate and its extremities in available CMIP5 level RCM Projections over a monsoonal South Asian country; in this case, Bangladesh.

The aim of this study is thus to explore the climate and its extremes over a monsoon dominated country like Bangladesh by following the latest RCP emission scenarios, considering fine scale regional physics, incorporating the uncertainties range, and also by conducting advance bias correction methods to accomplish most reliable future projections. In this relation, the article has attempted to analyze the future probabilistic climate of the country, by using five regional climate model projections driven by four

GCM results; i.e., EC-EARTH, CNRM-CM5, CCSM4, MPI-ESM-LR. All of the projections utilized three different RCP scenarios: historical, RCP 4.5 and RCP 8.5, to capture the whole range of future uncertainties. To remove the systematic biases from multi-model RCM outputs, latest QM bias correction methods are applied to a newly generated observed gridded data product. Developed by comparing six available observed datasets, the data product presents extreme events in a spatial gridded form.

The remainder of the study is organized as follows: in Section 2, a description of the observed and model data is presented. Method of bias-correction and description of selected extremes are also provided in the same section. The starting part of Section 3 explains the performance of past climate extremes considering different sets of observed data as well as the performance of the six RCM projections. The results are analyzed and a detailed discussion of the study and the potential implications are concluded in later part of Section 3.

2. Data and Methods

2.1. Observed data

The assessment of climate and associated extremes by incorporating climate models, requires evenly spaced data network with long term, reliable time series. Land-based station data has more reliable extreme information, especially in the monsoon dominated regions due to erratic occurrences of rainfall (Singh 2015). However, such datasets have lack of spatial coverage. On the other hand, gridded data products tend to provide spatially rich climate information although it loses some accuracy in terms of magnitudes of daily

extremes (Yatagai et al. 2007). Therefore, conjugating the land-based observed data with the best performed gridded product has the potential to provide most accurate information of climatic extremes (Khandu et al. 2015; Song et al. 2015). For our study region, Prasanna et al., (2007) conducted a similar approach over the entire GBM basin, but the dataset was limited to only ten years from 1997 to 2007, which was inadequate for the climate change study. In this study, we combined two types of suitable data products to develop a long term climate data series for the proposed study. As a daily land-based observation, data from 35 climate stations available from Bangladesh Meteorological Department (BMD) were used. The time period spans over 40 years, ranging from 1948-2010. After quality control and homogeneity test, 32 stations were selected for further analysis. Three meteorological variables; precipitation (PR), maximum temperature (TMAX), and minimum temperature (TMIN) were considered in this study. However, as the extremities of monsoon climate are more dependent on precipitation frequency and magnitude, we focused our comparison of observed data sets only on PR (Singh 2015). The gridded precipitation data products available over Bangladesh are, APHRODITE [the Asian Precipitation - Highly-Resolved Observational Data Integration Towards Evaluation of Water Resources] (Yatagai et al. 2012), CRU [Climatic Research Unit] (Harris et al. 2014), TRMM [Tropical Rainfall Measuring Mission] (Simpson et al. 1988), GPCP [Global Precipitation Climatology Project] (Huffman et al. 1997) and the ERA-Interim reanalysis (Dee et al. 2011) dataset. Among these datasets, CRU and GPCP data are only available at monthly scales and the focus of this study is on daily bias-correction, thus we did not considered the data sets. Also, TRMM data is not sufficient for climate data analyses as it has a limited range from 1998 to 2015. For the ERA-Interim reanalysis product, a number of atmospheric datasets are available over Bangladesh from 1979 to

until now. APHRODITE's highly resolved reanalysis rainfall and temperature records also cover a climatologic period of 1980-2007. Therefore, a comparative extreme analysis between ERA-Interim, APHRODITE and BMD was done where selected land-based BMD data were considered as the true value of observed precipitation. Yearly, monthly and daily investigations of decadal rainfall were conducted in two decadal segments: 1981-1990 and 1991-2000. Values of 32 stations were compared with the same locations of the gridded products, and the decadal mean of all the stations were interpreted. This assessment has revealed that the APHRODITE dataset performs better than ERA-Interim; thus the dataset was combined with BMD gage data to formulate a new gridded product. The detail of the results can be found in section 3.1.1.

To construct the gridded product, each time step of rain gauge observations of BMD was interpolated applying the ordinary co-kriging method with the best-fitted variogram and the entire interpolated surface were later converted to a 25×25 km grid. Geo-spatial kriging techniques are found to be most widely used method in interpolating gauge rainfall data sets (Goovaerts 2000). Best fitted interpolated surface values were extracted considering a 75 km distance threshold based on the assumption that a rainfall event could have influenced up to a 75 km distance of its surrounding. According to Wood and Field (2011), the 50th percentile of the size of clouds over the tropical region during dry spells is less than 100km. Thus, for the selected 25 km by 25 km grid resolution, the cloud length of less than 100km would be a representative of three grid cells or 75km spacing of the proposed grid. Thus, the values of the interpolated surface would be appropriate to explain the surrounding 75km distance of each station. Similarly, in the outside areas of these three grid buffer zones, the satellite derived gridded rainfall would be more relevant. Thus, the

missing values beyond 75 km buffers were filled with the APHRODITE dataset for each time step. In this way, we have implemented the 75 km buffer method to combine the interpolated rainfall values and APHRODITE data from 1981 to 2007 for generating the new gridded product. The performance assessment of the gridded product is also presented in section 3.1.2. A similar gridding approach was also applied to the temperature variables. For both minimum and maximum temperature, the only exception from the grid generation process of precipitation was the absence of a distance threshold after ordinary kriging. In that case, only BMD land-based data was used for temperature gridding. The refined gridded products were used as a basis for further climate analysis and referred as the observed data throughout the rest of the article.

2.2. Model data

Climate data derived from the five available RCM outputs have been selected for this study. The datasets were made available through COordinated Regional Climate Downscaling Experiment (CORDEX), a program that brought forth a collective effort to regional climate projections globally (Giorgi et al. 2009). The CORDEX aims to advance and coordinate the science and application of regional climate downscaling through global partnerships. The project defined some specific domains around the globe and invited communities to conduct regional downscaling in those designated domain. Through the project's data portal, several RCM results became available over South Asia (CORDEX, 2015). As domain selection could be sensitive in a regional modeling study (Bhaskaran et al. 2012), Giorgi et al. (2009) provided a detailed rationale behind domain selection and spatial resolution over CORDEX domains.

In this study, the choice of GCMs was limited due to the number of freely available RCM results. The selection of GCMs to conduct downscaling was the decision of the corresponding home institutions that simulated the RCMs for RCP scenarios. Therefore, we utilized RCM results that are publicly available over the domain in our selected time slices and scenarios. Several studies explained the performance of the selected RCMs (Jacob and Podzun 1997; Samuelsson et al. 2011; McGregor et al. 2013; Teichmann et al. 2013; Zhang et al. 2013; Iqbal et al. 2017). The RCM results selected in our study have reproduced satisfactory monthly rainfalls over the Himalayan region showed by Ghimire et al. (2015). The study conducted over the South Asian CORDEX domain and the selected region follows monsoon climate that is similar to the Bengal Delta (Bhatt and Nakamura 2005). Although the set of selected RCMs that performed satisfactory over the Himalayas do not guarantee to produce better results over the Bengal Delta region, due to similar monsoon climate, we expect that they give us a good direction in RCM selection over the region.

Some uncertainty could arise from the choice of RCM and their internal model physics (Giorgi and Mearns 2002). However, to address the various types of uncertainties, Giorgi and Gutowski Jr. (2015) explained the internal variability and the added value of RCMs in the framework of the CORDEX project. A detailed statistics of the driven GCMs and RCMs are provided in Table 1.

Representative Concentration Pathways (RCPs) are the four global greenhouse gas and aerosol concentration (not emissions) trajectories of futures, which are different than the

previous socio-economic scenarios that give rise to alternative greenhouse gas emissions (van Vuuren et al. 2011). In this study, three RCPs scenarios (historical, RCP 4.5 and RCP 8.5) for three meteorological variables from the five RCMs were utilized for the period of 1981-2010.

The performance of daily extremes, especially precipitation extremes also needs to be examined for the model evaluation. The evaluation of extremes was conducted based on five indices adopt from the CCL/CLIVAR/JCOMM Expert Team on Climate Change Detection and Indices (ETCCDI) (ETCCDI 2016). The selected indices are:

- (a) Number of heavy precipitation events (Rx10): Number of days per year when rainfall amount was greater than 10 mm
- (b) Number of extremely heavy precipitation events (Rx50): Number of days per year when rainfall amount was greater than 50 mm
- (c) Number of rainy days (Rx1):): Number of days per year when rainfall amount was greater than 1 mm
- (d) Minimum values of minimum temperature (TNn): Annual minimum temperature in °C.
- (e) Maximum values of maximum temperature (TXx): Annual maximum temperature in °C.

The selected indices from ETCCDI, were originally developed at the monthly scale. In this study, we have converted them as yearly indices, to make the study concise and more representative of the scope. All the monthly values of Rx1, Rx10 and Rx50 were thus summarized to yearly values. In case of TXx and TNn, the individual year values were

evaluated from the maximum and minimum monthly values, respectively. Due to the comparative large uncertainties, the precipitation extremes were only emphasized during the model evaluation analysis.

To replicate the distribution of mean climate as well as annual extremes derived from the model results, bias-correction methods are considered to be the effective tools in climate change study (Bürger et al. 2011; Cannon et al. 2015). Bias-correction methods can vary depending on the application and use of data. Annual or decadal scale corrections can be performed with conventional 'delta bias correction' method (Amengual et al. 2012). However, these methods are not suitable for preserving the daily extremes, which are crucial for hydrologic modelling, extremity analysis and risk assessment. A quartile-based method proposed by Wilcke et al. (2014) has demonstrated a successful application on regional climate model projections for several variables, including temperature and precipitation. We used an adaptation of this method in this study to retain the number of daily extremes over the 25 years' time period over Bangladesh. Another study, Ehret et al., (2012) presented limitations of bias-correction methods over climate projections. However, as solution to those limitations, they proposed detail representation of bias and unbiased products as 'short' term and multi-model projections as 'mid-term' solutions. In this study, we have adopted both of these solutions to cover the limitations of the bias-correction method.

2.3. Bias correction

In this study, we have conducted bias correction on high-resolution RCM results to

evaluate better climate projection. Previously published literature has shown that GCMs have limitations in the representation of the mean monsoon climate; thus their results need further refinement for regional studies (Dankers et al. 2007; Bhaskaran et al. 2012). In case of the bias-correction of GCMs, the coarsely simulated model results may impose a common projected trend over the finer-scale regional projections. If there are several observation stations located within the same GCM grid cell, after bias-correction, the projected climate of those stations will follow the same projected trend of that particular grid cell. However, in the regional scale, the observed trends may vary within the stations due to local geophysical characteristics such as orographic effects and land use/cover patterns (Wood et al. 2004; Jang and Kavvas 2014; Bieniek et al. 2016). On the other hand, dynamical resolved RCM projections retain these characteristics and provide more regional information of the projected climate within the same GCM cell. As a result, the bias-correction of RCM results provide better regionally representative projections compared to the bias-corrected GCMs (Dankers et al. 2007; Bhaskaran et al. 2012).

The statistical downscaling method applies downscaling by adopting the same bias-correction scheme of the GCMs. The method develops empirical relations based on historical observations that are assumed to be stationary over time. This is usually termed as assumption of stationarity. To evaluate this assumption, Salvi et al. (2016) implemented a design-of-experiments strategy set of experiments and showed a methodology to test the assumption in the climate projections. The study showed that the assumption of stationarity is getting violated over the India region. The findings of the study also confer the inability of the downscaling method to capture the changes of mean rainfall under a changed

greenhouse emission scenario. However, as dynamical downscaling incorporates regional physics into the modeling, it is an approach expected to better preserve the non-stationarity nature of the data (Giorgi and Gutowski Jr. 2015). The advantages of dynamical downscaling over statistical downscaling have been documented in various literature (Paul et al. 2008; Hong and Kanamitsu 2014; Kang et al. 2014; Lee et al. 2014; Lee and Hong 2014). As dynamically downscaled RCM provided better regional information than GCMs over South Asia (Dankers et al. 2007; Bhaskaran et al. 2012), the application of bias-correction in RCM projections were emphasized in recent studies (Wood et al. 2004; Bennett et al. 2014; Macadam et al. 2016; Kis et al. 2017).

Data ranging from 1981 to 2005, a 25-year time slice was used as ‘observed climatology’ for bias correction of the models, as observed data are more reliable after 1980 with lower number of missing values. Bias corrections were performed on each model projection using observed gridded data. Initially, model daily cumulative empirical distributions (ECDFs) were constructed for each individual day of a year with a 30 days’ window. Observed cumulative empirical distribution was also generated using no-parametric kernel approach. Comparing two ECDF, a relation of respective biases was established for each grid cell. Using the relation, RCM data from all models were bias corrected from 1981 to 2100. The process was adopted from Wilcke et al. (2013a), where they demonstrated the retainment of the RCM’s temporal structure and inter-variable dependencies. The method retains the quality of the temporal structure of multiple variables and improves RCM output at a daily time scale. It is true that the method might retain partial biases in the far future when non-stationarity of the model’s error characteristics occurs. However, even in non-stationarity,

the method is expected to improve the biases of raw RCMs (Wilcke et al. 2013).

The projections of bias corrected CMIP5 results over Bangladesh were further analyzed both spatially and temporally under moderate RCP 4.5 and the strongest RCP 8.5 scenarios with respect to baseline climate. Future states of precipitation, maximum and minimum temperature and four selected extremes (TXx, TNn, Rx10 & Rx50) are described in section 3.2.1. As our study focused on providing a comprehensive message of future extremes over the region, we presented both bias-corrected and uncorrected future results of selected extremes in the spatial analysis. It should be noted that, data from CISRO-CCSM4 simulation shows unrealistic deviation during 2006-2040 for all three climate variables. Therefore, we excluded the results of CISRO-CCSM4 model in our subsequent analysis.

3. Results and Discussion

3.1. Observed climate and Bias correction

3.1.1 Performance of observed gridded product

Prior to the generation of observed grid, we compared suitable existing gridded data, ERA-Interim and APHRODITE, with gaged values. The assessment was presented in Table 2. Annual values of the precipitation from both gridded products deviate from observed values, where for ERA-Interim, they exceed 400mm in both decades. At monthly scales however, during monsoon season, significant disagreement has been observed in ERA-Interim data. This finding agrees with those of Rahman et al., (2012b), which showed that ERA-40, a previous version of the ERA-Interim product poorly captured the monsoon rainfall, especially in the Sylhet region (North-eastern part of Bangladesh). Such dry biases

of ERA-Interim were also observed over north-eastern Bangladesh by Ménégoz et al., (2013). In case of APHRODITE data, it shows considerable difference in compare to BMD data in some of the daily climatic extremes like 50mm rainy days, 90th percentile of rainfall and wet days (Table 2). However, from the overall gridded product assessment, APHRODITE data has proven to be better than the ERA-Interim data product. Therefore, for further improvement of daily extremes, APHRODITE data were combined with BMD gauged data to formulate a new gridded data product.

The performance of precipitation and its extremes for the newly generated dataset also are also showed in Table 2. The gridded dataset not only increase the accuracy of the mean at yearly and monthly temporal scale but also provides improved values of the daily rainfall extremes over Bangladesh. Notable improvement of monthly rainfall is also observed in the new dataset during the monsoon season, which is ranging from month of July to September.

3.1.2. Performance of the models before bias-correction

Model requires comparative analogy in respect to the gridded product. The performance assessment of each model with the observed data is shown in Figs. 1a, b, c, at a monthly temporal scale.

The annual rainfall cycle in South Asia is dominated by the monsoon season during the months of June, July, August and September, when almost 70% of the rainfall occurs. Among the five regional models, only the RCA4-EC-EARTH model overestimates the

monsoon rainfall over the region. The simulations obtained by the CISRO RCMs show very similar temporal biases of precipitation, which makes it evident that the boundary data from GCMs plays a dominant role in those RCMs for simulating regional precipitation over the region. This argument is also supported by Ghimire et al., (2015), where similar annual patterns are also found in the far north of the country over the Himalayan area. The study revealed overestimation of rainfall over the Himalayan region, whereas, in our case monsoon rainfall is underestimated. This discrepancy might be due to the inaccuracy of the orographic rainfall at the high altitudes produce by the regional model. For REMO-MPI, there is a large dry bias during monsoon season. Similar findings have also been reported by Jacob et al., (2012). . In general, the temperatures derive from the models show better performance than precipitation in terms of monthly climatic biases. Minimum temperature produced by RCA4-EC-EARTH model, has cold biases during winter and post monsoon seasons. During the months of March and April, all of the RCMs show some biases in maximum temperature, but the rest of the annual cycle are consistent with observation.

The choice of convective schemes across the regional climate models could play a crucial role in reproducing monsoon rainfall, which eventually affect the dynamic downscaling process (Prein et al. 2015). In this study, we have utilized the results of three regional models (Table 2) that have their own convective schemes. The cloud formation scheme of REMO was adopted from the MPI global model and it is based on the approach from Sundqvist (1978). In case of CCAM from CSIRO, the atmospheric climate model utilizes a conformal cubic grid. It includes CSIRO's mass cumulus convection scheme that incorporates downdrafts and the evaporation of rainfall (McGregor 2005). For the RCA of

SMHI, the regional model resolves convective processes with an entraining and detraining plume model using the Kain–Fritsch (KF) scheme (Kain and Fritsch 1993; Kain 2004). In this context, using the Weather Research and Forecasting (WRF) model, Devanand et al. (2017) showed that among various convective schemes, the Kain–Fritsch (KF) scheme performed better in simulating Indian summer monsoon. Our analysis also found agreement, as RCA4-EC-EARTH produced comparable rainfall compared to other RCMs over the Bengal delta region.

It should be noted that the domain setup (i.e. a nested domain) is also important in regional climate downscaling (Devanand et al. 2017). Currently, the CORDEX domain of South Asia is defined as a single nest domain with a large spatial coverage. Due to the high resolution (0.44 degree by 0.44 degree), the domain is already computationally expensive for multiple scenarios with multiple ensembles. However, with the advancement of computational power, the CORDEX domain can be redefined in the future to incorporate nesting operations for better performance of the models.

After the assessment of mean climate, we also explored the efficiency of the models in generating selected extremes. Spatial and temporal evaluations of the precipitation indices have been shown in Fig. 2, 3, 4. The spatial analysis reveals dry biases in Rx50 for the REMO-MPI model results, especially in the northwestern region. All three CSIRO models have been able to capture Rx50 quite well and show little spatial variability among them. RCA4-EC-EARTH simulation data shows number of Rx50 lesser in the Sylhet region (north-eastern part), whereas in the east-central part Rx50 is much higher than observed

climate. In context of lower end of rainfall distribution, Rx1 are well captured by all three CSIRO simulations (Fig. 3). However, the CSIRO models estimate higher number Rx1 over the northwestern parts, while REMO-MPI and RCA4-EC-EARTH show lower Rx1 over the north and the northeastern areas compare to observed precipitation. In terms of heavy rainfall (Rx10), except RCA4-EC-EARTH simulation, all other RCM simulations suggest lower values compare to observation, but they preserved the existing spatial pattern during the baseline period (not shown in the figures). Spatial average of Rx10 and Rx50 from the models present some dry temporal biases than respective observed extremes (Fig. 4). As these model biases rapidly change between individual years for a particular model, average of all model results can give us a better picture of model performance over the country. After observing a constant dry biases in both indicators, correction of these biases become essential for further extreme analysis.

3.1.3. Performance of the models after bias-correction

Bias corrected data results along with raw model data are shown in the Taylor diagram (Figs. 1d, e). The daily bias correction has improved the correlation factor and standard deviations of the model results. The improvement is founded to be higher in the model temperature (correlation about 0.95) than precipitation (correlation about 0.85).

Spatial and temporal agreement in the climatic extremes is achieved from the bias correction of the RCM results. Rx50 and Rx10 values from all the models show similar spatial patterns during the base period. However, in terms of magnitude, exception has been observed in the corrected RCA4-EC-EARTH model result, where increased Rx10 values are found over the northeastern region (Fig. 3). The temporal analysis reveals that

bias-correction of precipitation actually made the model results much wetter than before. Similar comments about these wet biases from the quartile mapping were also found in previous studies (Wilcke et al. 2013). As stating tail of kernel distribution unable to capture accurate amount of dry days, such error might occurs (Wilcke et al. 2013). However, as Bangladesh is a monsoon dominated region, the pattern of normal to extreme precipitation have significant impacts on its agro-based economy and socio-economic outcomes (Ahmed 2003; Islam et al. 2005; Ahmed 2006). Deriving accurate information of precipitation variability from the climate models are essential for studying the climatic impacts for future decision making of the country (Shahid 2011). In this context, the daily bias corrections of RCM rainfall allowed significant improvement by providing a more realistic capture of high intensive rainfall events. Moreover, the corrected model results also exhibit improved accuracy of the mean climate over the region. For temperature, the daily bias correction method reduces the disagreement of models results drastically, where corrected model datasets are highly correlated (temporal correlations > 0.9) with observed data (Fig. 1). Therefore, spatial analyses of these datasets have not been shown in this study.

3.2. Future changes

3.2.1 Projected temporal state of PR, TMAX and TMIN

The mean annual PR over Bangladesh under RCP 4.5 and RCP 8.5 are shown in Fig. 5a, b, c, d. In general, projected annual average of PR show disagreements between the models under both scenarios, where most of them, suggest an increase in future years. An exception is noted in MPI projections, as it shows decrease of PR after 2050s under RCP 8.5. At the

end of 21st century, mean annual PR is estimated to be in range of 2400 to 3000 mm/year and 1900 to 3000 mm/year under RCP 4.5 and RCP 8.5 respectively. The model variability of RCP 4.5 is lesser during 2090s (2081-2090) compared to RCP 8.5, providing more confidence in RCP 4.5 scenarios. The RCP 4.5 scenario is developed considering the rising radiative forcing pathway leading to 4.5 W/m² at stabilization after 2100 where in the RCP 8.5 scenario energy continues to accumulate (van Vuuren et al. 2011). Therefore, fixed energy change of RCP 4.5 after 2100 could constrain the variability of model results. RCA4 and REMO models are much more variable in PR changes throughout the model projections, while CSIRO RCM shows much more consistent growth. Some insight of PR change over Bangladesh supports our results as well. Previous CMIP3 based reports suggested change of PR from -5% to over 30% in future years in comparison to the baseline period (Hasan and Islam, 2013; Hasan et al., 2013; Nowreen et al., 2014; Kumar et al., 2014, 2013). Change of yearly PR also found in the study conducted by Caesar et al. (2015), where they referred -0.5mm/day to 2mm/day (-180mm/year to 750mm/year) change in future rainfall. Some South Asia-based RCP projections also reported similar finding (Chaturvedi et al. 2012; Jayasankar et al. 2015; Sharmila et al. 2015). As we explained in previous sections that the advance bias correction can provide confident by removing model disagreement with observed, thus our results can be a more reliable as the similar correction mechanism applied for projecting the future climate of the country.

The annual TMAX from CMIP5 projections over Bangladesh are illustrated in Fig. 5c, d. The variable exhibits significant increase in both RCP projections. Mean annual TMAX, predicted to rise to 31.5°C-32°C under RCP 4.5 and to 32.5°C-34°C under RCP 8.5 in the

country. Increased absolute values of TMAX under RCP 8.5 indicates that mean annual TMAX of the 2080s will be as warm as the mean summer temperature (33.5°C) of present day, which hints alarming consequences for the country. These results are corroborated by similar findings in previous studies (Chaturvedi et al. 2012; Hasan and Islam 2013; Mittal et al. 2014).

The projected annual TMIN over Bangladesh also presented in Fig. 5e, f. From 21°C during 1990s, TMIN projected to increase up to $23\pm 0.5^{\circ}\text{C}$ at the end of century under RCP 4.5. Under RCP 8.5, CMIP5 models suggest that TMIN will increase to a range of 24.5 to 26.5 °C during 2080s. Such rapid increase in the strongest RCP scenario give us an indication of an appalling future, where the number of winter days will be much lower than the current state. It is also noteworthy that TMIN shows a much faster increase than TMAX (about 1°C higher by the end of the 21st century) under both scenarios. Thus, it signals a reduced variation between day temperature-TMAX and night temperature-TMIN over the region.

3.2.2. Projected spatial changes of PR and average temperature

Spatial changes of PR over Bangladesh are assessed based on bias corrected CMIP5 climate projections (Fig. 6). RCA4-EC-EARTH and all three CSIRO projections show an increase of rainfall in future years. The projected increase is not gradual in the earlier decades (2050s), but by the 2080s, most of the projections show steady increase of precipitation over the northwestern parts of the country. The RCA4 projection shows much higher changes of PR over the Teesta river basin area (northwestern part). CISRO-CCSM4

and CSIRO-CCNRM projections predicted an increase of PR over the Sylhet region (northeastern part) under the RCP 8.5 scenario, where CSIRO-MPI-ESM shows such increase in the Chittagong Hill Tracts region (southeastern part) of the country. Contrary to other model projections, the model results from REMO-MPI show projected decrease of rainfall under both RCP 4.5 and RCP 8.5 scenarios. In this projection, a faster decrease of rainfall is observed in the northern parts than southern parts for both pathways. It is notable that, under RCP 8.5, estimated decrease of 900mm annual rainfall is observed in Sylhet region by the end of the century.

As TMAX and TMIN changes are very similar to each other, spatial changes of average temperature by averaging TMAX and TMIN are presented in the study (Fig. 7). The Fig. shows the spatial distribution of mean annual changes in average temperature in the 2050s (2041-2070) and 2080s (2071-2100) under RCP 4.5 and RCP 8.5 scenarios, relative to baseline. The southwestern coastal zone of the country projected to be the most affected with definite increase in temperature. Interestingly, all projections strongly agreed with such observations, strengthening the CMIP3 climate model results and the argument that the southwestern part of Bangladesh is the most vulnerable due to its socio-economic condition and population density (Ali and Islam 2014; Dastagir 2015). Vulnerability due to such increase of overall temperature ranges will result in disastrous outcomes for this region by the end of the 21st century. During 2050s, projected temperature estimated to increase by 0.75°C-1.75°C under RCP 4.5 and by 1°C-2.5°C under RCP 8.5 in the southern parts of the country. Although RCP 4.5 scenarios are known to be less ambitious and CO₂ controlled emission scenarios, most of the climate models still suggest at least a 2°C

increase of temperature during 2080s over most part of the country. On the other hand, the RCP 8.5 scenarios provided an alarming projection of up to 4.5°C within 2100 over the whole country. It should be noted that CCSM4 model result shows much lesser increments of temperature among CSIRO RCMs.

In general, north-western part of Bangladesh experiences lower rainfall compared to the hilly regions located in the eastern parts of the country. Analyzing model projections and their bias correction, it is observed that RCA4 and REMO show an increase of temperature over low rainfall zones. Contrary to that, CSIRO models conclude higher increase of temperature in the wet hilly regions. The contrasting characteristics of the projected results reaffirm that the relationship of rainfall depends on complex interaction of ocean, land and atmosphere, and not just temperature characteristics. Thus, it again emphasized the importance of dynamic over statistical downscaling considering regional scales (5km to 50km) for a clear understanding of the future climate.

3.2.3. Projected changes of climatic extremes

In this study, we have tried to portrait the effect of bias-correction on future extremes. Therefore, we demonstrated the difference between bias-corrected and uncorrected climate in a spatial analysis of the extreme indices. The spatial changes of two precipitation (Rx10 and Rx50) and two temperature (TXx, TNn) indices, both bias-corrected and uncorrected versions, are presented in Fig. 8, 9. The uncorrected changes of Rx10 and Rx50 differs from bias-corrected values of same variables, both in terms of pattern and magnitude. The pattern of uncorrected Rx10 deviates drastically from 2050s to 2080s in both scenarios,

where changes in the pattern between the time-slices were gradual in the bias-corrected results. In terms of magnitude, uncorrected Rx10 shows smaller changes under RCP 4.5, but more increase on the southern parts of country during 2080s of RCP 8.5 in compare to bias-correction.

The changing variability is also much higher in the uncorrected than the bias-corrected projections, under both scenarios. For example, northern parts of the country experience about 7 ± 5 (which means changes are observed from 2 days to 12 days) increase of Rx10 under bias-corrected projection during 2050s of RCP 4.5 where, in case of uncorrected values, the increment is 3 ± 6 for the same period and scenario. In case of RX50, uncorrected projections change the signal from positive to negative under RCP4.5 scenarios, especially in the north-central region of the country. The uncorrected values of Rx50 also shows a higher uncertainty range in respect to the bias-corrected range, with accordance to Rx10. In cases of the temperature extremes, the uncorrected and bias-corrected pattern is more agreeable than the precipitation extremes, as expected, due to fact that the models in hindcast simulation better captured temperatures. However, the variability between uncorrected and bias-corrected changes are still persistent, where uncorrected extremes shows hotter climate with a higher uncertainty range. Both figures for extremes suggest that the uncorrected changes give much wider uncertainties and exhibit erratic pattern of changes in future projections.

In addition, for uncorrected projections, the policy makers need to keep in mind that the changes that are represented in the Figures are not changes from past climate, rather the

changes are from the individual model results of the baseline run. This can cause a great ambiguity in conferring the results in the prospective decision-making process. In this context, the uncorrected climate projections can give idea of the wider range of uncertainties, where bias-corrected model results can provide a higher level of confidence. Utilizing the projected changes in extremes by the bias-correction techniques, the decision maker might have a smaller uncertainty range but they will have a realization of changes from the actual observed climate. As the focus of this study is to convey assertive information of extremes for decision makers, the bias corrected results should be more relevant in this context. Therefore, we have described the bias-corrected results as the projected result in the following sections.

Projected mean of precipitation extremes (Rx10 and Rx50) suggest an increase of rainfall all over the country, where northeastern part indicate higher increment rate than the rest of the country under both RCP scenarios. The region is mostly hilly and important for industrial tea plantation (Islam and Miah 2003). As almost all models conclude the increase of extreme rainfall at end of the 21st century, such changes may have significant impact on the tea plantations of the area. These areas are also prone to high amount of intense rainfall events and flash flooding. Thus, increase of heavy rainfall events will eventually extend the risk of flash flooding to an alarming level. In addition, heavy rainfall events (Rx10) will increase in much faster rate than extremely heavy rainfall events (Rx50) all over the country. The projected Rx10 of model mean refers an increase of at least 80 or more of the heavy rainfall days within a decade (8 days per year) from current climate. Majority of model result also suggest that the country will experience at least four more days of

extremely heavy rainfall annually from present time to the end of the century. By looking at variance of Rx50 between model projections, it can be said that all five models show more confidence in projecting extremes over the western parts than other parts of the country.

Figure 9 shows the changes of TXx and TNn during 2050s and 2080s under both RCP 4.5 and RCP 8.5 scenarios. All the model under both scenarios refers a faster rise of TNn than TXx. Minimum temperature (TNn) increase might be favorable for cold-vulnerable crops or destructive for cold-loving crops (Parmesan 2006). Eastern parts in general shows much higher rise of TXx other areas of the country, with more confidence due to the low values of variability.

In conjunction with precipitation and temperature increases, it is found that the eastern part of the country will experience more changes in terms of both mean climate and extremes than western parts of the country. Heavy and extremely heavy rainfalls in majority models show a significant increase over the hilly regions (northeastern and southeastern part) of the county in both time slices. Interestingly, temperature extremities will also increase over the same regions.

Probability distribution (PD) of the two precipitation extremes (Rx10, Rx50) and two temperature extremes (TXx & TNn) are presented in Fig. 10a, b, c, d, e, f (are bias-corrected). To examine the extremity of precipitation, knowledge of future changes in number of heavy rainy days and extreme rainy days are required which are presented as

Rx10 and Rx50 respectively. Most of the PD of Rx10 formulated from bias corrected projections shows increase of heavy rainfall under both scenarios, where only REMO-MPI shows the opposite. According to REMO-MPI model results, under the RCP 4.5 scenario, decreasing trends of RX10 will stop at 2050s, where under RCP 8.5 it will continue to decrease till the end of the 21st century. Other models suggest that under both scenarios the PD will be shifted toward higher number. Such shift will likely cause at least 10 more days of heavy rainfall per year. A significant shift of probability in extreme precipitation is only observed in RCA4-EC-EARTH model result under RCP 8.5 scenarios. All other models show higher probability that Rx50 will decrease at 2050s under the same scenario but projected changes are not significant.

Changes in the highest daytime temperature (TXx) in a year are presented in Fig. 10e, f. Under RCP 4.5, shift in the PD of TXx is uncertain in all models. However, the flatter distribution from the baseline in EC-EARTH and REMO model suggest that the variation of TXx will be high between the years during 2080s. Under RCP 8.5, the significant shift of the lower tail of the TXx distribution indicates a definite increase in summer days. Based on the EC-Earth and REMO model results, such increase can reach up to 5°C at the end of current century over the country.

Projected probability of minimum temperatures during winter season is also illustrated in Fig. 10g, h. Gradual shift toward a higher TNn have been noticed in all model projections under RCP 4.5 at 2050s, but such a shift will not continue up to 2080s under the same scenario. RCP 8.5 scenario suggests a significant increase in probability of TNn based on

all model results. In contrary to much colder temperatures from other hypotheses, TNn shows a reduction of its extremity in future years. However, such results can be uncertain due to the inability of GCMs to produce such extremes (Barros et al. 2014). It is evident that, increase of TNn during 2080s is much higher than increase of TXx during the same period. Such incremental shift in PD can lead to a less variable diurnal temperature range over Bangladesh.

In this study, we have utilized five combinations of RCMs and GCMs that gave the projections of future probable climate and its extremes over Bangladesh. A larger set of RCMs and GCMs can cover a wider uncertainty range, and provides us more information of the projected future. However, we have a limited choice of GCMs and RCMs available for this study due to unavailability of projections and computational constrains over the CORDEX domain (explained in the Methods section). This limitation could potentially improve in the future as additional CMIP5 RCM projections become available.

The replication of non-stationarity by climate models is important for climate projections. To explore the confidence of the projections, Salvi et al. (2016) demonstrated a strategy to check the assumption of stationarity for statistical downscaling methods and also recommended to test the framework on dynamical downscaling as well as on GCM results. This framework could potentially be very useful for the bias-corrected and uncorrected RCM results over Bangladesh. However, it was not covered in this study, and thus provides an opportunity for future improvement.

4. Conclusion

To examine future changes in climate and climatic extremes in a monsoon-dominated region, we have analyzed the results from the five available regional climate models from IPCC AR5 over Bangladesh for the present (1961-1990) and future (2005-2100). For a climatic extremes analysis, we have generated a new gridded rainfall data product over the country to address information gap on extremes, insufficient observed grid-data at a daily scale, and uncorrected high bias values of future projections over the region. Moreover, the most recent CMIP5 Regional Climate Models with higher accuracy under emission trajectories have been evaluated. The summarized findings can be presented as follows:

After bias correction with newly generated observed data product, the patterns of extreme climate events are preserved between the model and observations over Bangladesh. The comparison of Taylor diagram also validated the performance of bias correction between observed and model data. Under the RCP 4.5 and RCP 8.5 scenarios, rainfall increase has been observed significantly and with high confidence over the eastern hilly regions, especially in the northern parts. A possible reduction of rainfall will be more prominent in the northern zones than southern zones of the country. Maximum and minimum temperature changes are more incremental in the southwestern parts compare to other parts. The model result under RCP 4.5 scenario shows large uncertainly in rainfall and much steady rise of temperature in the middle of the 21st century. Under RCP 8.5, the projected increase in rainfall events is observed over the areas where temperature will increase faster and vice-versa. Due to the energy difference between RCP 4.5 and RCP 8.5, the rainfall

projections of RCP 8.5 shows more uncertainty than RCP 4.5 at 2100. The projected model results have also indicated the changes in the frequency of extreme precipitation and temperature events. The extremities of rainfall tend to be more variable than temperature extremes and the number of heavy rainfall days will be much higher in future years. The results imply that there would be much higher heavy rainfall events over the northeastern hilly regions than other parts of the country. Alarming, the temperature extremity also tends to have a drastic increase over the same regions.

Although bias correction of RCM provides a useful basis for the impact studies, considerable uncertainties remain in GCM, RCM and the bias correction method itself. Despite these uncertainties, bias-corrected projections at the appropriate spatial-temporal scales are the most reliable tools for understanding hydro-climatic impacts. In this study, an initial investigation of the hydroclimatic extremes has been performed with an appropriate daily scale bias correction method with a new gridded climate dataset over a monsoon region, the Bengal Delta region of South Asia. Further analyses of monthly or seasonal extremities in precipitation and temperature should be pursued in future years.

Acknowledgements:

The authors would like to sincerely thank the NASA Health and Air Quality Program [grant number NNX15AF71G] and the University of Rhode Island College of Engineering Dean's Fellowship program for supporting this study. Dr. A.K.M. Saiful Islam is supported by the European Union Seventh Framework Programme FP7/2007-2013 [grant number 603864] (HELIX: High-End cLimate Impacts and eXtremes; <http://www.helixclimate.eu>).

We also like thanks the anonymous reviewers for their thoughtful comments.

References:

Ahmed AU (2006) Bangladesh Climate Change Impacts and Vulnerability: A Synthesis.

Ahmed R (2003) Climate of Bangladesh. *Banglapedia* 45–48.

Alexander L V., Arblaster JM (2017) Historical and projected trends in temperature and precipitation extremes in Australia in observations and CMIP5. *Weather Clim Extrem* 15:34–56. doi: 10.1016/j.wace.2017.02.001

Ali K, Islam A (2014) Assessing risks from climate variability and change for disaster-prone zones in Bangladesh. *Int J Disaster Risk Reduct* 10:236–249. doi: 10.1016/j.ijdrr.2014.08.008

Amengual A, Homar V, Romero R, et al (2012) Projections of the climate potential for tourism at local scales: Application to Platja de Palma, Spain. *Int J Climatol* 32:2095–2107. doi: 10.1002/joc.2420

Apurv T, Mehrotra R, Sharma A, et al (2015) Impact of climate change on floods in the Brahmaputra basin using CMIP5 decadal predictions. *J Hydrol* 527:281–291. doi: 10.1016/j.jhydrol.2015.04.056

Barros VR, Field CB, Dokken DJ, et al (2014) IPCC AR5. In: *Climate Change 2014: Impacts, Adaptation, and Vulnerability. Part B: Regional Aspects. Contribution of Working Group II to the Fifth Assessment Report of the Intergovernmental Panel on Climate Change*. Cambridge University Press, Cambridge, United Kingdom and New York, NY, USA, pp 1–51

- Bennett JC, Grose MR, Corney SP, et al (2014) Performance of an empirical bias-correction of a high-resolution climate dataset. *Int J Climatol* 34:2189–2204. doi: 10.1002/joc.3830
- Bhaskaran B, Ramachandran a., Jones R, Moufouma-Okia W (2012) Regional climate model applications on sub-regional scales over the Indian monsoon region: The role of domain size on downscaling uncertainty. *J Geophys Res Atmos* 117:1–12. doi: 10.1029/2012JD017956
- Bhatt BC, Nakamura K (2005) Characteristics of Monsoon Rainfall around the Himalayas Revealed by TRMM Precipitation Radar. *Mon Weather Rev* 133:149–165. doi: 10.1175/MWR-2846.1
- Bieniek PA, Bhatt US, Walsh JE, et al (2016) Dynamical Downscaling of ERA-Interim Temperature and Precipitation for Alaska. *J Appl Meteorol Climatol*. doi: 10.1175/JAMC-D-15-0153.1
- Bürger G, Schulla J, Werner AT (2011) Estimates of future flow, including extremes, of the Columbia River headwaters. *Water Resour Res* 47:1–18. doi: 10.1029/2010WR009716
- Caesar J, Janes T, Lindsay A, Bhaskaran B (2015) Temperature and precipitation projections over Bangladesh and the upstream Ganges, Brahmaputra and Meghna systems. *Environ Sci Process Impacts* 17:1047–1056. doi: 10.1039/C4EM00650J
- Cannon AJ, Sobie SR, Murdock TQ (2015) Bias correction of GCM precipitation by quantile mapping: How well do methods preserve changes in quantiles and extremes?

J Clim 28:6938–6959. doi: 10.1175/JCLI-D-14-00754.1

Chaturvedi RK, Joshi J, Jayaraman M, et al (2012) Multi-model climate change projections for India under representative concentration pathways. *Curr Sci* 103:791–802.

Christidis N, Stott PA (2016) Attribution analyses of temperature extremes using a set of 16 indices. *Weather Clim Extrem* 14:24–35. doi: 10.1016/j.wace.2016.10.003

Dankers R, Christensen OB, Feyen L, et al (2007) Evaluation of very high-resolution climate model data for simulating flood hazards in the Upper Danube Basin. *J Hydrol* 347:319–331. doi: 10.1016/j.jhydrol.2007.09.055

Dastagir MR (2015) Modeling recent climate change induced extreme events in Bangladesh: a review. *Weather Clim Extrem* 7:49–60. doi: 10.1016/j.wace.2014.10.003

Dee DP, Uppala SM, Simmons AJ, et al (2011) The ERA-Interim reanalysis: Configuration and performance of the data assimilation system. *Q J R Meteorol Soc* 137:553–597.

Déqué M (2007) Frequency of precipitation and temperature extremes over France in an anthropogenic scenario: Model results and statistical correction according to observed values. *Glob Planet Change* 57:16–26. doi: 10.1016/j.gloplacha.2006.11.030

Devanand A, Ghosh S, Paul S, et al (2017) Multi-ensemble regional simulation of Indian monsoon during contrasting rainfall years: role of convective schemes and nested domain. *Clim Dyn* 0:1–21. doi: 10.1007/s00382-017-3864-x

Ehret U, Zehe E, Wulfmeyer V, et al (2012) HESS Opinions “should we apply bias

- correction to global and regional climate model data?” *Hydrol Earth Syst Sci* 16:3391–3404. doi: 10.5194/hess-16-3391-2012
- ETCCDI (2016) ETCCDI Extremes Indices Archiveo Title. In: ETCCDI Extrem. Indices Arch. <http://www.cccma.ec.gc.ca/data/climdex/>. Accessed 1 Jan 2016
- Freychet N, Hsu HH, Chou C, Wu CH (2015) Asian summer monsoon in CMIP5 projections: A link between the change in extreme precipitation and monsoon dynamics. *J Clim* 28:1477–1493. doi: 10.1175/JCLI-D-14-00449.1
- Ghimire S, Choudhary a., Dimri a. P (2015) Assessment of the performance of CORDEX-South Asia experiments for monsoonal precipitation over the Himalayan region during present climate: part I. *Clim Dyn.* doi: 10.1007/s00382-015-2747-2
- Giorgi F, Gutowski Jr. WJ (2015) Regional Dynamical Downscaling and the CORDEX Initiative. *Annu Rev Environ Resour* 40:150724171620008. doi: 10.1146/annurev-environ-102014-021217
- Giorgi F, Jones C, Asrar GR (2009) Addressing climate information needs at the regional level: the CORDEX framework.
- Giorgi F, Mearns LO (2002) Calculation of average, uncertainty range, and reliability of regional climate changes from AOGCM simulations via the “Reliability Ensemble Averaging” (REA) method. *J Clim* 15:1141–1158. doi: 10.1175/1520-0442(2003)016<0883:COCOAU>2.0.CO;2
- Goovaerts P (2000) Geostatistical approaches for incorporating elevation into the spatial

interpolation of rainfall. *J Hydrol* 228:113–129. doi: 10.1016/S0022-1694(00)00144-X

Harris I, Jones PD, Osborn TJ, Lister DH (2014) Updated high-resolution grids of monthly climatic observations – the CRU TS3.10 Dataset. *Int J Climatol* 34:623–642. doi: 10.1002/joc.3711

Hartmann DL, Tank AMGK, Rusticucci M (2013) IPCC Fifth Assessment Report, *Climatic Change 2013: The Physical Science Basis*. IPCC AR5:31–39.

Hasan MA, Islam AKMS (2013) Changes of Seasonal Temperature Extremes in Future over Bangladesh using Projections by a Regional Climate Model. *Natl Semin Clim Chang Impact Adapt* 116–120.

Hasan MA, Islam AKMS, Bhaskaran B (2013) Predicting future precipitation and temperature over Bangladesh using high resolution regional scenarios generated by multi-member ensemble climate. In: 4th International Conference on Water & Flood Management (ICWFM-2013). pp 575–582

Ho CK, Stephenson DB, Collins M, et al (2012) Calibration strategies a source of additional uncertainty in climate change projections. *Bull Am Meteorol Soc* 93:21–26. doi: 10.1175/2011BAMS3110.1

Hong SY, Kanamitsu M (2014) Dynamical downscaling: Fundamental issues from an NWP point of view and recommendations. *Asia-Pacific J Atmos Sci* 50:83–104. doi: 10.1007/s13143-014-0029-2

- Huffman GJ, Adler RF, Arkin P, et al (1997) The global precipitation climatology project (GPCP) combined precipitation dataset. *Bull Am Meteorol Soc* 78:5–20.
- Hussain MA, Islam AKMS, Hasan MA (2013) Changes of the Seasonal Salinity Distribution At the Sundarbans Coast Due To Impact of Climate Change. 4th Int Conf Water Flood Manag 4:637–648.
- IPCC (2007) IPCC Fourth Assessment Report (AR4). IPCC 1:976.
- Iqbal W, Syed FS, Sajjad H, et al (2017) Mean climate and representation of jet streams in the CORDEX South Asia simulations by the regional climate model RCA4. *Theor Appl Climatol* 129:19.
- Islam MN, Terao T, Uyeda H, et al (2005) Spatial and Temporal Variations of Precipitation in and around Bangladesh. *J Meteorol Soc Japan* 83:21–39. doi: 10.2151/jmsj.83.21
- Islam S, Miah S (2003) *Banglapedia: national encyclopedia of Bangladesh*.
- Jacob D, Elizalde A, Haensler A, et al (2012) Assessing the transferability of the regional climate model REMO to different coordinated regional climate downscaling experiment (CORDEX) regions. *Atmosphere (Basel)* 3:181–199. doi: 10.3390/atmos3010181
- Jacob D, Podzun R (1997) Sensitivity studies with the regional climate model REMO. *Meteorol Atmos Phys* 63:119–129. doi: 10.1007/BF01025368
- Jang S, Kavvas ML (2014) Statistical Downscaling versus Dynamic Downscaling: An Assessment Based upon a Sample Study. In: *World Environmental and Water*

Resources Congress 2014. American Society of Civil Engineers, Reston, VA, pp 591–595

Jayasankar CB, Surendran S, Rajendran K (2015) Robust signals of future projections of Indian summer monsoon rainfall by IPCC AR5 climate models: Role of seasonal cycle and interannual variability. *Geophys Res Lett* 1–8. doi: 10.1002/2015GL063659. Received

Kain JS (2004) The Kain–Fritsch Convective Parameterization: An Update. *J Appl Meteorol* 43:170–181. doi: 10.1175/1520-0450(2004)043<0170:TKCPAU>2.0.CO;2

Kain JS, Fritsch JM (1993) Convective parameterization for mesoscale models: The Kain–Fritsch scheme. In: *The representation of cumulus convection in numerical models*. Springer, pp 165–170

Kang S, Hur J, Ahn JB (2014) Statistical downscaling methods based on APCC multi-model ensemble for seasonal prediction over South Korea. *Int J Climatol* 2005:3801–3810. doi: 10.1002/joc.3952

Khandu, Awange JL, Forootan E (2015) An evaluation of high-resolution gridded precipitation products over Bhutan (1998–2012). *Int J Climatol* 1087:1067–1087. doi: 10.1002/joc.4402

Kis A, Pongracz R, Bartholy J (2017) Multi-model analysis of precipitation-related climatological extremes for the Carpathian Region. *Int J Climatol* 17:2100. doi: 10.1002/joc.5104

- Knutti R, Sedláček J (2012) Robustness and uncertainties in the new CMIP5 climate model projections. *Nat Clim Chang* 1–5. doi: 10.1038/nclimate1716
- Lee JW, Hong SY (2014) Potential for added value to downscaled climate extremes over Korea by increased resolution of a regional climate model. *Theor Appl Climatol* 117:667–677. doi: 10.1007/s00704-013-1034-6
- Lee JW, Hong SY, Chang EC, et al (2014) Assessment of future climate change over East Asia due to the RCP scenarios downscaled by GRIMs-RMP. *Clim Dyn* 42:733–747. doi: 10.1007/s00382-013-1841-6
- Li H, Sheffield J, Wood EF (2010) Bias correction of monthly precipitation and temperature fields from Intergovernmental Panel on Climate Change AR4 models using equidistant quantile matching. *J Geophys Res Atmos*. doi: 10.1029/2009JD012882
- Macadam I, Argüeso D, Evans JP, et al (2016) The effect of bias correction and climate model resolution on wheat simulations forced with a regional climate model ensemble. *Int J Climatol* 4591:4577–4591. doi: 10.1002/joc.4653
- Mcgregor J, Katzfey J, Thatcher M, et al (2013) AN UPDATE ON CCAM MODELLING ACTIVITIES AT CSIRO. 51–53.
- McGregor JL (2005) C-CAM: Geometric aspects and dynamical formulation. CSIRO Atmospheric Research Dickson ACT
- Ménégoz M, Gallée H, Jacobi HW (2013) Precipitation and snow cover in the Himalaya:

From reanalysis to regional climate simulations. *Hydrol Earth Syst Sci* 17:3921–3936.
doi: 10.5194/hess-17-3921-2013

Mirza MMQ, Warrick RA, Ericksen NJ (2003) The implications of climate change on floods of the Ganges, Brahmaputra and Meghna rivers in Bangladesh. *Clim Change* 57:287–318.

Mittal N, Mishra A, Singh R, Kumar P (2014) Assessing future changes in seasonal climatic extremes in the Ganges river basin using an ensemble of regional climate models. *Clim Change* 123:273–286. doi: 10.1007/s10584-014-1056-9

Murshed SB, Nowreen S, Islam AKMS, et al (2013) Change of extreme precipitation indices for the eight hydrological regions of Bangladesh. In: *International Conference on Climate Change Impact and Adaptation (I3CIA-2013)*. pp 462–471

Nowreen S, Murshed SB, Islam AKMS, et al (2014) Changes of rainfall extremes around the haor basin areas of Bangladesh using multi-member ensemble RCM. *Theor Appl Climatol* 1–15. doi: 10.1007/s00704-014-1101-7

Parmesan C (2006) Ecological and Evolutionary Responses to Recent Climate Change. *Annu Rev Ecol Evol Syst* 37:637–669. doi: 10.1146/annurev.ecolsys.37.091305.110100

Paul S, Liu CM, Chen JM, Lin SH (2008) Development of a statistical downscaling model for projecting monthly rainfall over East Asia from a general circulation model output. *J Geophys Res Atmos* 113:1–16. doi: 10.1029/2007JD009472

- Prasanna V, Subere J, Das DK, Govindarajanc, Srinivasan Yasunarid T (2007) Development of daily gridded rainfall dataset over the Ganga, Brahmaputra and Meghna river basins. *Meteorol Appl* 14:117–129. doi: 10.1002/met.13
- Prein AF, Langhans W, Fosser G, et al (2015) A review on regional convection-permitting climate modeling: Demonstrations, prospects, and challenges. *Rev Geophys* 53:323–361. doi: 10.1002/2014RG000475
- Rahman MM, Islam MN, Ahmed AU, Georgi F (2012a) Rainfall and temperature scenarios for Bangladesh for the middle of 21st century using RegCM. *J Earth Syst Sci* 121:287–295. doi: 10.1007/s12040-012-0159-9
- Rahman MM, Islam MN, Ahmed AU, Georgi F (2012b) Rainfall and temperature scenarios for Bangladesh for the middle of 21st century using RegCM. *J Earth Syst Sci* 121:287–295. doi: 10.1007/s12040-012-0159-9
- Rahman MM, Singh Arya D, Goel NK, Mitra AK (2012c) Rainfall statistics evaluation of ECMWF model and TRMM data over Bangladesh for flood related studies. *Meteorol Appl* 19:501–512. doi: 10.1002/met.293
- Rajib MA, Rahman M, Mcbean EA (2011) Global Warming in Bangladesh Perspective : Temperature Projections upto 2100. In: *Proceedings of the Global Conference on Global Warming 2011* 11-14. Lisbon, Portugal Global, pp 43–48
- Rajib MA, Rahman MM (2012) A comprehensive modeling study on regional climate model (RCM) application-Regional warming projections in monthly resolutions under IPCC A1B scenario. *Atmosphere (Basel)* 3:557–572. doi:

10.3390/atmos3040557

Raneesh K, Thampi S (2013) Climatology & Weather Forecasting Bias Correction for RCM Predictions of Precipitation and Temperature in the Chaliyar River Basin. 1:1–6. doi: 10.4172/2332-2594.1000105

Rao KK, Patwardhan SK, Kulkarni A, et al (2014) Projected changes in mean and extreme precipitation indices over India using PRECIS. Glob Planet Change 113:77–90. doi: 10.1016/j.gloplacha.2013.12.006

Revadekar J V., Patwardhan SK, Rupa Kumar K (2011) Characteristic Features of Precipitation Extremes over India in the Warming Scenarios. Adv Meteorol 2011:1–11. doi: 10.1155/2011/138425

Salvi K, Ghosh S, Ganguly AR (2016) Credibility of statistical downscaling under nonstationary climate. Clim Dyn 46:1991–2023. doi: 10.1007/s00382-015-2688-9

Samuelsson P, Jones CG, Willén U, et al (2011) The Rossby Centre Regional Climate model RCA3: Model description and performance. Tellus, Ser A Dyn Meteorol Oceanogr 63:4–23. doi: 10.1111/j.1600-0870.2010.00478.x

Schiermeier Q (2011) Increased flood risk linked to global warming. Nature 470:316.

Shahid S (2010) Rainfall variability and the trends of wet and dry periods in Bangladesh. Int J Climatol 30:2299–2313. doi: 10.1002/joc.2053

Shahid S (2011) Trends in extreme rainfall events of Bangladesh. Theor Appl Climatol 104:489–499. doi: 10.1007/s00704-010-0363-y

- Sharmila S, Joseph S, Sahai a. K, et al (2015) Future projection of Indian summer monsoon variability under climate change scenario: An assessment from CMIP5 climate models. *Glob Planet Change* 124:62–78. doi: 10.1016/j.gloplacha.2014.11.004
- Shashikanth K, Salvi K, Ghosh S, Rajendran K (2014) Do CMIP5 simulations of Indian summer monsoon rainfall differ from those of CMIP3? *Atmos Sci Lett* 15:79–85. doi: 10.1002/asl2.466
- Simpson J, Adler RF, North GR (1988) A proposed tropical rainfall measuring mission (TRMM) satellite. *Bull Am Meteorol Soc* 69:278–295.
- Singh D (2015) South Asian monsoon: Tug of war on rainfall changes. *Nat Clim Chang* 6:20–22. doi: 10.1038/nclimate2901
- Song C, Ke L, Richards KS, Cui Y (2015) Homogenization of surface temperature data in High Mountain Asia through comparison of reanalysis data and station observations. *Int J Climatol* 1101:n/a-n/a. doi: 10.1002/joc.4403
- Sundqvist H (1978) A parameterization scheme for non-convective condensation including prediction of cloud water content. *Q J R Meteorol Soc* 104:677–690. doi: 10.1002/qj.49710444110
- Taylor KE (2001) Summarizing multiple aspects of model performance in a single diagram. *J Geophys Res* 106:7183. doi: 10.1029/2000JD900719
- Taylor KE, Stouffer RJ, Meehl GA (2012) An Overview of CMIP5 and the Experiment Design. *Bull Am Meteorol Soc* 93:485–498. doi: 10.1175/BAMS-D-11-00094.1

- Teichmann C, Eggert B, Elizalde A, et al (2013) How does a regional climate model modify the projected climate change signal of the driving GCM: A study over different CORDEX regions using REMO. *Atmosphere (Basel)* 4:214–236. doi: 10.3390/atmos4020214
- Thiemeßl JM, Gobiet A, Leuprecht A (2011) Empirical-statistical downscaling and error correction of daily precipitation from regional climate models. *Int J Climatol* 31:1530–1544. doi: 10.1002/joc.2168
- van Vuuren DP, Edmonds J, Kainuma M, et al (2011) The representative concentration pathways: An overview. *Clim Change* 109:5–31. doi: 10.1007/s10584-011-0148-z
- Wilcke RAI (2014) Evaluation of Multi-Variable Quantile Mapping on Regional Climate Models. University of Graz
- Wilcke RAI, Mendlik T, Gobiet A (2013) Multi-variable error correction of regional climate models. *Clim Change* 120:871–887. doi: 10.1007/s10584-013-0845-x
- Wood a. W, Leung LR, Sridhar V, Lettenmaier DP (2004) Hydrologic implications of dynamical and statistical approaches to downscaling climate model outputs. *Clim Change* 62:189–216. doi: 10.1023/B:CLIM.0000013685.99609.9e
- Wood R, Field PR (2011) The Distribution of Cloud Horizontal Sizes. *J Clim* 24:4800–4816. doi: 10.1175/2011JCLI4056.1
- Yatagai A, Kamiguchi K, Arakawa O, et al (2012) Aphrodite constructing a long-term daily gridded precipitation dataset for Asia based on a dense network of rain gauges.

Bull Am Meteorol Soc 93:1401–1415. doi: 10.1175/BAMS-D-11-00122.1

Yatagai A, Xie P, Alpert P (2007) Development of a daily gridded precipitation data set for the Middle East. *Adv Geosci* 12:165–170. doi: 10.5194/adgeo-12-165-2008

Zhang H, Fraedrich K, Blender R, Zhu X (2013) Precipitation Extremes in CMIP5 Simulations on Different Time Scales. *J Hydrometeorol* 14:923–928. doi: 10.1175/JHM-D-12-0181.1

Figure Captions:

Fig. 1 Monthly climatology of rainfall (a), maximum temperature(b) and minimum temperature (c) that found from the five CMIP5 regional models and the observed gridded data over Bangladesh. (d-e) Taylor diagram (after Taylor, 2001) for annual mean rainfall and mean temperature over the period 1981–2000 over Bangladesh in reference to observed BMD data, showing raw RCM results and bias-corrected RCM results generated from CMIP5 models.

Fig. 2 The temporal mean (1981–2005) of Rx50 (i.e. Number of days greater than 50mm rainfall per year) over Bangladesh derived from observed (a) BMD Grid, from the raw RCM of (b) RCA4-EC-EARTH, (c) REMO-MPI, (d) CSIRO-CCSM4, (e) CSIRO-CCSM4, (f) CSIRO-CCSM4 and from the respective error-corrected RCMs (g-k).

Fig. 3 The temporal mean (1981–2005) of Rx1 (i.e. Number of days greater than 1mm rainfall per year) over Bangladesh derived from observed (a) BMD Grid, from the raw RCM of (b) RCA4-EC-EARTH, (c) REMO-MPI, (d) CSIRO-CCSM4, (e) CSIRO-CCSM4, (f) CSIRO-CCSM4 and from the respective error-corrected RCMs (g-k).

Fig. 4 Rx10 and Rx50 values from multi-models and observed data over Bangladesh from 1981 to 2005 are presented with shaded time series plot. Blue and yellow region represent the range of model before correction and after correction respectively.

Fig. 5 Projected annual precipitation, maximum temperature and minimum temperature over Bangladesh in RCP 4.5 (top) and RCP 8.5 (bottom) scenarios.

Fig. 6 Changes of annual precipitation from baseline (1981-2005) to 2050s (2041-2070) and 2080s (2071-2100) observed in RCA4-EC-EARTH, REMO-MPI, CSIRO-CCSM4, CSIRO-CCNRM and CSIRO-CNRM-CM5 RCMs in RCP 4.5 scenario. Similar results, but in RCP 8.5 are also shown in (k-t).

Fig. 7 Changes of average temperature from baseline to 2050s (2041-2070) and 2080s (2071-2100) derived from RCA4-EC-EARTH, REMO-MPI, CSIRO-CCSM4, CSIRO-CCNRM and CSIRO-CNRM-CM5 RCMs in RCP 4.5 scenario. Similar result but in RCP 8.5 are also shown in (k-t).

Fig. 8 Projected mean changes of heavy precipitation (Rx10) and extreme precipitation (Rx90) from five RCMs for 2050s and 2080s relative to 1981–2005. Changes are showed in decadal scale and contour line represents the variability of the five models from its mean values. Bias corrected (top) and bias uncorrected (bottom) regional climate projections have been compared.

Fig. 9 Projected mean changes of highest summer temperature (TXx) and lowest winter temperature (TNn) from five RCMs for 2050s and 2080s relative to 1981–2005. Changes are showed in annual scale and contour line represents the variability of the five models from its mean values. Bias corrected (top) and bias uncorrected (bottom) regional climate

projections have been compared.

Fig. 10 Annual probability distribution functions for Rx1, Rx50, TXx and TNn indices for five regional climate model in three time periods of 21st Century. The solid line represents the observed period and dashed line represent mean of the five models in future time slices.

Fig 1. Monthly climatology of rainfall (a), maximum temperature(b) and minimum temperature (c) that found from the five CMIP5 regional models and the observed gridded data over Bangladesh. (d-e) Taylor diagram (after Taylor, 2001) for annual mean rainfall and mean temperature over the period 1981–2000 over Bangladesh in reference to observed BMD data, showing raw RCM results and bias-corrected RCM results generated from CMIP5 models.

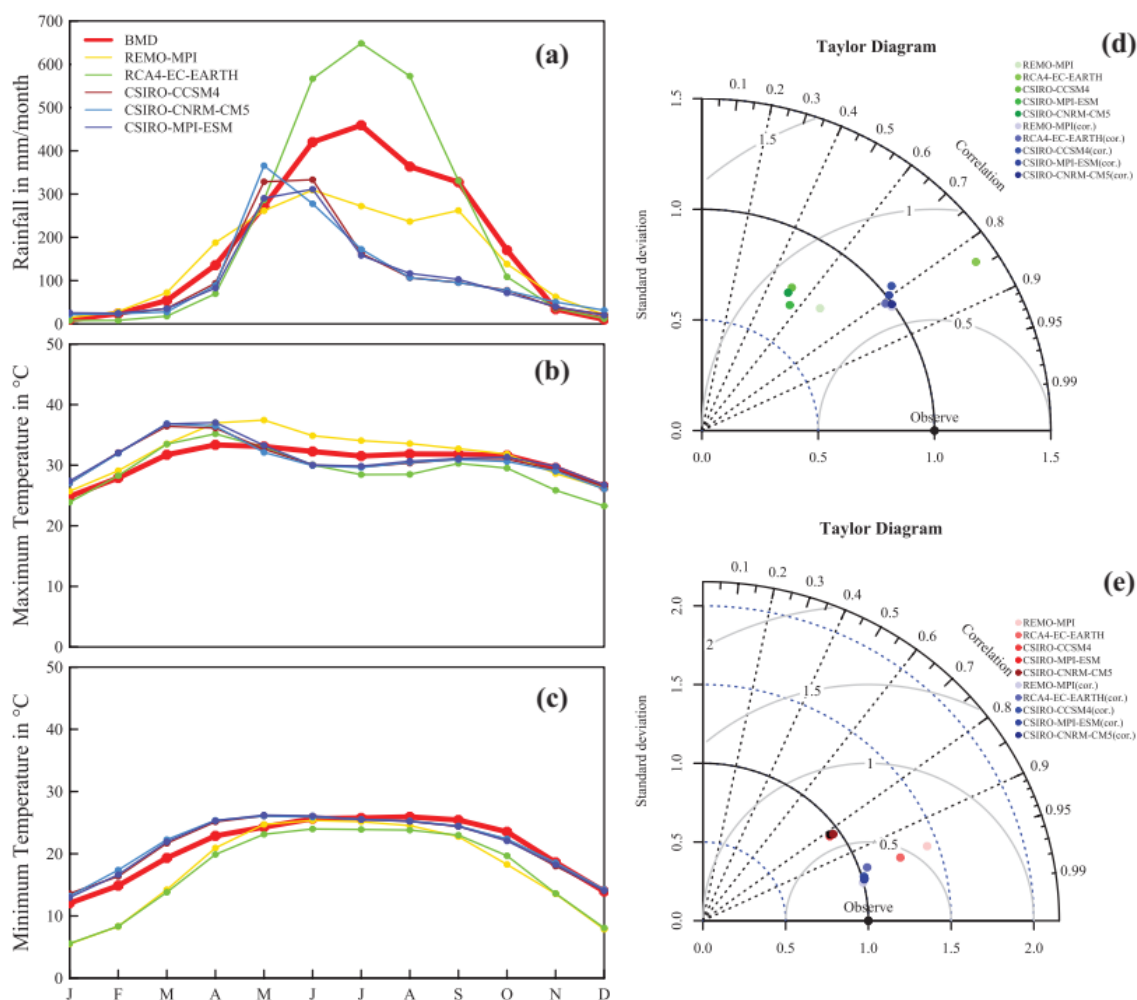


Fig 2. The temporal mean (1981–2005) of Rx50 (i.e. Number of days greater than 50mm rainfall per year) over Bangladesh derived from observed (a) BMD Grid, from the raw RCM of (b) RCA4-EC-EARTH, (c) REMO-MPI, (d) CSIRO-CCSM4, (e) CSIRO-CCSM4, (f) CSIRO-CCSM4 and from the respective error-corrected RCMs (g-k).

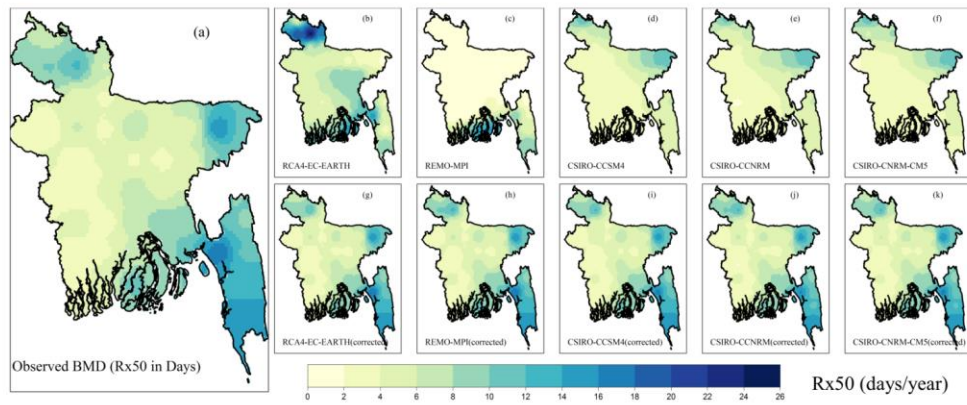


Fig. 3 The temporal mean (1981–2005) of Rx1 (i.e. Number of days greater than 1mm rainfall per year) over Bangladesh derived from observed (a) BMD Grid, from the raw RCM of (b) RCA4-EC-EARTH, (c) REMO-MPI, (d) CSIRO-CCSM4, (e) CSIRO-CCSM4, (f) CSIRO-CCSM4 and from the respective error-corrected RCMs (g-k).

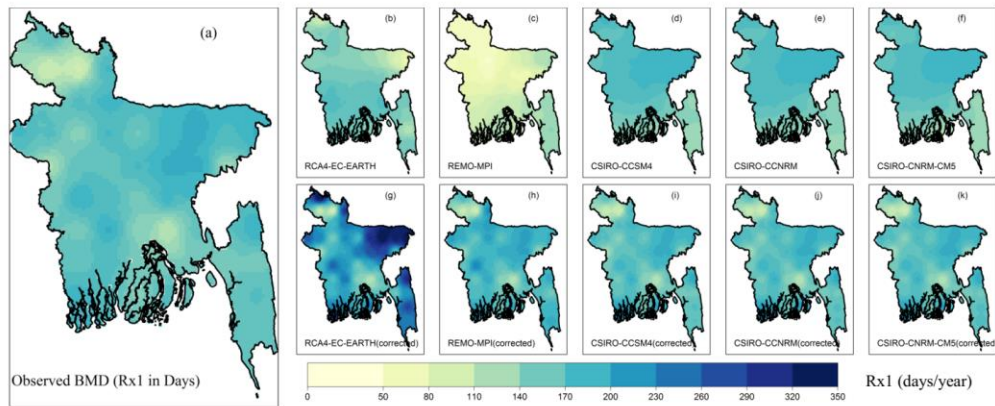


Fig. 4 Rx10 and Rx50 values from multi-models and observed data over Bangladesh from 1981 to 2005 are presented with shaded time series plot. Blue and yellow region represent the range of model before correction and after correction respectively.

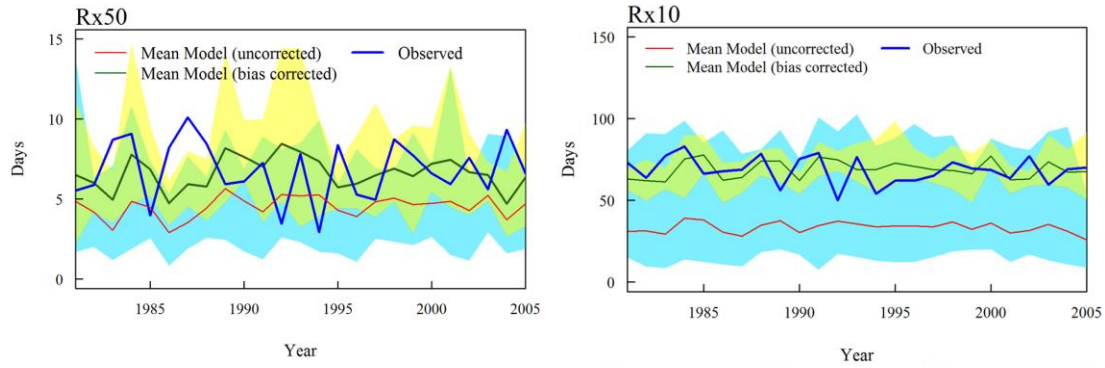


Fig. 5 Projected annual precipitation, maximum temperature and minimum temperature over Bangladesh in RCP 4.5 (top) and RCP 8.5 (bottom) scenarios.

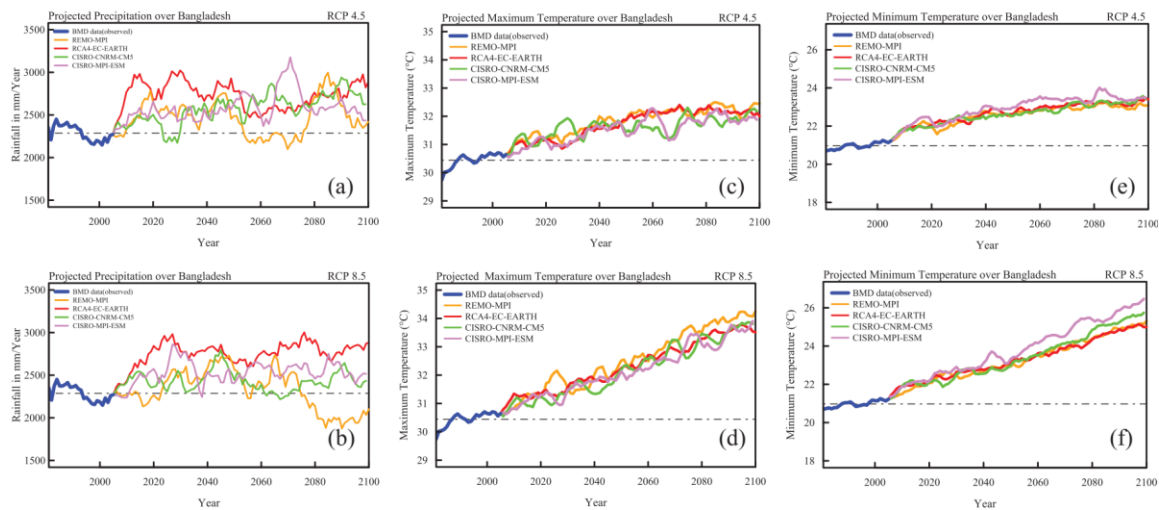


Fig. 6 Changes of annual precipitation from baseline (1981-2005) to 2050s (2041-2070) and 2080s (2071-2100) observed in RCA4-EC-EARTH, REMO-MPI, CSIRO-CCSM4, CSIRO-CCNRM and CSIRO-CNRM-CM5 RCMs in RCP 4.5 scenario. Similar results, but in RCP 8.5 are also shown in (k-t).

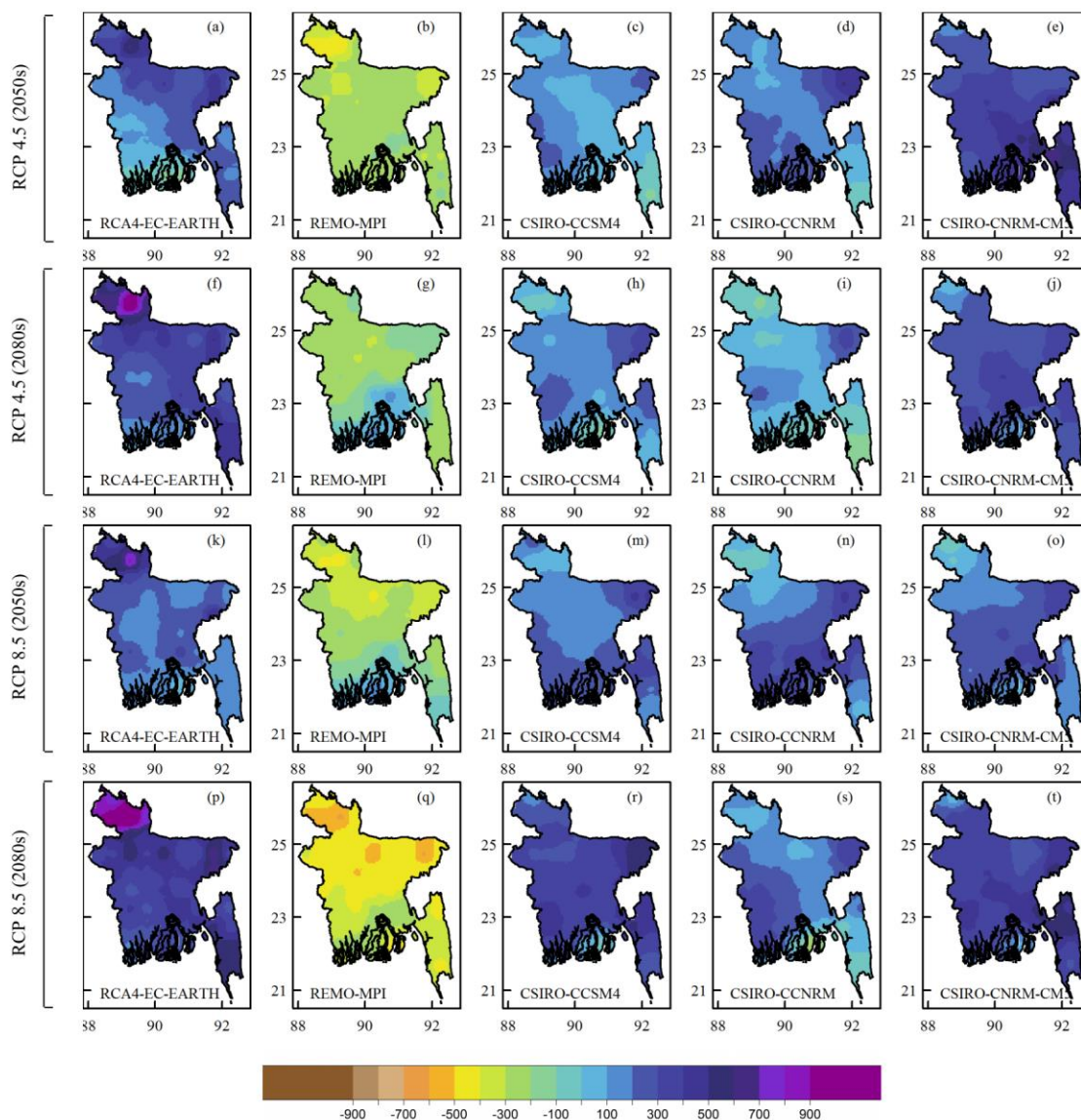


Fig. 7 Changes of average temperature from baseline to 2050s (2041-2070) and 2080s (2071-2100) derived from RCA4-EC-EARTH, REMO-MPI, CSIRO-CCSM4, CSIRO-CCNRM and CSIRO-CNRM-CM5 RCMs in RCP 4.5 scenario. Similar result but in RCP 8.5 are also shown in (k-t).

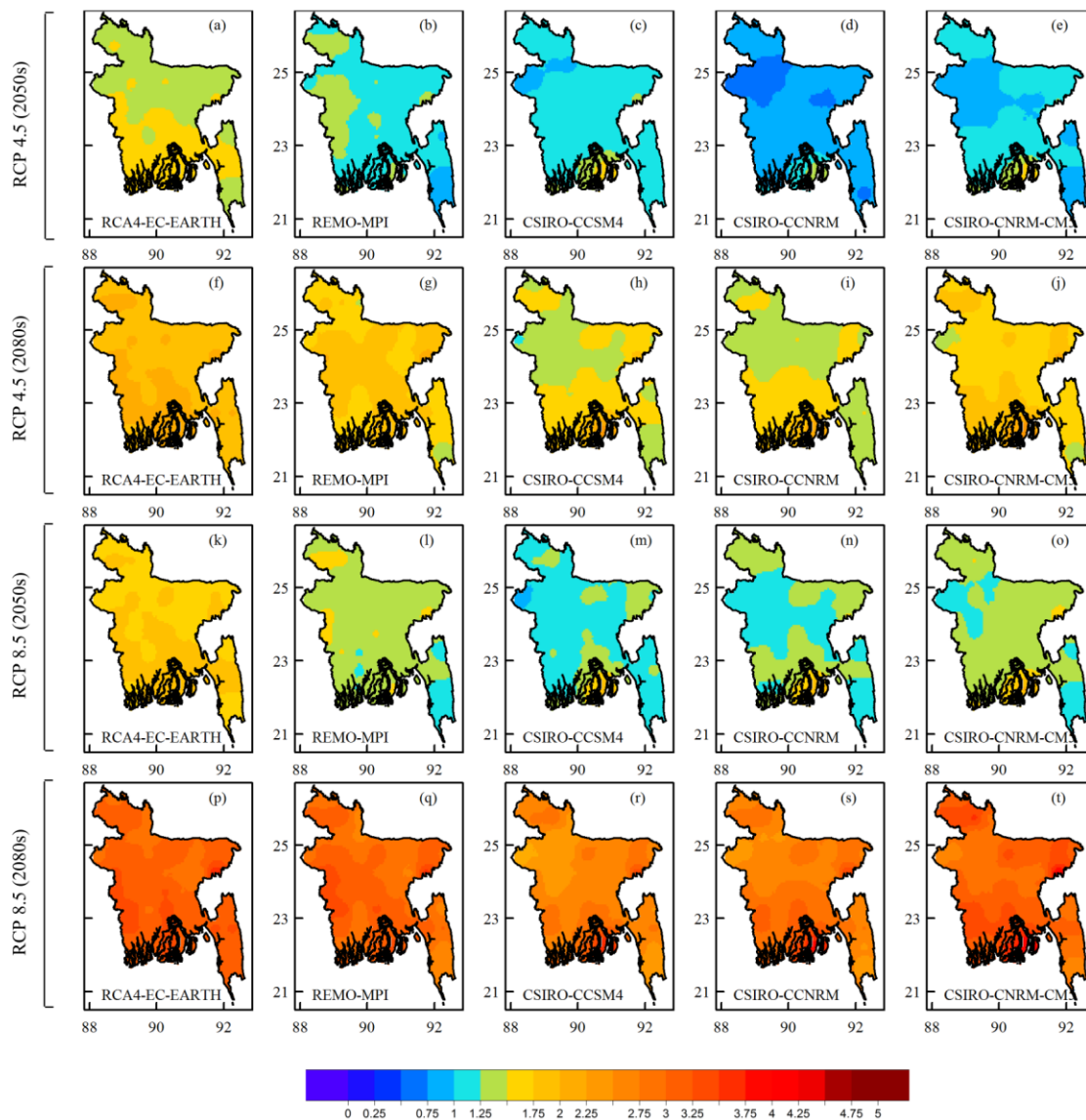


Fig. 8 Projected mean changes of heavy precipitation (Rx10) and extreme precipitation (Rx90) from five RCMs for 2050s and 2080s relative to 1981–2005. Changes are showed in decadal scale and contour line represents the variability of the five models from its mean values. Bias corrected (top) and bias uncorrected (bottom) regional climate projections have been compared.

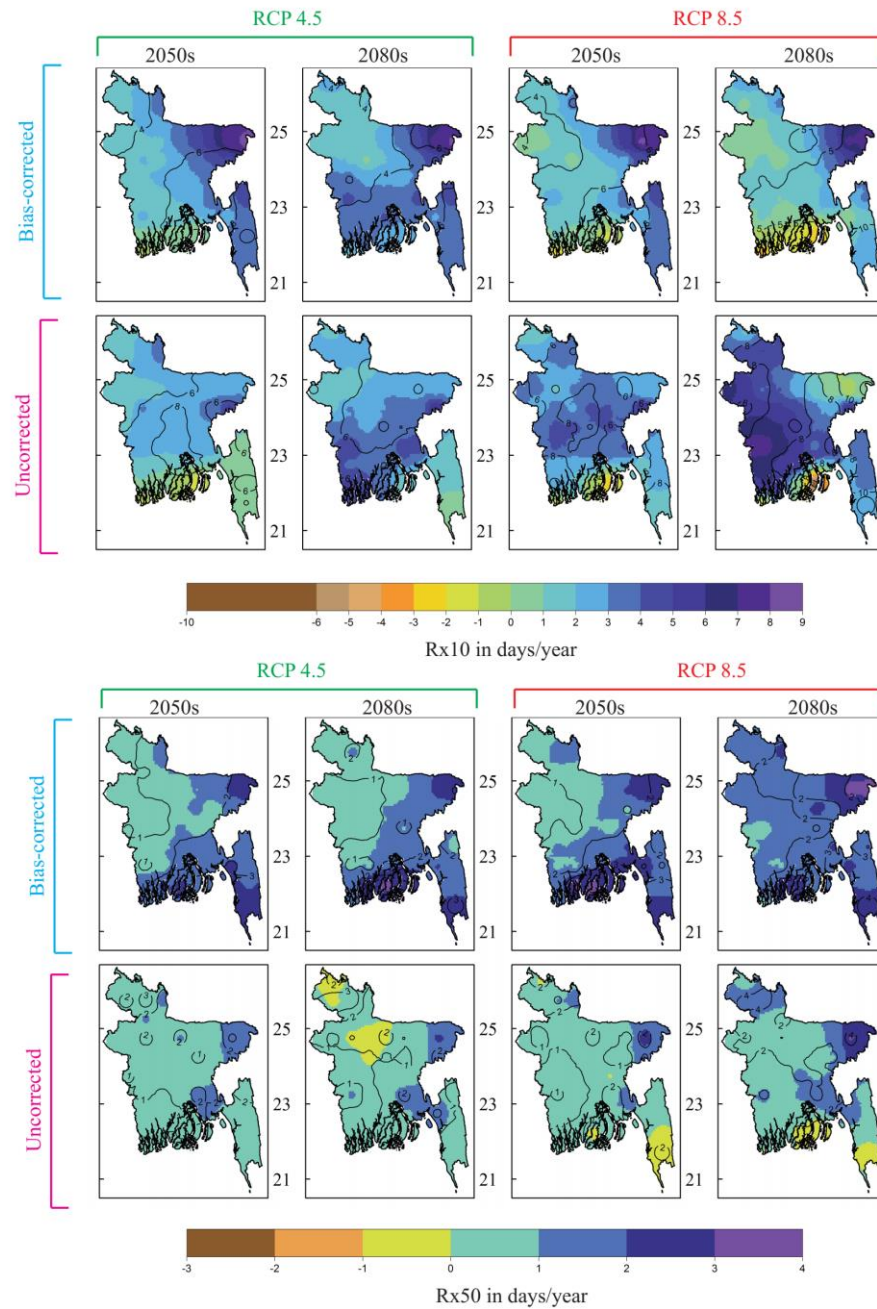


Fig. 9 Projected mean changes of highest summer temperature (TXx) and lowest winter temperature (TNn) from five RCMs for 2050s and 2080s relative to 1981–2005. Changes are showed in annual scale and contour line represents the variability of the five models from its mean values. Bias corrected (top) and bias uncorrected (bottom) regional climate projections have been compared.

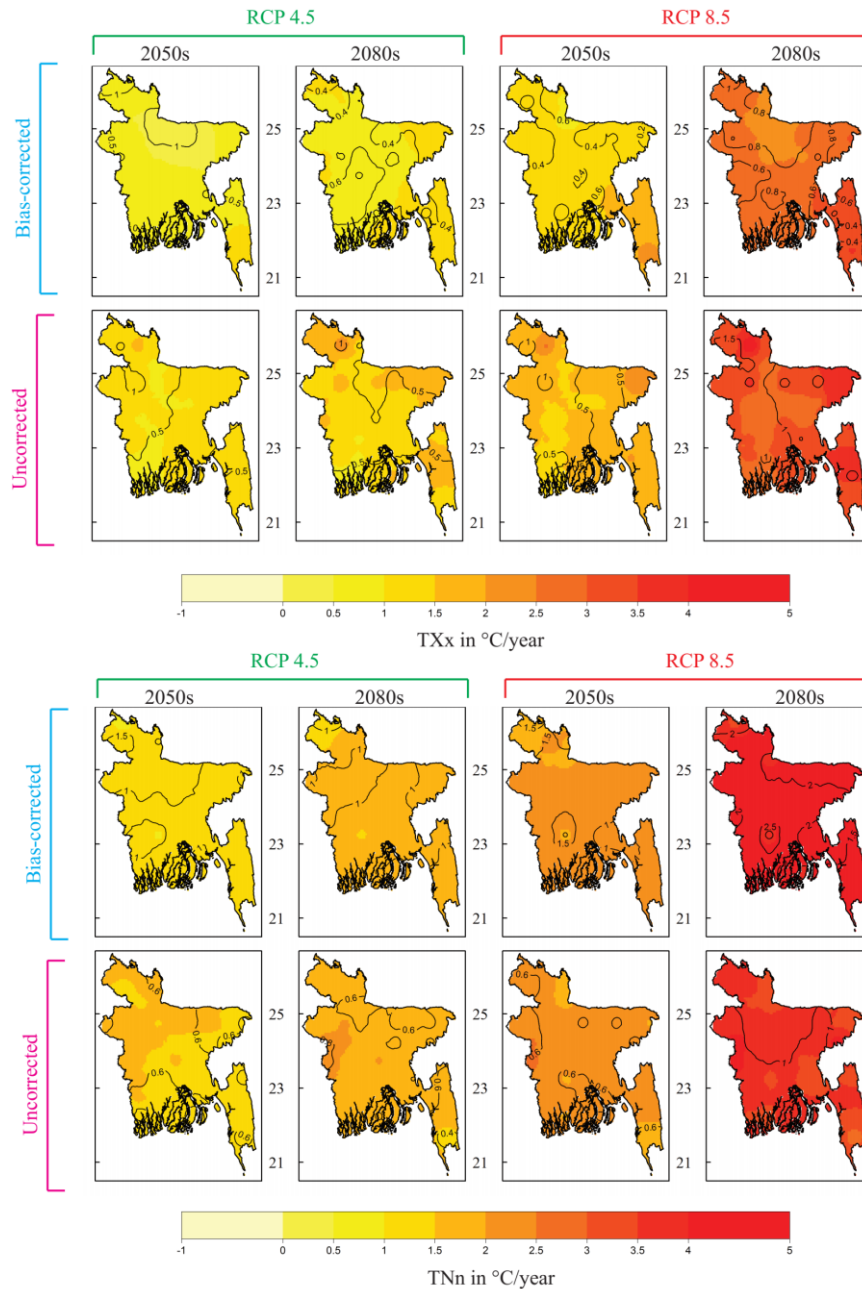


Fig. 10 Annual probability distribution functions for Rx1, Rx50, TXx and TNn indices for five regional climate model in three time periods of 21st Century. The solid line represents the observed period and dashed line represent mean of the five models in future time slices.

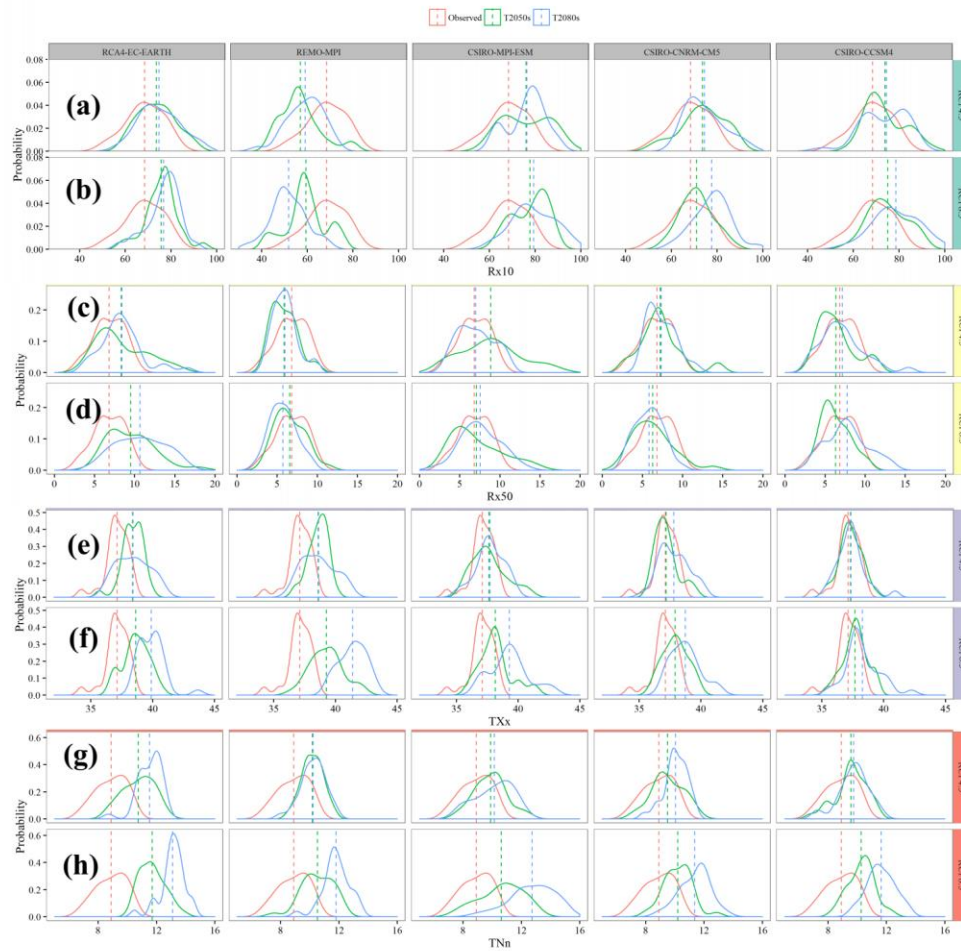


Table 1: Yearly, monthly and daily statistics of BMD stations, Aphrodite, Era-interim and newly developed BMD gridded datasets over Bangladesh from 1981 to 2000. Bracket values represent the difference between BMD station data and respective gridded data value.

Rainfall Statistics	(1) BMD Stations		(2) Aphrodite		(3) Era-INTERIM		(4) BMD Grid		
	1990s	2000s	1990s	2000s	1990s	2000s	1990s	2000s	
<i>Annual rainfall(mm)</i>	2588	2441	2258 (329)	2220 (368)	1948 (640)	2041 (400)	2477 (111)	2370 (71)	
<i>Monthly rainfall (mm)</i>	<i>Jan</i>	6	12	7 (1)	12 (6)	5 (1)	13 (2)	9 (3)	13 (1)
	<i>Feb</i>	22	31	18 (4)	26 (4)	20 (1)	24 (8)	22 (1)	30 (1)
	<i>Mar</i>	59	62	51 (8)	58 (1)	42 (11)	54 (5)	59 (6)	60 (2)
	<i>Apr</i>	165	110	147 (18)	100 (64)	107 (54)	103 (5)	166 (5)	113 (6)
	<i>May</i>	290	298	269 (20)	274 (16)	224 (52)	245 (47)	307 (31)	296 (5)
	<i>Jun</i>	455	436	399 (55)	419 (35)	361 (121)	388 (68)	435 (47)	422 (33)
	<i>Jul</i>	561	494	502 (60)	457 (105)	407 (178)	397 (123)	543 (43)	473 (48)
	<i>Aug</i>	417	433	370 (47)	388 (29)	336 (95)	350 (99)	413 (18)	412 (37)
	<i>Sep</i>	329	328	312 (17)	304 (25)	292 (47)	292 (45)	338 (2)	344 (7)
	<i>Oct</i>	166	175	136 (30)	145 (21)	111 (58)	141 (41)	159 (10)	163 (19)
	<i>Nov</i>	48	36	36 (12)	28 (21)	28 (23)	27 (11)	40 (11)	33 (5)
	<i>Dec</i>	12	11	11 (1)	9 (3)	12 (0)	8 (3)	13 (1)	10 (0)
<i>Wet days</i>	118	120	154 (36)	159 (40)	181 (63)	191 (71)	147 (29)	143 (23)	
<i>Dry days</i>	247	245	211 (36)	207 (40)	184 (63)	175 (71)	218 (29)	222 (23)	
<i>90th p*/year</i>	22	22	19 (3)	19 (3)	15 (7)	16 (6)	21 (1)	20 (2)	
<i>50mm days/year</i>	14	13	8 (6)	7 (7)	1 (13)	1 (12)	10 (4)	9 (3)	
<i>10mm days/year</i>	64	62	65 (1)	65 (3)	85 (21)	89 (27)	70 (5)	66 (5)	

* Number of days when rainfall was greater or equal to 90th Percentile of decade in a year.

Table 2. Description of selected regional climate models over Bangladesh

Simulation names	Regional Climate Model	Driving GCM	Institute	Scenarios	Resolution
RCA4-EC-EARTH	Rosby Centre regional atmospheric model version 4 (RCA4) (Samuelsson et al. 2011)	European Consortium ESM (EC-EARTH)	Rosby Centre, Swedish Meteorological and Hydrological Institute (RCA4), Sweden	Historical RCP 4.5 RCP 8.5	25km
CSIRO-CNRM-CM5	Commonwealth Scientific and Industrial Research Organisation (CSIRO), Conformal-Cubic Atmospheric Model (CCAM) (Jacob and Podzun 1997)	Centre National de Recherches Météorologiques Climate Model, version 5 (CNRM-CM5)	CSIRO Marine and Atmospheric Research, Melbourne, Australia	Historical RCP 4.5 RCP 8.5	50km
CSIRO-CCSM4	Commonwealth Scientific and Industrial Research Organisation (CSIRO), Conformal-Cubic Atmospheric Model (CCAM) (Jacob and Podzun 1997)	The Community Climate System Model, version 4 (CCSM4)	CSIRO Marine and Atmospheric Research, Melbourne, Australia	Historical RCP 4.5 RCP 8.5	50km
CSIRO-MPI-ESM-LR	Commonwealth Scientific and Industrial Research Organisation (CSIRO), Conformal-Cubic Atmospheric Model (CCAM) (Jacob and Podzun 1997)	Earth system model of Max Planck Institute for Meteorology (MPI-ESM-LR)	CSIRO Marine and Atmospheric Research, Melbourne, Australia	Historical RCP 4.5 RCP 8.5	50km
REMO-MPI	The Regional Model of Max Planck Institute for Meteorology (REMO) (Teichmann et al. 2013)	Earth system model of Max Planck Institute for Meteorology (MPI-ESM-LR)	Climate Service Center, Hamburg, Germany	Historical RCP 4.5 RCP 8.5	50km

CHAPTER 2

Manuscript II

Published in *Geo Health*, 2018

Assessment of Critical Modern Recharge to Arid Region Aquifer Systems Using an Integrated Geophysical, Geochemical, and Remote Sensing Approach

M. Alfi Hasan¹, Colleen Moww², Antarpreet Jutla³, Ali S. Akanda¹

- 1) Department of Civil and Environmental Engineering, University of Rhode Island, Kingston, Rhode Island 02881
- 2) Graduate School of Oceanography, University of Rhode Island, Kingston, Rhode Island 02881
- 3) Department of Civil and Environmental Engineering, West Virginia University, PO Box 6103, Morgantown, WV 26506

Key Points:

- Rotavirus shows strong mortality and morbidity, as well as strong spatial and temporal variability in South Asia.
- Strong winter and weak monsoon transmission cycles dominate South Asia, modulated by regional climatic extremes.
- Satellite-derived hydroclimatic information has potential to help forecasting of rotavirus risk over Bengal Delta.

Abstract

Rotavirus is the most common cause of diarrheal disease among children under five. Especially in South Asia, rotavirus remains the leading cause of mortality in children due to diarrhea. As climatic extremes and safe water availability significantly influence diarrheal disease impacts in human populations, hydroclimatic information can be a potential tool for disease preparedness. In this study, we conducted a multivariate temporal and spatial assessment of thirty-four (34) climate indices calculated from ground and satellite earth observations to examine the role of temperature and rainfall extremes on the seasonality of rotavirus transmission in Bangladesh. We extracted rainfall data from the Global Precipitation Measurement (GPM) and temperature data from the Moderate Resolution Imaging Spectroradiometer (MODIS) sensors to validate the analyses and explore the potential of a satellite-based seasonal forecasting model. Our analyses found that the number of rainy days and nighttime temperature range from 16°C to 21°C are particularly influential on the winter transmission cycle of rotavirus. The lower number of wet days with suitable cold temperatures for an extended time accelerates the onset and intensity of the outbreaks. Temporal analysis over Dhaka also suggested that water logging during monsoon precipitation influences rotavirus outbreaks during a summer transmission cycle. The proposed model shows lag components, which allowed us to forecast the disease outbreaks one to two-months in advance. The satellite data-driven forecasts also effectively captured the increased vulnerability of dry-cold regions of the country, compared to the wet-warm regions.

1. Introduction

Living in the age of satellites and nanotechnology, a significant fraction of the global human population is still threatened by diarrheal diseases. A major contributor to global mortality and morbidity, diarrheal diseases account for an estimated 3.1% of the total burden of diseases in terms of Disability-Adjusted Life Year (DALY) and 1.3 million deaths annually, including a majority of children under five years (Troeger et al., 2017; WHO, 2014). Two of the most infectious and fatal diarrheal diseases, *Rotavirus* and *Cholera*, comprise more than one-third of the diarrheal burden in the developing countries of South Asia (Siddique et al., 2011). Yet, there is much room for improvement in understanding the underlying processes and the assessment of diarrheal disease risk over vulnerable regions (Akanda et al., 2014).

The transmissions of these diseases both at endemic and epidemic scales are primarily due to insufficient safe water access, inadequate sanitation and drainage infrastructures, and poor access to health care compounded by natural disasters or social upheavals. However, the development of water, sanitation and health infrastructures as a solution to intervene in the disease pathway requires a long timeframe and continuous financial commitment (Hutton and Bartram, 2008). Many developing countries failed to meet the 2015 Millennium Development Goals set by the United Nations in 2000, predominantly in the sanitation sectors. As the global community transitions from the Millennium Development Goals (MDGs) to the Agenda 2030 Sustainable Development Goals (SDGs), the need to monitor and track the impact and progress of the global prevention efforts has become vital (H. Wang et al., 2016).

Recent studies indicate that hydrologic processes and climatic variability strongly influence the outbreak of these diseases (Gurarie and Seto 2009; Remais, Liang, and Spear 2008; Bandyopadhyay, Kanji, and Wang 2012; Jutla et al. 2015; Akanda et al., 2013). Moreover, the risk posed of the diarrheal diseases and uncertainty of the impacts are increasing under ongoing climate change (Maantay & Becker, 2012). Thus, innovative ways of advancing surveillance efforts to assess baseline conditions and strengthening health efforts through identifying disease hotspots in vulnerable regions is a critical need (Akanda, Jutla, and Colwell 2014). Here, we focus on rotavirus diarrhea as it has one of the highest number of diarrhea-related mortalities in children younger than five years of age, globally (WHO, 2011).

Most studies have explored the influence on rotavirus transmission for particular climatic extreme or related natural disasters, but the integration of multiple variables with disease cases has been limited. Martinez et al. (2016) explored the effect of flood and rainfall on rotavirus transmission of Dhaka, where the importance of multiple extremes was pointed out. Moors et al. (2013) integrated several climatic effects to explain the pattern of diarrheal disease outbreaks over India; however, a deterministic quantification of the diseases based on the climatic effects was absent. Jagai et al. (2012) has conducted a meta-analysis of rotavirus over South Asia, but did not consider the climate extremes. Accurate identification of climatic events is also important for disease modeling. For example, waterlogging causes diarrheal outbreaks in many parts of the world after consecutive rainfall for several days. Due to the combined effect of heavy intensive rainfall-runoff and inefficient drainage systems, flood waters flow into low lying areas, causing water logging

(Tawhid 2004). These areas help to connect the fecal-oral route of the disease transmission cycle through continued use of these interconnected and infected water bodies. As a result, diarrheal outbreaks spread from one locality to another (Bhavnani et al., 2014). Thus, evaluating the disease outbreak with extreme rainfall intensity but without considering the cumulative impact of consecutive rainy days left gaps in the understanding. Moreover, specific temperature conditions during daytime or nighttime could also influence pathogen survivability (Lambrechts et al., 2011). Therefore, the relationships of specific climate phenomena with rotavirus need to be explored in more detail.

The development of satellite technologies and proliferation of earth observation datasets in recent years has enabled collection and analyses of hydro-climatic information from all over the globe in unprecedented time (Emamifar, Rahimikhoob, and Noroozi 2013; Hou et al. 2014; Brown et al., 2011). The satellites not only provide advanced knowledge of environmental variables, but also high-resolution spatial and temporal information. Most of these data products are available freely within six hours to one-week intervals after their acquisition. For example, the Global Precipitation Measuring (GPM) mission can provide rainfall information every 30 minutes with a 0.1° spatial resolution, globally (Huffman et al., 2015). The Tropical Rainfall Measuring Mission (TRMM) data is another widely evaluated satellite data and has shown strong performance in detecting rainfall in various applications (Kummerow et al., 1998). Similarly, the Moderate Resolution Imaging Spectroradiometer (MODIS) land surface data product can provide daily temperature data at 1-km spatial resolution (Pagano & Durham, 1993). These datasets, not only improve

data acquisition intervals compared to station data, but also provide more spatial information in a near-real-time basis.

With establishment of the links between diarrheal diseases and new generation earth data, including satellite observations, there is a great potential to develop models for disease prediction at higher spatial and temporal resolutions. Such systems are especially crucial in developing countries, where the population faces a massive burden of rotavirus related mortality and morbidity each year. Bangladesh, a South Asian country with an emerging economy, still suffers a heavy toll every year due to rotavirus. In this study, we have explored the effect of climatic extremes on the rotavirus infection cycle in Bangladesh both spatially and temporally. We have evaluated rotavirus patterns over several cities inside the country and across South Asia to understand the larger context in relation to regional hydroclimatic processes. We also implemented a deterministic multivariate modeling for risk assessment and integrating near real-time satellite products (with GPM for rainfall and MODIS for temperature).

2. Methodology

2.1 Study Area:

A robust epidemiologic assessment of rotavirus diarrheal outbreak with climate requires a sufficiently long time series and good spatial coverage of disease data. Unfortunately, only few places in South Asia have such information. Located in the fast growing megacity of Dhaka, the International Centre for Diarrheal Disease Research, Bangladesh (ICDDR,B) has published rotavirus surveillance data since 2003, thus providing an opportunity to

explore the relationship between the disease and regional climate. As ICDDR,B conducts surveillance over the metropolitan city of Dhaka, we have selected the city as our primary study area. Dhaka is the capital city of Bangladesh with a population of nearly 14 million, and immensely vulnerable to rotavirus diarrhea. Situated in the tropical zone, the city has a warm climate dominated by monsoon dynamics. The average temperature of city is usually high (~28°C-30°C) during April through October and relatively low (~20°C-22°C) from November through February. We have also incorporated data from five other cities of Bangladesh namely; Rajshahi, Kishoreganj, Sylhet, Barisal and Chittagong for this study. In addition, we have included data from four more cities of South Asia: Delhi, Kathmandu, Thimpu and Karachi for a wider spatial assessment. The cities are all located in the tropical monsoon region and rotavirus is endemic in all of those (Mullick et al., 2014; Sherchand et al., 2009; Shetty et al., 2016; Wangchuk et al., 2015)

2.2 Disease Data:

The cases of rotavirus incidences over Dhaka were obtained from the hospital-based surveillance system of ICDDR,B over a period from January 2003 to May 2015. The ICDDR,B Centre for Health and Population Research runs an urban hospital situated in Kamalapur, Dhaka, where more than 100,000 patients are treated for diarrhea each year. At the hospital, cholera as well as rotavirus surveillance are conducted regularly; stool samples are collected to determine the presence of enteric pathogens in every 50th (2%) patient attending the hospital for treatment of diarrhea. From the hospital surveillance reports, information on monthly rotavirus isolates were summarized and a time series was formulated.

The rotavirus data from other cities within Bangladesh were collected from the national surveillance campaign of the Institute of Epidemiology, Disease Control and Research (IEDCR). The cities within Bangladesh resemble similar demographic and climatic patterns. Bangladesh, this is the only available spatial data set with the same temporal length, to the best of our knowledge. Therefore, we have selected the surveillance data (January 2013 to December 2015) of these cities in the analysis. The rotavirus information for Delhi, Kathmandu and Thimpu were gathered from secondary literature, where the datasets range from 2005 to 2013 (Mullick et al., 2014; Sherchand et al., 2009; Shetty et al., 2016; Wangchuk et al., 2015). However, each city has only about two years of reliable data and distributed over different time periods. Thus, the disease outbreak information of these cities was avoided in the main analysis and was only utilized to validate the larger spatio-temporal rotavirus pattern in South Asia.

2.3 Weather Data:

We obtained daily maximum (TMax) and minimum temperatures (TMin), and precipitation (PR) data for Dhaka from the Bangladesh Meteorological Department (BMD) for the period 2000 to 2014. We collected climatologic records for other cities from The Global Historical Climatology Network - Daily (GHCN-Daily), version 3 from January, 2013 to December, 2016 (Menne et al., 2012). Homogeneity and quality control tests were conducted to ensure the removal of outliers. The tests were carried out using the RHtestsV4 software package which was developed by the joint CCI/CLIVAR/JCOMM Expert Team (ET) on Climate Change Detection and Indices (ETCCDI) (X. L. Wang & Feng, 2013).

For detecting spatial variability, we utilized two types of satellites data products in this study. The Global Precipitation Measurement (GPM) data were used as the source of the satellite precipitation, collected from March 2015 to December 2015. The GPM mission is an international network of satellites that provides the next-generation global observations of rain and snow (Hou et al., 2014). We also utilized an additional satellite-derived rainfall dataset from the Tropical Rainfall Measuring Mission (TRMM) for validation purposes. Among the various products that are available, we used the TRMM3b42v7 version with a spatial resolution of 0.25 degree x 0.25 degree and a temporal resolution of 3-hour. A global Land Surface Temperature (LST) data product was acquired from the Moderate Resolution Imaging Spectroradiometer (MODIS)-Aqua satellite (MYD11A1.005 version) for both day and night temperatures at a 1-km spatial resolution.

2.4 Method

Our study approach can be separated into three sections: temporal assessment, spatial analysis, and multi-variate modeling and validation with satellite data.

A robust analysis of the hydro-climatic influence on the transmission cycle of a disease requires specific climate realizations. For example, the mean or maximum state of a monthly temperature may not directly influence a disease outbreak, but a specific temperature range or consecutive rainfall events can trigger an epidemic. Therefore, for a comprehensive examination of environmental drivers on rotavirus diarrhea, we selected 36 climate indices based on various properties of weather events (Table 1). We either applied or adopted the climate indices from the Expert Team on Climate Change Detection and Indices (ETCCDI)(WMO, 2007). These indices were used in various climate studies to

analyze the extremity of the climatic phenomenon (Alexander, 2015; Hasan, Islam, and Akanda 2017; Keggenhoff et al., 2015). The selections of the indices in those studies were conducted based on particular objectives of individual studies. In this case, we selected the indices that are most relevant to rotavirus transmission dynamics.

In Table 1, we have defined the indices based on extremity, intensity, duration and magnitude of climate variables to capture the whole spectrum of short scale weather phenomenon. The average day or night temperatures and their variations in a month were defined by TMax, Tmin and DTR indices. For TxijGE and TnijGE, we categorized the mean monthly range of TMax and Tmin into 3°C intervals to understand the seasonal effects of various temperature range on rotavirus infections. During an annual cycle, the mean (monthly) TMax and Tmin varies about 9°C over the region (Islam & Hasan, 2012). Therefore, we selected 3°C as threshold interval to classify 9°C temperature range for developing TxijGE and TnijGE indices. As the minimum monthly DTR of Bangladesh is 6°C, we selected half of that (which is 3°C) to capture the temperature effect in both day and night (Islam & Hasan, 2012). Any threshold interval lower than 3°C will result in redundant indices. On the other hand, any threshold interval higher than 3°C will plausibly miss the variation of temperature that can influence rotavirus. The duration of hot or cold days based on a particular threshold were described by the rest of temperature indices (i.e. Tn10, Tx90, etc.).

In case of rainfall, intensity and amount were characterized with SDII and PRECIPTOT. The magnitude of rainfall was described with Rx1and Rx5 indices. The durations of

various kinds of storms were classified using the rest of the precipitation indices. However, among all the indices, many are season specific and have interdependency among them. On this ground, we categorized the indices into two seasons; October to April as the dry *winter* season and July to September as the wet *monsoon* season. The indices that have 60% or more zero values were dropped and eventually we concluded with 22 and 28 indices among 36 indices for winter and monsoon seasons, respectively. For example, we did not select Tn1618GE for the monsoon season. As days with minimum temperature range of 16 to 18 degree will be zero for monsoon months, any correlation value between rotavirus and Tn1618 will result in misleading information. Therefore, some indices were dropped from the pool of 36 indices, when we conducted the season specific analysis. All the indices for temporal and spatial analysis are generated from BMD observed data, where the validation analysis of the indices is generated with daily satellite data.

Evaluating spatial risk of a disease can be modeled with existing stochastic methods like the Bayesian approach (Cheng & Berry, 2013), Monte Carlo simulations (Prosser et al., 2016) or Susceptible-Infectious-Recovered (SIR) (Grassly & Fraser, 2008) models. While the stochastic methods are useful to capture probable spatial patterns of diseases transmission, the complexity of the methods sometimes miss the deterministic influence of a particular driver. As the goal of our paper is to evaluate the influences of climate indices on rotavirus diarrhea, we utilized a deterministic model to formulate the risk of the disease and avoided the population effect. In the process to eliminate the influence of population, we standardized and scaled the disease cases for each of the selected cities and combined the disease cases into a single series of the same time frame (January 2013 to June 2015)

to conduct spatial analysis. The standardization method was adopted from Jagai et al. (2012), where we considered our scaled values as z-scores of rotavirus risk. As a result of removing the effect of population, the analysis thus represents the severity of disease cycle rather than actual cases of diseases. Any value that exceeds one (1) is considered as an outbreak.

From selected climate indices, we conducted a univariate correlation analysis considering three levels of relationships in each season. In the first level, we considered lag relationships of indices with rotavirus cases. In the next level, we considered one and two-months moving average of rotavirus infections, and in the final level, we considered a cross-correlation of moving average and lags. In all three levels, we examined the two seasonal periods both temporally and spatially. As rotavirus outbreaks are more prevalent during winter seasons (supportive analyses related to the phenomenon are provided in the results section), we have examined the winter cycle in more detail. For the winter season, the evaluation of the transmission cycle was conducted into three phases; the rising, the peak and the falling phase. A descriptive definition of the phases is presented in the results section. From the spatial and temporal correlations, the most influential climate relationships were identified and utilized in multivariate regression modeling.

From the correlation assessment, we generated a deterministic model that can project the risk of rotavirus based on climate indices. The model was comprised of the selected three-phase winter cycle that can quantify the rotavirus outbreak from the influence of climatic factors. Finally, the model was utilized to forecast disease outbreaks using precipitation

data from GPM and temperature data from MODIS sensors. As the data of GPM satellite are available from 2015, we performed validation of the model for October 2015 and November 2015, during the dominant winter transmission cycle. As our results showed that the climate indices influence only the winter cycle significantly in all selected cities of Bangladesh, we selected the winter cycle for validation purposes. On the other hand, as the disease data for all cities are available up to December 2015 (during the time of this study), we were only able to validate the rising phase of the winter transmission cycle using satellite data. As rotavirus data from several regions were available for 2 years only, we were unable to utilize data before 2013 or beyond 2015 for spatial validation. However, to demonstrate the spatial capability of our model, we utilized TRMM data in conjunction with MODIS for formulating spatial risk maps of rotavirus for the 2014 winter season.

3. Results

3.1 Seasonal characteristics of Rotavirus in South Asia:

In this section, we discuss the general spatio-temporal pattern of rotavirus outbreaks seen in South Asian cities. Annual rotavirus cycles over South Asia are presented in Figure 2(a). December and January are the peak months of the outbreak for the Bangladeshi cities, with the exception of Sylhet. Thimpu of Bhutan experiences the peak in a post-winter month (March) where Delhi experiences the peak earlier than Bangladeshi cities. Similar to Dhaka, Kathmandu also experiences the annual peak during the month of December. Among the cities of South Asia, a monsoon outbreak is observed (smaller relative to the winter outbreak) in Delhi (population ~19 million) and Dhaka (population ~ 14 million),

where both cities have a much higher population compared to other selected cities (World Population Review, 2017).

The rotavirus endemic cycle exhibits significant seasonal variability over South Asia (Figure 2(a)). The dominant cycle starts in October, reaches its peak in January and is followed by a recession phase in February and March. The autocorrelation analysis over Dhaka for the original monthly time series validates the presence of the dominant winter cycle. In Figure 2(c), the monthly autocorrelation function shows the presence of the strong annual winter peak. The auto-correlation figure also suggests a weaker outbreak during the monsoon season, typically during July, August and September. The z-score of the rotavirus over Dhaka also supports similar findings, where, as in 2004, the monsoon magnitude of rotavirus was higher than that of the winter (Figure 2(b)).

Characteristics of rotavirus incidences over Dhaka were analyzed following a 13-year time series data set (2003-2015) (Figure 2(b)). Rotavirus outbreaks during the winter of 2008, 2011 and 2012 were the most intense in recent history. Typically, rotavirus incidence becomes the highest during January, but some exceptions were observed during March 2009 and July 2004. In most years, the lowest incident rate of rotavirus diarrhea was observed during May. However, in 2012 and 2014, the lowest incidences were observed in August.

In this analysis, we calculated temporal correlation only over Dhaka and not the other cities due to lack of data availability (the disease data of other cities starts from 2012). Among

the precipitation indicators over the city, RR1 was found to be one of the influential indicators on rotavirus. The correlation analysis suggests (Figure 3(a)) that a decrease in RR1 in September affects the winter rotavirus cycle especially for the month of November. The secondary outbreak during the July, August and September is affected by the number of days with rainfall events of 70mm or more (RR70) (Figure 3(b)). However, both the rotavirus cases and RR70 were higher during the 2007 floods over the city.

3.2 Univariate correlation between climate indices and rotavirus

To assess the effect of individual climate variables and indices on rotavirus transmission, we conducted univariate analysis considering moving average and lag of related variables. The correlations for the winter and monsoon seasons are presented in Figure 4.

During the winter season, rotavirus outbreak in Dhaka shows a strong negative lag relation (1-month) with the selected rainfall-related indices (Figure 4(a)). In case of other cities (Figure 4(b)), the same indices show significant but lower correlation values. Unlike Dhaka, the correlations of indices in other cities do not exhibit any substantial lag effect. Thus, we can say that the low duration of rainfall events seems to be an influential driver for the season, where the effects come with a delay (1-month) over Dhaka compared to other places. The temperature indices related to the colder spells strongly impact the winter epidemics in both spatial and temporal analysis. However, the spatial correlations are weaker than the temporal values in both types of indices, probable due to the varying rainfall patterns between the six locations. The temperature indices that display the strongest correlation (0.5 or more) are Tmax, Tmin, Tn1621GE (number of nights with

temperature between 16°C to 21°C) and Tn1921GE (number of nights with temperature between 19°C to 21°C). All these indicators confirm the effect of colder temperatures on the rotavirus cycle similar to Atchison et al. (2010).

During the monsoon season, the temporal investigation of rotavirus indicates significant correlation with all rainfall indices where such relationships are absent in the spatial assessment (Figure 4(c-d)). The outcome is expected, as the secondary monsoon outbreak and its impacts are most profound in Dhaka among the six selected cities of Bangladesh (Figure 4(a)). Tn2225GE significantly correlates with 2-month lag rotavirus outbreak, which is the strongest relationship among the indices. The relationship suggests that a night temperature range of 22°C to 25°C has a potent role in the monsoon cycle of rotavirus over Dhaka.

From Figure 2 and 4, it is evident that the winter cycle of rotavirus is more prominent than the monsoon cycle over the study region and is strongly influenced by climatic factors. Thus, we focused the investigation on the winter epidemic for the rest of the study. For a detailed understanding of the winter cycle, we characterized it into three phases; rising, peak and falling phases. The rotavirus outbreak starts to appear during the months of October and November, thus can be classified as the 'rising' phase. As the cycle, typically reaches its 'peak' during the months of December, January and February, we considered it as the 'peak' phase. From February to April, the cycle enters in its recession phase, therefore, this phase was defined as the 'falling' phase. Based on the three phases, we conducted two levels of correlation analysis as described previously between rotavirus

cases and climate indices. As temperature and precipitation indices have dependency among them, many indices show similar correlation in particular phases. Therefore, to make a concise judgment, we presented only the most significant correlation for each phase of the epidemic cycle in Table 2.

The rising phase of rotavirus cycle has significant influence by the night temperature as Tn1621GE shows spatial and temporal correlation of 0.61 and 0.51 respectively. The lower number of 25 degree days (SU) were found to be influential on the spatial scale, where Tx2932GE also represented a similar message in the temporal scale. Number of rainy days (RR1) is strongly correlated (negatively) with rotavirus cases in both tests, more so for the onset of the epidemics in Dhaka. The rising phase of Dhaka is influenced by 2-month prior RR1, where the same index in other cities exhibits a no-lag relation. This analysis suggests that the dry and cold days in fall are potential drivers for the start of outbreak, where the timing of rainfall deviates the timing of outbreak from place to place. During the peak phase, both the number of hot days (SU) and Tmax shows negative correlation spatially. Therefore, the relationship suggests that the upper temperature threshold of cold days or nights affects the rotavirus magnitude in the peak phase. The values of the rainfall indices (except PRECIPTOT) during the peak are close to zero, thus any significant correlation of these indices will be misleading. Hence, we avoided such values in conferring our results. During the falling phase as well, RR1 plays an influential negative role on the rotavirus cycle. Both temporal and spatial time series exhibits correlation of -0.61 and -0.69, respectively. However, the temporal correlations show no lag compared to the spatial correlations of the six cities during the phase. Tx10 and DTR demonstrated the strongest

association with rotavirus in the temporal and spatial scales, respectively. Similar to the rising phase, the falling phase shows strong connections with dryness and demonstrates variability in the timing of the infections depending on the location.

The synthesis of the analyses revealed that Tn1621GE and RR1 are commonly correlated during the rising and falling phases, both temporally and spatially (Table 2). The longest time series for Dhaka cases also disclose the significant relationship of Tn1621GE at the winter peak. On that account, we can say that a specified night temperature range with dry weather is a prominent force to the spread of the disease during the winter.

The assessment between three selected phases of the rotavirus winter cycle confers the effect of climate more strongly in the rising and falling phases rather than peak phase. Therefore, to achieve more clarity, we conducted a moving average analysis of one, two and three months between indices and rotavirus. The month-wise temporal analysis indicates a strong correlation of -0.81 between Tn1621GE and rotavirus cases during the peak month (December). Tmin also showed a robust correlation (-0.84) with same month's epidemic cycle (Figure 3). The consistent pattern of the two indices with rotavirus cycle from 2003-2014 confirms the relationship in Figure 3. It should be noted here that, the values of Tmin during this period varied between 14.5°C and 16.5°C (only 2°C). Such small changes in temperature variation can be misleading regarding the effect of a minimum temperature.

The month-wise correlation analysis for the individual cities would be statistically insignificant, as a common data period between the six cities are only available for approximately 3 years (for a seasonal analysis, it will generate 3 points in three years). In this case, we considered two of the most influential variables of the winter cycle; Tn1621GE and RR1, and compared them with rotavirus proportions of these cities in Figure 5. Both of the indices reflect an ensuing pattern with rotavirus cases in six selected cities of South Asia. Between the observed dual cycles of Tn1621GE, the first cycle tends to trigger the rotavirus peak in same month in the Sylhet area. Similarly, the same cycle of Tn1621GE of Mymensingh have influence on the next month's rotavirus cases. In case of Rajshahi, the same cycle shows a two-month lag relation instead of one. Moreover, the rotavirus peak also follows distinct patterns with RR1 or rainy days. In case of Barisal and Sylhet, the peak of rotavirus occurs during the driest month (or lowest RR1) without showing any lag. Over Rajshahi, this relationship extends for a two-months lag. This variation in lag for both indices explains why there is no significant relationship found during the peak phase (Table 2) in the spatial analysis.

3.3 Multivariate assessment

From the univariate analysis, we identified the RR1 and Tn1621GE as the most influencing variables on the winter rotavirus cycle. Using these climatic indices, we developed a multivariate regression model for evaluating the winter cycle. As the indices poses different correlation values in explaining the transmission process in different phases, we conducted three separate multivariate models for the three phases of the cycle and combined them into a single model. As we explored the spearman rank correlation values, we also

incorporated non-linear relationship between the indices and rotavirus cases. For checking the distribution of the response (response here is z-score of rotavirus) variable of the model, we conducted Shapiro-Wilk (Shapiro & Wilk, 1972) and Kolmogorov-Sminov (Massey, 1951) tests. The tests confirm that the response variable follow a gamma distribution and rejects the null hypothesis of normality. Considering the gamma distribution, we generated optimized models with the most dominant climate indices by utilizing both linear and non-linear regression. We selected the best model for each phase of the cycle by evaluating the Akaike information criterion (AIC). The combined model from the three individual phases is presented in Eq. 1.

$$\begin{aligned}
 X_t = & -0.1 * RR1_{m-1} + 0.04 * Tn1621GE_m - 0.07 * RR1_{n-1} + 0.07 * \\
 & Tn1621GE_{n-1} - 0.03 * RR1_{o-1} + 0.02 * (Tn1621GE_{o-1} + Tn1621GE_o) + \\
 & 7.47
 \end{aligned}
 \tag{1}$$

The subscript of RR1 and Tn1621GE refers their respective month's value in the equation. 'm', 'n' and 'o' represent the values for month of October-November-December and January-February-March, respectively. X is the scaled z-score of rotavirus for any selected month of the winter cycle. The R value of the equation is 0.67, referring to one-third of the explained variance for the whole transmission cycle. The result is higher than the previously reported climatic influence on rotavirus over South Asia (Jagai et al., 2012).

Using the formulated model, we can forecast rotavirus prevalence all over Bangladesh with localized climatic indices. In this context, based on the reported results of this study,

reliable real time information of RR1 and Tn1621GE can give advance information one-to-two months prior to the occurrence of an impending outbreak. To calculate near real-time RR1 and Tn1621GE, we utilized GPM daily precipitation data and MODIS temperature data. Magnitude of GPM rainfall products poses a magnitude bias with observed daily rainfall. However, for 1mm rainy days in a month (RR1), the GPM data provide same value as in-situ observed (BMD) data from June 2015 to December 2015. In case of MODIS land surface temperature data; we replaced the missing values in night temperature with GHCN data to formulate a complete Tn1621GE time series over the selected cities.

The calculated indices from GPM and MODIS are inserted in Eq. 1 to validate the model results for October and November 2015. Figure 6 shows the spatial prevalence of observed and model estimated rotavirus over Bangladesh. For October, the eastern parts of the country largely agree with the observed disease incidences, where magnitude slightly deviates. In case of November, the observed patterns are well captured by the model; however, magnitude deviates over the Barisal and Rajshahi regions. We also presented the potential of using TRMM satellite with MODIS datasets (Figure 7) to predict disease risk over the focus region. Figure 7 shows the October and November outbreaks from model and observed data during 2014. The TRMM derived disease map is able to capture the pattern better than GPM derived product. However, it should be noted that 2014 winter data are also utilized in model formulation, thus it cannot be considered as a validation result.

4. Discussion

Our initial assessment infers that the rotavirus cycle is strongly influenced by the dry and cold winter season climate in Dhaka. In Great Britain, Atchison et al. (2010) explored the temperature dependence of rotavirus and conferred that above the 5°C threshold, an increase of the average temperature decreased the infection rate of the disease. A similar understanding was also found in Australia (D'Souza et al., 2008), where rotavirus diarrhea admissions are associated with lower temperatures and lower humidity. Although these two studies were conducted in different climatic zones altogether, we believe that the dearth of overall number of studies linking rotavirus with climatic indices, these findings are still important evidences towards the influence of temperature on rotavirus incidence. In South Asia, Jagai et al. (2012) also showed that the reduction in annual temperature and precipitation increases the level of infections of rotavirus, supporting our findings.

As our assessment separated the timeframe into two seasonal cycles, the correlation from winter cycle over all six selected cities strengthens the findings of previous studies. However, we also found significant positive association of rotavirus infections during monsoon over Dhaka. Dhaka is a densely populated city with a high number of informal settlements, or slums, with poor water and sanitation conditions (Akanda & Hossain, 2012). As rotavirus pathogens can be transmitted through the fecal oral route, high precipitation events can create waterlogging and eventually connects to the pathogen transmission pathways (Dennehy, 2000). Thus, Dhaka experienced an additional monsoon outbreak compared to other cities and the outbreak may be influenced by heavy rainfall events. Such phenomena also clarify why the monsoon indicators showed insignificant

relationships with rotavirus in other cities. Dhaka typically observes the annual highest rotavirus incidence during January, but some exceptions were observed during March 2009 and July 2004 (Figure 2(b)). The 2004 flood event was one of the most devastating floods in the last decade in Bangladesh (Schwartz et al., 2006). Floods connect the fecal oral transmission route of the disease thus results unusual outbreak (Levy et al., 2009). In many years, the lowest incident rate of rotavirus diarrhea was observed during May. However, in 2012 and 2014, the cycle reached its lowest crest during August. In 2012 and 2014, medium flooding happened in outskirts of Dhaka, which might act as the hindering phenomenon of rotavirus outbreaks (FFWC, 2012, 2014). Dhaka experienced one of the highest rotavirus outbreaks during the flood of 2007 (Figure 2(b)). Our analysis showed that the outbreak was correlated to extreme rainfall events (RR70), a potential indicator of floods. During the floods of 2007, there was a massive outbreak of diarrheal diseases in Dhaka including cholera, rotavirus, and dysentery (Harris et al., 2008, Cash et al., 2014)).

Our study also provides some detailed assessment of the winter rotavirus cycle. We found that the rising phase of rotavirus is negatively correlated with SU or Tx2532GE, which represents the amount of warm days in month. As the virus prefers low temperature environments, the lower number of warm days eventually helps to initiate the spread of the disease. Previous studies indicated that the virus can be active in the environment for up to 4 weeks or one month without a host body (Levy et al., 2009). Therefore, reduction of warm days may increase the rotavirus sensitivity and the effect can be delayed up to one month. Our findings also suggest that the beginning of the winter cycle (October-November) is highly correlated with RR1 and Tn1621GE, both spatially and temporally.

Average night temperature during September-October are 25°C. As Tn1621GE represents the night temperature of 16°C to 21°C, some nights in September start to experience temperatures below 21°C. Therefore, the index can be reflected as colder nights of that month. In a laboratory test, rotavirus was found to be active for several days in 4°C and 20°C temperatures without human contact (Moe & Shirley, 1987). In aerosol, the virus is also infectious in low temperatures (Moe & Harper, 1983). Therefore, higher values of Tn1621GE, which act as cold nights during September-October, may promote the infectivity of rotavirus up to a 4-week delay.

On the other hand, the RR1 index represents the number of wet days in a month rather than magnitude or intensity of rainfall events. As rotavirus transmission can be driven with air, reduction of rainfall may raise the propensity of aerial transport (Ansari et al., 1991) of contaminated fecal matter. Therefore, RR1 can be considered a barrier to air-borne transport of rotavirus. Consequentially, the joint effect of RR1 and Tn1621GE triggers the one month delayed outbreak during the rising phase of the winter cycle. During the peak month of rotavirus in December, RR1 becomes nearly zero over Dhaka, thus allowing aerial transport of the virus to its highest potential. In this phase, the correlation with Tn1621GE shifts from positive to negative. During the month of December, the average nighttime temperature also drops below 21°C. Such a drop of night temperature, transforms the Tn1621GE index to a representative of a warm night, as temperatures can be higher than 21°C during this month. As Atchison et al. (2010) and Cunliffe et al. (1998) both referred, lower temperatures can increase the infection rate of rotavirus; higher number of Tn1621GE inversely affects the rotavirus incidence during December. Similarly, this

understanding is also supported by T_{min} values over Dhaka. Therefore, as the number of warm nights increase, the magnitude of rotavirus cases decrease in the peak month. During the falling phase, when it starts to rain again from February, the air-borne transport of the virus starts to be limited again and alongside the temperature remains under 21°C, until March. Thus, Tn1621GE serves as an indicator of warm nights during winter and lower rotavirus infection.

In other cities of Bangladesh, the timing of the cycles did not match in the same way, thus correlation values decreased. In spatial cases, the rising and falling phase still showed a significant correlation with RR1 and Tn1621GE, but values of the correlation coefficient are lower than the values of the temporal analysis. During September, Tn1621GE acts as an indicator of cold night. In Sylhet and Barisal, as the increase of cold and dry nights coincide, rotavirus infection experiences a sharp rise, thus no lag relationship is observed. However, in places like Dhaka and Mymensingh, where dryness comes early but temperature suitability comes in a delayed manner, the places experience a one-month delay in an outbreak. If these two phenomena have a much wider gap, it can result in up to a two-month delay, which was observed in Rajshahi. Therefore, our findings suggest that the timing of coldness and dryness can locally affect the spread of a rotavirus epidemic. This finding increases the potential of using a high-resolution satellite data product in forecasting the local onset of the outbreaks. It is difficult to draw a generality from only three or four years of rotavirus observations; upon availability of more surveillance data, such analysis can be explored in more detail in future.

From the multivariate analysis, we are also able to confirm our hypothesis through the model selection process. All components of Equation 1 significantly influence corresponding prevalence values of the rotavirus cycle and confirm the role of environmental factors on the whole rotavirus transmission cycle. The forecasted prevalence matched some spatial areas of observed values during November but not in October. As we conducted a detailed analysis of the climate extremes that are able to explain about 44% variance, such discrepancy was expected in spatial mapping. Due to the lack of sufficient spatial disease and climate data, the spatial signature was not captured properly, thus the accuracy of the model suffers. Moreover, factors like population dynamics and social behavior, or environmental factors such as flood and soil moisture can be important in improving modeling accuracy. In addition to that, the accuracy of satellite datasets can also be a plausible reason for the less than satisfactory performance of the spatial mapping. However, the satellite products such as GPM, TRMM and MODIS not only give near real-time information, but also great spatial coverage, and have great potential to improve the resolution of the risk maps for such infectious diseases.

Understanding the role of climatic extremes can contribute to several pre- outbreak and post-outbreak solutions. As the developed disease model suggests, with the knowledge of an imminent outbreak one month ahead, the health management organizations can implement extra vaccination efforts as well as awareness in the most vulnerable communities. In the developing world, where preventive resources are limited, prioritizing vaccination efforts and locations by public health authorities could save significant morbidity and mortality. During the epidemic, further outbreaks can be prevented by

implementing disinfectant byproducts in water sources, improving drainage in the most vulnerable areas, and ensuring potable water in the infected communities. The post-outbreak measures can be improvement of sanitation situations by developing sewage structures, or educating the high-risk communities about the transmission pathways of rotavirus. Structural solutions such as dikes, canals or sewage networks can also be constructed to reduce water logging and improve sanitary and drainage conditions.

Immunization efforts targeting vulnerable communities would be another preventive measure to reduce the spread of rotavirus diarrhea. The efficacy of the vaccination is found to be 51% effective in reducing morbidity and mortality in recent trials in developing countries (Jiang et al., 2010). Two primary rotavirus vaccines have been certified (RotaTeq, Merck & Co and Rotarix, GSK Biologicals) in major countries of the world and are slated to be incorporated across the developing world (Ruiz-Palacios et al., 2006; Vesikari et al., 2006). The vaccination is usually administered to children under one year of age and typically costs from \$1 to \$7 per dose (Atherly et al., 2009).

5. Conclusions

In this study, we have analyzed the relationship of various climate variables and indices with rotavirus outbreaks in South Asia, formulated outbreak models and proposed a forecast mechanism. In the validation process, we have utilized satellite-derived climate products, which have the capacity to provide climatic information within a 24-hour latency period after the acquisition of data. To quantify the disease outbreaks, we used a spatial risk indicator to show the spatial pattern of rotavirus outbreaks throughout Bangladesh and

South Asia, and validated forecasted values with observed number of cases for October 2015 and November 2015.

The study strongly distinguished the effect of night and day time temperatures on the epidemiology of rotavirus. While previous studies pointed out that the cold and dry climate is favorable for rotavirus spread, the role of day and night temperature remained unexplored. Our analyses found that the number of colder nights one month before an epidemic dictates the magnitude of the rotavirus outbreak in subsequent months. This effect also matches with the number of 1 mm rainy days, as fewer numbers of rainy days or drier winters facilitate the transmission of the disease. Higher number of cold nights with less amount of rainfall during September and October may trigger the outbreak and the relationship was significant in all six cities of Bangladesh. Metropolitan areas of Dhaka and Chittagong experience similar, but smaller outbreaks during the monsoon season due to the number of heavy rainfall events. As the cities have poor water supply, sanitation and drainage systems, heavy rainfall events eventually connect the fecal-oral route of rotavirus transmission pathway. Our analysis also showed that the rainfall and temperature products from GPM and MODIS, respectively, could be utilized to predict the occurrences and magnitudes of rotavirus outbreaks. The forecasted spatial patterns derived from these products matched with observed progression of rotavirus over Bangladesh.

The proposed disease forecasting mechanism provides great potential to improve the existing disease preparedness and vaccination strategies. The detection of risky hotspots can facilitate vaccination programs in similar climatic regions. As our model

deterministically explained the environmental variability of the disease, future investigations can incorporate population-based disease models to improve the performance of the forecasts. As shown in our study, satellite-based forecasting has great potential to improve the health and well-being, and contribute towards sustainable development of the growing population of the planet.

Acknowledgments, Samples, and Data

This research was supported, in part, by a NASA Health and Air Quality grant (NNX15AF71G). The authors would like to thank Emine Bihter Yalcin and Soroush Kouhi Anbaran for their constructive comments. We also like to thank the anonymous reviewers for their detailed and insightful comments.

The incidence rate of rotavirus over Dhaka can be found from icddr,b Health and Science Bulletins (<http://dspace.icddr.org/jspui/handle/123456789/6349>). The rotavirus outbreak information for other cities in Bangladesh are available on the IEDCR website (<http://www.iedcr.gov.bd/index.php/surveillance-rotavirus>). The BMD and GHCN climate data can be obtained from BMD (<http://bmd.gov.bd/?/home>) and National Climatic Data Center (NCDC) website (<https://www.ncdc.noaa.gov/cdo-web/datatools/findstation>), respectively. The satellite datasets (GPM, MODIS and TRMM) can be retrieved from the Google Earth Engine (<https://earthengine.google.com/datasets/>).

References

- Akanda, A., & Jutla, A. (2013). Understanding climate change impacts on global diarrhoeal disease burden. Retrieved July 5, 2016, from <http://outreach.stakeholderforum.org/index.php/previous-editions/cop-19/193-cop-19-day-3-climate-change-and-health/11582-understanding-climate-change-impacts-on-global-diarrhoeal-disease-burden>
- Akanda, A. S., Jutla, A. S., & Colwell, R. R. (2014). Global diarrhoea action plan needs integrated climate-based surveillance. *The Lancet Global Health*, 2(2), e69–e70. [https://doi.org/10.1016/S2214-109X\(13\)70155-4](https://doi.org/10.1016/S2214-109X(13)70155-4)
- Akanda, A. S., & Hossain, F. (2012). The climate-water-health nexus in emerging megacities. *Eos, Transactions American Geophysical Union*, 93(37), 353–354.
- Alexander, L. V. (2015). Global observed long-term changes in temperature and precipitation extremes: A review of progress and limitations in IPCC Assessments and beyond1. *Weather and Climate Extremes*. <https://doi.org/http://dx.doi.org/10.1016/j.wace.2015.10.007>
- Ansari, S. A., Springthorpe, V. S., & Sattar, S. A. (1991). Survival and vehicular spread of human rotaviruses: possible relation to seasonality of outbreaks. *Reviews of Infectious Diseases*, 13(3), 448–61. Retrieved from <http://www.ncbi.nlm.nih.gov/pubmed/1866549>
- Atchison, C. J., Tam, C. C., Hajat, S., Van Pelt, W., Cowden, J. M., & Lopman, B. A. (2010). Temperature-dependent transmission of rotavirus in Great Britain and The Netherlands. *Proceedings of the Royal Society B*, 277, 933–942.

<https://doi.org/10.1098/rspb.2009.1755>

Atherly, D., Dreibelbis, R., Parashar, U. D., Levin, C., Wecker, J., & Rheingans, R. D. (2009). Rotavirus Vaccination: Cost-Effectiveness and Impact on Child Mortality in Developing Countries. *The Journal of Infectious Diseases*, 200(s1), S28–S38. <https://doi.org/10.1086/605033>

Bandyopadhyay, S., Kanji, S., & Wang, L. (2012). The impact of rainfall and temperature variation on diarrheal prevalence in Sub-Saharan Africa. *Applied Geography*, 33(1), 63–72. <https://doi.org/10.1016/j.apgeog.2011.07.017>

Bhavnani, D., Goldstick, J. E., Cevallos, W., Trueba, G., & Eisenberg, J. N. S. (2014). Impact of rainfall on diarrheal disease risk associated with unimproved water and sanitation. *The American Journal of Tropical Medicine and Hygiene*, 90(4), 705–11. <https://doi.org/10.4269/ajtmh.13-0371>

Brown, M. E., Escobar, V., Moran, S., Entekhabi, D., O'neill, P. E., Njoku, E. G., ... Entin, J. K. (2013). NASA's soil moisture active passive (SMAP) mission and opportunities for applications users. *Bulletin of the American Meteorological Society*, 94(8). <https://doi.org/10.1175/BAMS-D-11-00049.1>

Cash, B. A., Rodo, X., Emch, M., Yunus, M. D., Faruque, A. S. G., & Pascual, M. (2014). Cholera and shigellosis: Different epidemiology but similar responses to climate variability. *PLoS ONE*, 9(9). <https://doi.org/10.1371/journal.pone.0107223>

Cheng, J. J., & Berry, P. (2013). Development of key indicators to quantify the health impacts of climate change on Canadians. *International Journal of Public Health*, 58(5), 765–775. <https://doi.org/10.1007/s00038-013-0499-5>

- Cunliffe, N. A., Kilgore, P. E., Bresee, J. S., Steele, A. D., Luo, N., Hart, C. A., & Glass, R. I. (1998). Epidemiology of rotavirus diarrhoea in Africa: a review to assess the need for rotavirus immunization. *Bulletin of the World Health Organization*, 76(5), 525–37. Retrieved from <http://www.ncbi.nlm.nih.gov/pubmed/9868844>
- D'Souza, R. M., Hall, G., & Becker, N. G. (2008). Climatic factors associated with hospitalizations for rotavirus diarrhoea in children under 5 years of age. *Epidemiology and Infection*, 136(1), 56–64. <https://doi.org/10.1017/S0950268807008229>
- Dennehy, P. H. (2000). Transmission of rotavirus and other enteric pathogens in the home. *The Pediatric Infectious Disease Journal*, 19(10 Suppl), S103-5. Retrieved from <http://www.ncbi.nlm.nih.gov/pubmed/11052397>
- Emamifar, S., Rahimikhoob, A., & Noroozi, A. A. (2013). Daily mean air temperature estimation from MODIS land surface temperature products based on M5 model tree. *International Journal of Climatology*, 33(15), 3174–3181. <https://doi.org/10.1002/joc.3655>
- FFWC, F. F. and W. C. (2012). *FFWC Annual Report 2012*. <https://doi.org/10.1002/ejoc.201200111>
- FFWC, F. F. and W. C. (2014). *FFWC Annual Report 2014*.
- Grassly, N. C., & Fraser, C. (2008). Mathematical models of infectious disease transmission. *Nature Reviews Microbiology*. <https://doi.org/10.1038/nrmicro1845>
- Gurarie, D., & Seto, E. Y. W. (2009). Connectivity sustains disease transmission in environments with low potential for endemicity: modelling schistosomiasis with hydrologic and social connectivities. *Journal of the Royal Society, Interface*, 6(35),

495–508. <https://doi.org/10.1098/rsif.2008.0265>

Harris, A. M., Chowdhury, F., Begum, Y. A., Khan, A. I., Faruque, A. S. G., Svennerholm, A.-M., ... Qadri, F. (2008). Shifting Prevalence of Major Diarrheal Pathogens in Patients Seeking Hospital Care during Floods in 1998, 2004, and 2007 in Dhaka, Bangladesh. *The American Journal of Tropical Medicine and Hygiene*, 79(5), 708–714. <https://doi.org/10.4269/ajtmh.2008.79.708>

Hasan, M. A., Islam, A. K. M. S., & Bhaskaran, B. (2013). Predicting Change of Future Climatic Extremes Over Bangladesh in High Resolution Climate Change. In *4th International Conference on Water & Flood Management (ICWFM-2013)* (pp. 583–590). Dhaka, Bangladesh.

Hou, A. Y., Kakar, R. K., Neeck, S., Azarbarzin, A. A., Kummerow, C. D., Kojima, M., ... Nakamura, K. (2014). *The Global Precipitation Measurement Mission (GPM)*.

Huffman, G. J., Bolvin, D. T., & Nelkin, E. J. (2015). Integrated Multi-satellite Retrievals for GPM (IMERG) technical documentation. *NASA/GSFC Code*, 612, 47. Retrieved from <ftp://arthurhou.pps.eosdis.nasa.gov/gpmdata/>

Hutton, G., & Bartram, J. (2008). Global costs of attaining the Millennium Development Goal for water supply and sanitation. *Bulletin of the World Health Organization*, 86(1), 13–19. <https://doi.org/10.2471/BLT.07.046045>

Islam, A. K. M. S., & Hasan, M. A. (2012). Climate induced changes of precipitation extremes over Bangladesh. In *Proceedings of International Conference On Environmental Aspects Of Bangladesh* (pp. 67–105). Retrieved from <http://www.binbd.com/benjp/iceab12/ICEAB12proceeding4.pdf>

- Jagai, J. S., Sarkar, R., Castronovo, D., Kattula, D., McEntee, J., Ward, H., ... Naumova, E. N. (2012). Seasonality of rotavirus in south asia: A meta-analysis approach assessing associations with temperature, precipitation, and vegetation index. *PLoS ONE*, 7(5). <https://doi.org/10.1371/journal.pone.0038168>
- Jiang, V., Jiang, B., Tate, J., Parashar, U. D., & Patel, M. M. (2010). Performance of rotavirus vaccines in developed and developing countries. *Human Vaccines*, 6(7), 532–42. <https://doi.org/10.4161/HV.6.7.11278>
- Jutla, A., Huq, A., & Colwell, R. R. (2015). Diagnostic Approach for Monitoring Hydroclimatic Conditions Related to Emergence of West Nile Virus in West Virginia. *Frontiers in Public Health*, 3(February), 10. <https://doi.org/10.3389/fpubh.2015.00010>
- Keggenhoff, I., Elizbarashvili, M., & King, L. (2015). Recent changes in Georgia's temperature means and extremes: Annual and seasonal trends between 1961 and 2010. *Weather and Climate Extremes*, 8, 3445. <https://doi.org/10.1016/j.wace.2014.11.002>
- Kummerow, C., Barnes, W., Kozu, T., Shiue, J., & Simpson, J. (1998). The tropical rainfall measuring mission (TRMM) sensor package. *Journal of Atmospheric and Oceanic Technology*, 15(3), 809–817.
- Lambrechts, L., Paaijmans, K. P., Fansiri, T., Carrington, L. B., Kramer, L. D., Thomas, M. B., & Scott, T. W. (2011). Impact of daily temperature fluctuations on dengue virus transmission by *Aedes aegypti*. *Proceedings of the National Academy of Sciences of the United States of America*, 108(18), 7460–5. <https://doi.org/10.1073/pnas.1101377108>

- Levy, K., Hubbard, A. E., & Eisenberg, J. N. S. (2009). Seasonality of rotavirus disease in the tropics: a systematic review and meta-analysis. *International Journal of Epidemiology*, 38(6), 1487–96. <https://doi.org/10.1093/ije/dyn260>
- Maantay, J., & Becker, S. (2012). The health impacts of global climate change: A geographic perspective. *Applied Geography*, 33, 1–3. <https://doi.org/10.1016/J.APGEOG.2011.08.008>
- Martinez, P. P., King, A. A., Yunus, M., Faruque, A. S. G., & Pascual, M. (2016). Differential and enhanced response to climate forcing in diarrheal disease due to rotavirus across a megacity of the developing world. *Proceedings of the National Academy of Sciences of the United States of America*, 113(15), 1518977113-. <https://doi.org/10.1073/pnas.1518977113>
- Massey, F. J. (1951). The Kolmogorov-Smirnov Test for Goodness of Fit. *Journal of the American Statistical Association*, 46(253), 68–78. <https://doi.org/10.1080/01621459.1951.10500769>
- Menne, M. J., Durre, I., Korzeniewski, B., McNeal, S., Thomas, K., Yin, X., ... Houston, T. G. (2012). Global Historical Climatology Network - Daily (GHCN-Daily). *Journal of Atmospheric and Oceanic Technology*, 29, 897–910. <https://doi.org/doi:10.1175/JTECH-D-11-00103.1>
- Moe, K., & Harper, G. J. (1983). Archives of Virology The Effect of Relative Humidity and Temperature, 216, 211–216.
- Moe, K., & Shirley, J. A. (1987). Archives of Virology, 117, 197–214.
- Moors, E., Singh, T., Siderius, C., Balakrishnan, S., & Mishra, A. (2013). Climate change

- and waterborne diarrhoea in northern India: Impacts and adaptation strategies. *Science of the Total Environment*, 468–469, S139–S151.
<https://doi.org/10.1016/j.scitotenv.2013.07.021>
- Mullick, S., Mandal, P., Nayak, M. K., Ghosh, S., De, P., Rajendran, K., ... Chawla-Sarkar, M. (2014). Hospital based surveillance and genetic characterization of rotavirus strains in children (<5 years) with acute gastroenteritis in Kolkata, India, revealed resurgence of G9 and G2 genotypes during 2011-2013. *Vaccine*, 32(S1), A20–A28.
<https://doi.org/10.1016/j.vaccine.2014.03.018>
- Pagano, T. S., & Durham, R. M. (1993). Moderate resolution imaging spectroradiometer (MODIS). In *Sensor Systems for the Early Earth Observing System Platforms* (Vol. 1939, pp. 2–18).
- Prosser, D. J., Hungerford, L. L., Erwin, R. M., Ottinger, M. A., Takekawa, J. Y., Newman, S. H., ... Ellis, E. C. (2016). Spatial Modeling of Wild Bird Risk Factors for Highly Pathogenic A(H5N1) Avian Influenza Virus Transmission. *Avian Diseases*, 60(1s), 329–336. <https://doi.org/10.1637/11125-050615-Reg>
- Remais, J., Liang, S., & Spear, R. C. (2008). Coupling hydrologic and infectious disease models to explain regional differences in schistosomiasis transmission in southwestern China. *Environmental Science & Technology*, 42(7), 2643–9. Retrieved from <http://www.ncbi.nlm.nih.gov/pubmed/18505010>
- Ruiz-Palacios, G. M., Pérez-Schael, I., Velázquez, F. R., Abate, H., Breuer, T., Clemens, S. C., ... O’Ryan, M. (2006). Safety and Efficacy of an Attenuated Vaccine against Severe Rotavirus Gastroenteritis. *New England Journal of Medicine*, 354(1), 11–22.

<https://doi.org/10.1056/NEJMoa052434>

- Schwartz, B. S., Harris, J. B., Khan, A. I., Larocque, R. C., Sack, D. A., Malek, M. A., ... Ryan, E. T. (2006). Diarrheal epidemics in Dhaka, Bangladesh, during three consecutive floods: 1988, 1998, and 2004. *The American Journal of Tropical Medicine and Hygiene*, 74(6), 1067–73. Retrieved from <http://www.ncbi.nlm.nih.gov/pubmed/16760521>
- Shapiro, S. S., & Wilk, M. B. (1972). An Analysis of Variance Test for the Exponential Distribution (Complete Samples). *Technometrics*, 14(2), 355–370. <https://doi.org/10.1080/00401706.1972.10488921>
- Sherchand, J. B., Nakagomi, O., Dove, W., Nakagomi, T., Yokoo, M., Pandey, B. D., ... Cunliffe, N. a. (2009). Molecular epidemiology of rotavirus diarrhea among children aged <5 years in nepal: predominance of emergent G12 strains during 2 years. *The Journal of Infectious Diseases*, 200 Suppl(Suppl 1), S182–S187. <https://doi.org/10.1086/605046>
- Shetty, R. S., Kamath, V. G., Nayak, D. M., Hegde, A., & Saluja, T. (2016). Rotavirus associated acute gastroenteritis among under-five children admitted in two secondary care hospitals in southern Karnataka, India. *Clinical Epidemiology and Global Health*, 1–5. <https://doi.org/10.1016/j.cegh.2016.06.002>
- Siddique, A. K., Ahmed, S., Iqbal, A., Sobhan, A., Poddar, G., Azim, T., ... Sack, R. B. (2011). Epidemiology of rotavirus and cholera in children aged less than five years in rural Bangladesh. *Journal of Health, Population and Nutrition*, 29(1), 1–8. <https://doi.org/10.3329/jhpn.v29i1.7560>

- Tate, J. E., Burton, A. H., Boschi-Pinto, C., Steele, A. D., Duque, J., Parashar, U. D., ... al., et. (2012). 2008 estimate of worldwide rotavirus-associated mortality in children younger than 5 years before the introduction of universal rotavirus vaccination programmes: a systematic review and meta-analysis. *The Lancet Infectious Diseases*, 12(2), 136–141. [https://doi.org/10.1016/S1473-3099\(11\)70253-5](https://doi.org/10.1016/S1473-3099(11)70253-5)
- Tawhid, K. G. (2004). *Causes and Effects of Water Logging in Dhaka City, Bangladesh*. Retrieved from https://s3.amazonaws.com/academia.edu.documents/31161625/LWR_EX_04_45.pdf?AWSAccessKeyId=AKIAIWOWYYGZ2Y53UL3A&Expires=1508416266&Signature=yJgO5T20jTWLKAagbA2MR5WAgd4%3D&response-content-disposition=inline%3Bfilename%3DCauses_and_effects_of_water_loggi
- Troeger, C., Forouzanfar, M., Rao, P. C., Khalil, I., Brown, A., Reiner, R. C., ... Others. (2017). Estimates of global, regional, and national morbidity, mortality, and aetiologies of diarrhoeal diseases: A systematic analysis for the Global Burden of Disease Study 2015. *The Lancet Infectious Diseases*, 909–948. [https://doi.org/10.1016/S1473-3099\(17\)30276-1](https://doi.org/10.1016/S1473-3099(17)30276-1)
- Vesikari, T., Matson, D. O., Dennehy, P., Van Damme, P., Santosham, M., Rodriguez, Z., ... Heaton, P. M. (2006). Safety and Efficacy of a Pentavalent Human–Bovine (WC3) Reassortant Rotavirus Vaccine. *New England Journal of Medicine*, 354(1), 23–33. <https://doi.org/10.1056/NEJMoa052664>
- Wang, H., Naghavi, M., Allen, C., Barber, R. M., Carter, A., Casey, D. C., ... Zuhlke, L. J. (2016). Global, regional, and national life expectancy, all-cause mortality, and cause-specific mortality for 249 causes of death, 1980–2015: a systematic analysis for

- the Global Burden of Disease Study 2015. *The Lancet*, 388(10053), 1459–1544.
[https://doi.org/10.1016/S0140-6736\(16\)31012-1](https://doi.org/10.1016/S0140-6736(16)31012-1)
- Wang, X. L., & Feng, Y. (2013). *RHtestsV4 User Manual*.
- Wangchuk, S., Dorji, T., Tsheten, Tshering, K., Zangmo, S., Pem Tshering, K., ... Ahmed, K. (2015). A Prospective Hospital-based Surveillance to Estimate Rotavirus Disease Burden in Bhutanese Children under 5 Years of Age. *Tropical Medicine and Health*, 43(1), 63–68. <https://doi.org/10.2149/tmh.2014-22>
- WHO, W. H. O. (2011). Rotavirus surveillance worldwide-2009. *Wkly Epidemiol Rec*, 86(18), 174–176.
- WHO, W. H. O. (2014). *Preventing diarrhoea through better water, sanitation and hygiene: exposures and impacts in low-and middle-income countries*. World Health Organization.
- WMO, W. M. O. (2007). *Joint CCL/CLIVAR/JCOMM Expert Team on Climate Change Detection And Indices (ETCCDI)*.
- World Population Review. (2017). World Population Review. Retrieved April 6, 2017, from <http://worldpopulationreview.com/world-cities/dhaka-population/>

Figure Captions:

Figure 1. The location of the rotavirus prevalent cities in South Asia. The cities with green dots were selected for the spatial analysis.

Figure 2. (a) Annual monthly rotavirus outbreaks over South Asian cities. (b) Z-score of rotavirus over Dhaka from 2003 to 2015 (c) Auto-correlation function of rotavirus in the city of Dhaka from 2003 to 2015.

Figure 3. (a) Rotavirus incidence for the month of November with RR1 of September (the y-axis is plotted in reverse order); (b) rotavirus of June-July-August with RR70 of June-July-August; (c) Rotavirus incidence for the month of December with Tmin (left); and (d) Tn1621GE (right) of same month (the y-axis of the indices are plotted in reverse order).

Figure 4. (a) Temporal correlation of rotavirus in winter months over Dhaka from January 2003 to May 2015 and (b) Spatial correlation of rotavirus in winter months over six cities of Bangladesh from July 2012 to May 2015. (c) Temporal correlation of rotavirus in monsoon months over Dhaka from January 2003 to May 2015 and (d) Spatial correlation of rotavirus in monsoon months over six cities of Bangladesh from July 2012 to May 2015.

Figure 5. The rotavirus cycle in the six selected cities with compared to RR1 and Tn1621GE from June 2012 to May 2015.

Figure 6. Spatial distribution of the observed (left) and model-estimated (right, GPM + MODIS) z-score of rotavirus incidence for (a-b) October and (c-d) November, 2015.

Figure 7. Spatial distribution of the observed (left) and model-estimated (right, TRMM + MODIS) z-score of rotavirus incidence for (a-b) October and (c-d) November, 2014.

Tables Captions:

Table 1. Description of climate indices parameters.

Table 2. The spatial and temporal correlations between climatic indices and the three phases of the winter rotavirus epidemic.

Figure 1:

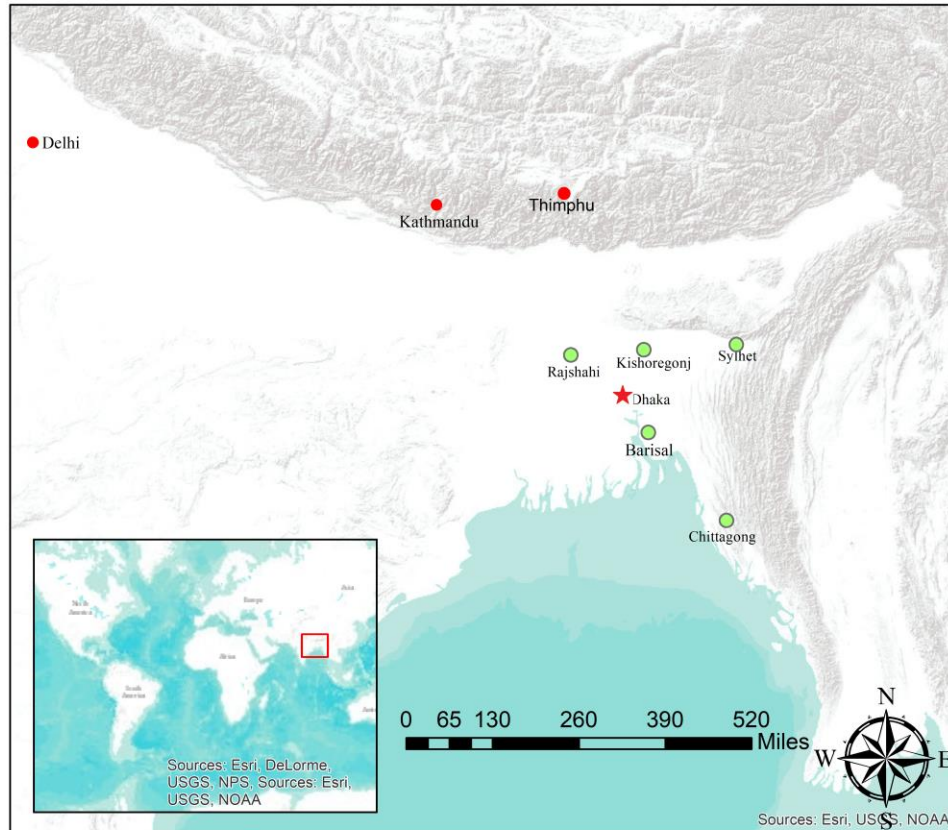


Figure 2:

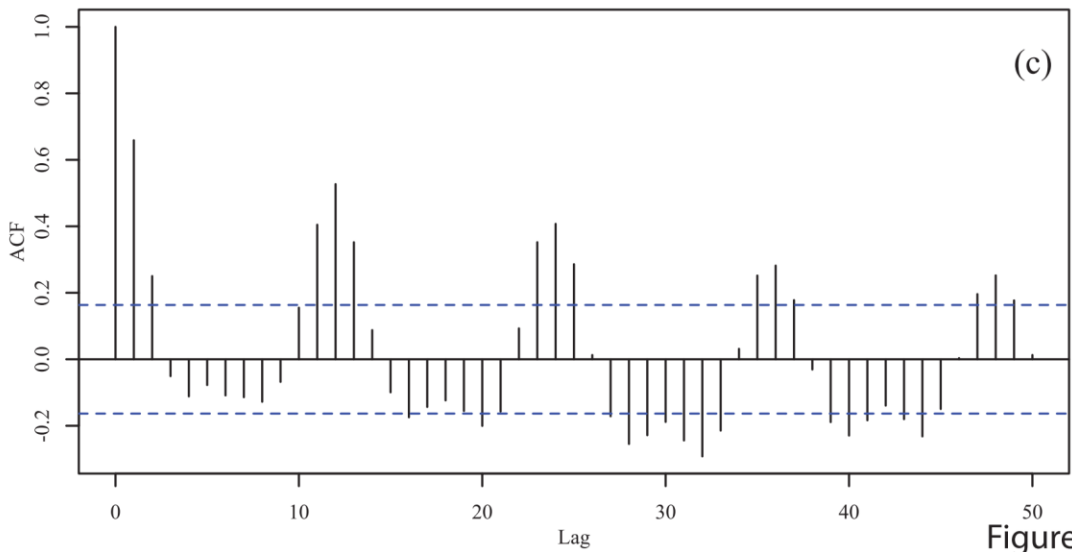
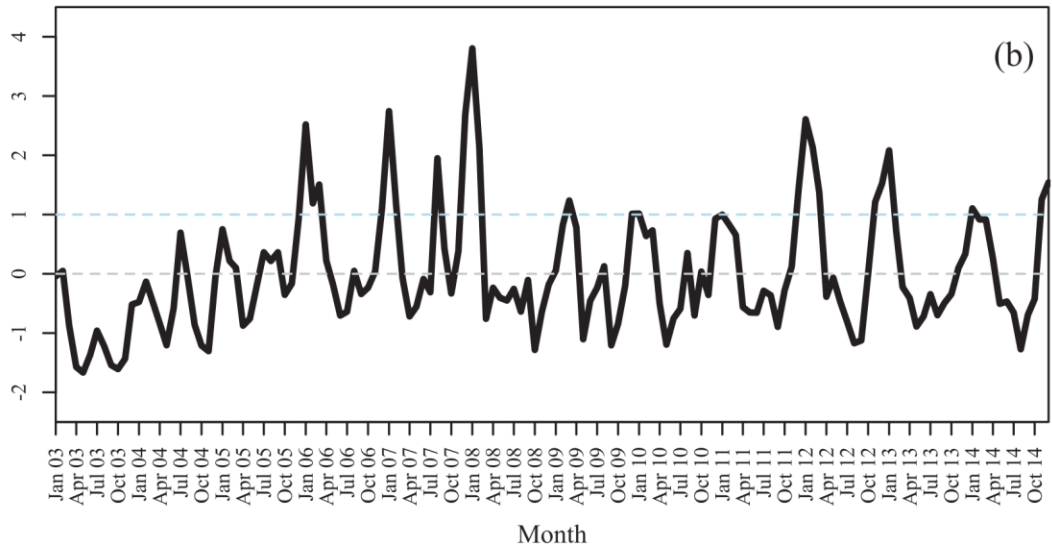
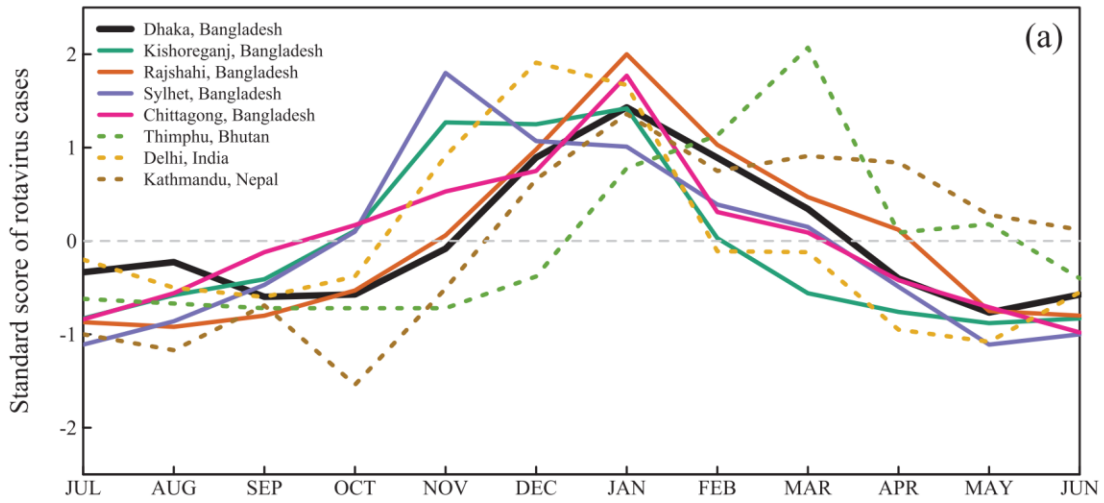


Figure 02

Figure 3:

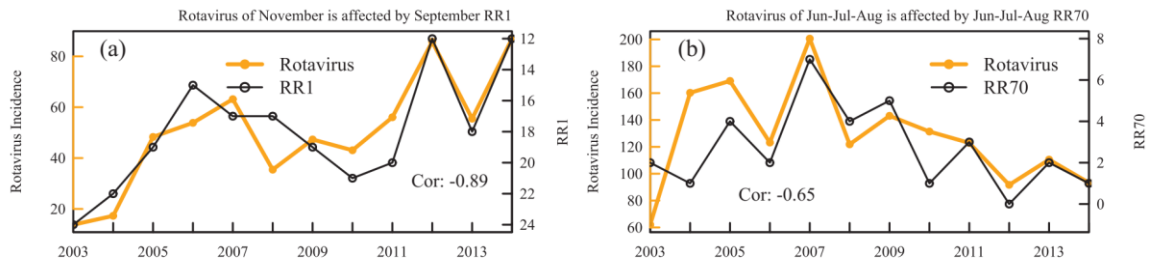


Figure 4:

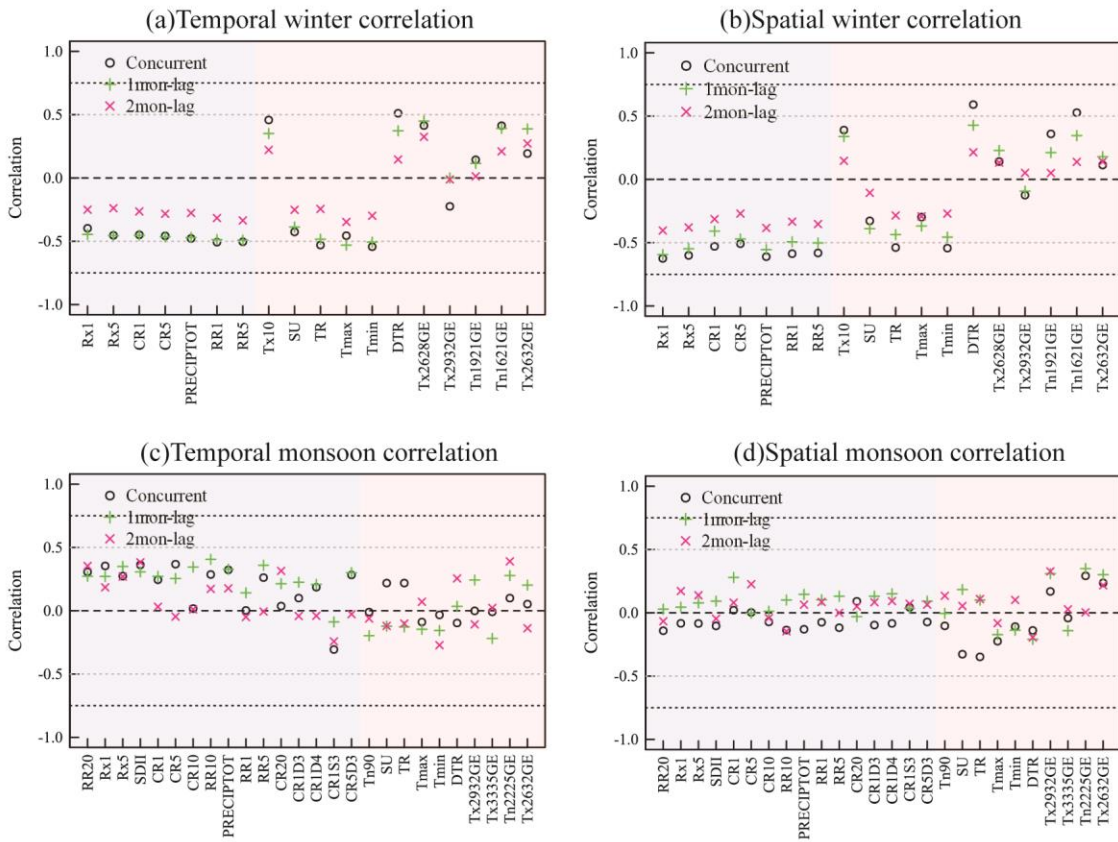


Figure 5:

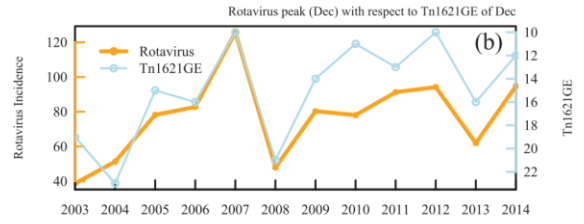
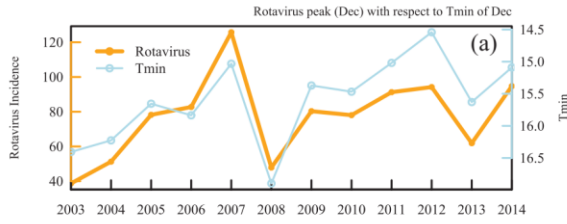


Figure 05

Figure 6:

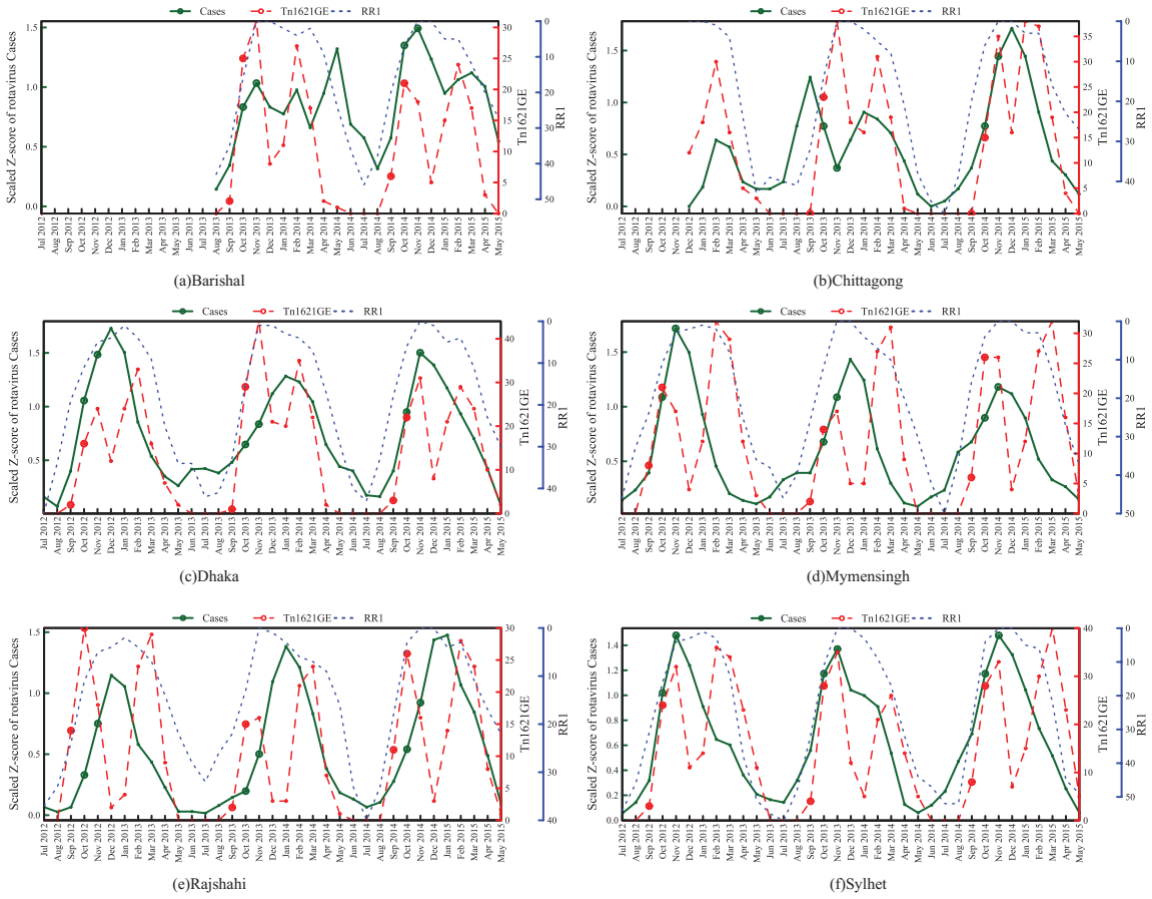


Figure 7:

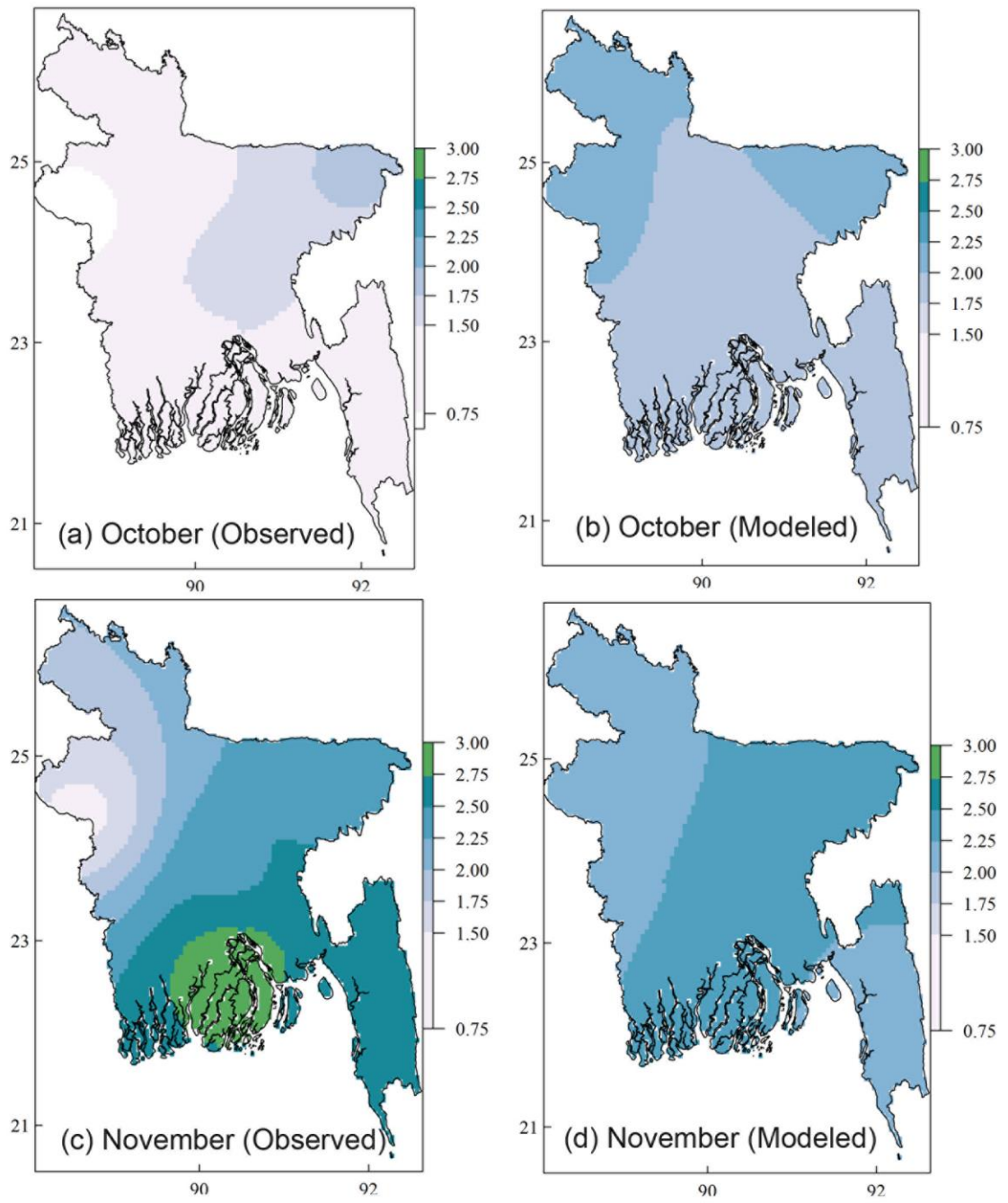


Figure 8:

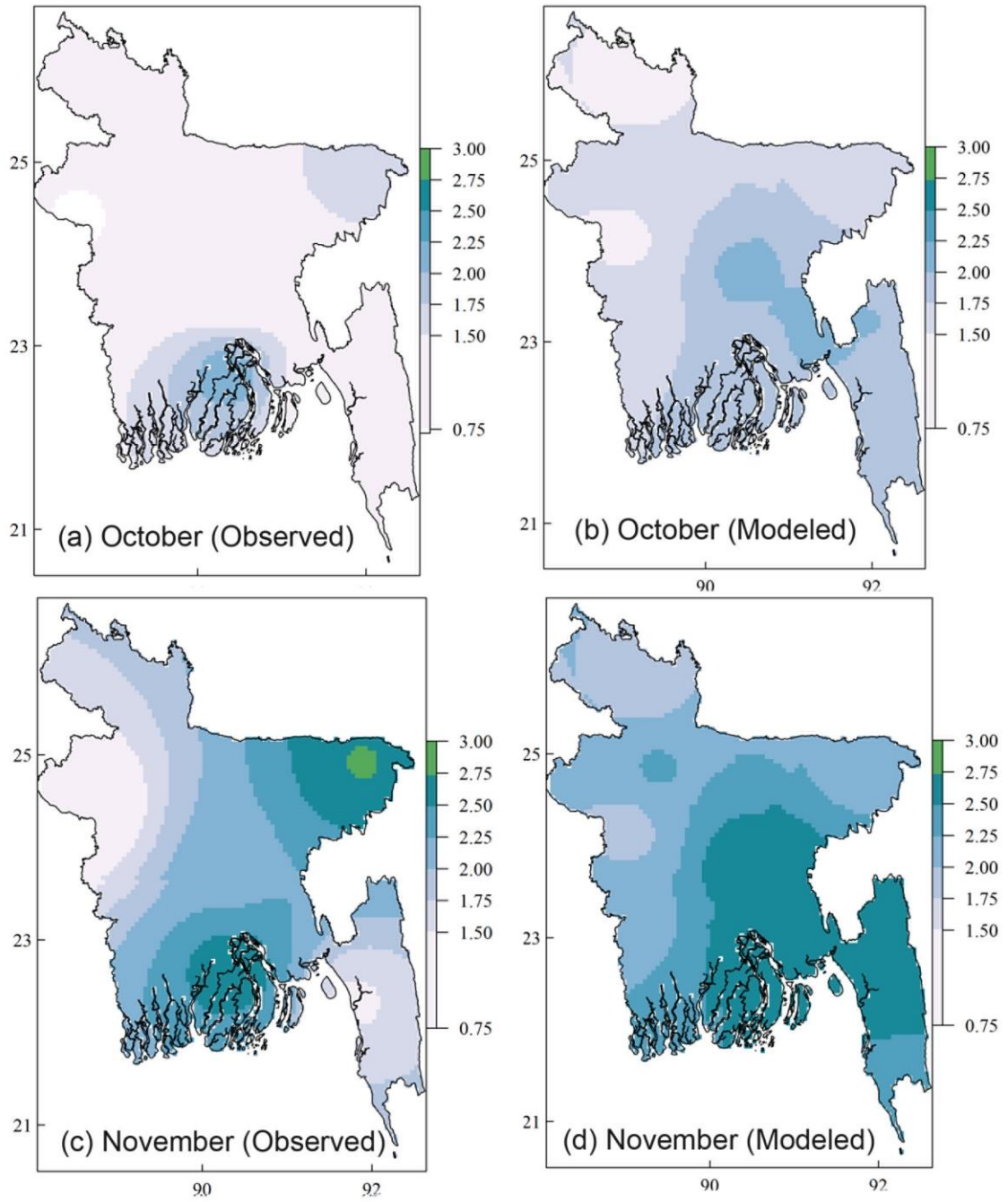


Table 1. Description of climate indices parameters.

Name (Number of indices represented)	Description	Types of indices
Tmin (1)	Average daily minimum temperature of a month.	Temperature
Tmax (1)	Average daily maximum temperature of a month.	Temperature
Tx10 / Tx90 (2)	Number of days in a month when TMax < 10 th percentile* / when Tmax > 90 th percentile*.	Temperature
Tn10 / Tn90 (2)	Number of days in a month when TMin < 10 th percentile* / when TMin > 90 th percentile*.	Temperature
SU (1)	Number of days in a month when TMax > 25°C.	Temperature
TR (1)	Number of days in a month when TMin > 20°C.	Temperature
DTR (1)	Monthly mean difference between TX and TN.	Temperature
TxijGE (4)	Number of days in a month when TMax is in between i °C and j °C., where, i = {26,29,33,26} and j = {28,32,35,32} ⁱ	Temperature
TnijGE (4)	Number of days in a month when TMin is in between i and j °C., where, i = {16,19,22,16} and j = {18,21,25,21} ⁱⁱ	Temperature
SDII (1)	Intensity of rainfall in a month (in mm/day)	Precipitation
CR _m (4)	Highest number of consecutive <i>m</i> mm rainfall events in a month, where, <i>m</i> = 1, 5, 10, 20 ⁱⁱⁱ	Precipitation
CR _n S3 (2)	Number of 3-days or more storm with rainfall > <i>n</i> mm where, <i>n</i> =1,5 ^{iv}	Precipitation
CR _n D _f (4)	Number of rainfall events in a month with rainfall > <i>n</i> mm for <i>f</i> days where, <i>n</i> =1,5 and <i>f</i> =4,5 ^v	Precipitation
PRECIPTOT (1)	Total amount of rainfall in a month. (in mm)	Precipitation
RR _j (5)	Number of rainy days with <i>j</i> mm or more rainfall, where, <i>j</i> = 1, 5, 10, 20,70. ^{vi}	Precipitation
Rx1 / Rx5 (2)	Maximum amount of 1-day / 5- day rainfall in a month	Precipitation

* Percentile are calculated based on 10-year baseline period of 2003 to 2013.

ⁱ For example, when i=26 and j=28, name of index would be Tx2628GE: The Number of days in a month when Tmax is between 26 °C to 28 °C.

ⁱⁱ For example, when i=16 and j=18, name of index would be Tn1618GE: The Number of days in a month when Tmin is between 16 °C to 18 °C.

ⁱⁱⁱ For example, when m=1 and j=28, name of index would be CR1: Highest number of 1 mm rainfall events in a month.

^{iv} For example, when n=1, name of index would be CR1S3: Number of 3-days or more storm with rainfall greater than 1 mm.

^v For example, when n=1 and f=4, name of index would be CR1D4: Number of rainfall in a month that greater than 1 mm for 4 days.

^{vi} For example, when j=1, name of index would be RR1: Number of rainy days with 1 mm or more rainfall.

Table 2. The spatial and temporal correlations between climatic indices and the three phases of the winter rotavirus epidemic.

		Rising phase (Oct- Nov)				Peak phase (Dec-Jan-Feb)				Falling phase (Jan-Feb-Mar-Apr)			
	Index Name	Correlation	Lag from Outbreak	Monthly assumption of moving average	Index Name	Correlation	Lag from Outbreak	Monthly assumption of moving average	Index Name	Correlation	Lag from Outbreak	Monthly assumption of moving average	
Spatial	SU	-0.58	2	1	SU	-0.64	0	2	Tn1621GE	-0.45	1	2	
	RR1	-0.48	1	2	Tmax	-0.57	0	2	Tx10	0.62	0	1	
	Tn1621GE	0.61	1	1	Tx10	-0.52	2	2	RR1	-0.61	1	2	
	Tn1921GE	0.68	1	1	Rx1	-0.47	0	2	Tmin	-0.62	0	1	
Temporal	Tn1621GE	0.51	1	1	Tn1621GE	-0.44	0	2	RR5	-0.7	0	2	
	RR1	-0.69	2	2	Tn1621GE	-0.43	0	1	RR1	-0.69	0	2	
	RR5	-0.69	2	2					PRECIPTOT	-0.66	0	2	
	Tx2932GE	-0.61	2	1					DTR	0.73	0	2	

*The bold indices are common in all three phases.

CHAPTER 3

Manuscript III

The future risk of diarrheal disease over Bengal delta based on climatic driven epidemic models: a case study with bias-corrected regional climate model results.

Department of Civil and Environmental Engineering, University of Rhode Island,
Kingston, RI 02881, USA

KEYWORDS

Diarrheal diseases, Climate Extremes, RCM, Bias-correction, RCP Projections

Abstract

Despite the human advancement in medical science and human wellbeing, diarrheal diseases are a major threat to human health and still represent a leading cause of morbidity and mortality worldwide. Being a major contributor of global mortality, diarrheal diseases account for an estimated 3.1% of the total burden of disease in terms of Disability-Adjusted Life Year (DALY) where cholera and rotavirus diarrhea comprise more than two-thirds of the diarrheal morbidity in developing countries of South Asia. Research studies show that hydrologic processes and climatic variabilities influence the outbreak of these diseases. Therefore, in this study, we explored the pre-existing role of the hydro-climate drivers of the diarrheal diseases during previous climate and projected the probable risks of the diseases using the results from dynamic downscaled climate models. Using prolonged surveillance data time-series of cholera and rotavirus from Bangladesh, we used the five bias-corrected Regional Climate Model (RCM) results under the RCP 4.5 scenario to integrate with the developed seasonal models and project the probabilistic risks of the diseases. As the cholera considered to be influenced by the extreme rainfalls, the mean of the projected results showed a significant increase of the cholera risk in the 20th century. The probabilistic projections also showed that the future risk of climate driven rotavirus would decrease about 5%. Most of the RCM results suggest a warmer winter in the future years, which eventually may translate to reduced risk of rotavirus outbreaks. Such understanding of the probabilistic risk of diarrheal diseases with respect to hydroclimatic variability will not only improve the local policymaking processes, but also facilitate the identification of climate-diarrheal hotspots around the globe.

Introduction:

Despite tremendous technological advancement in medical sciences and global healthcare delivery, diarrheal diseases remain the leading cause of child malnutrition and responsible for nearly half a million child-death each year (WHO/UNICEF 2015). Studies showed that the diarrheal diseases like cholera and rotavirus epidemics occur seasonally and are significantly influenced by climatic and environmental factors (Akanda et al. 2009; Akanda and Jutla 2013; Ali et al. 2016). The accelerated global warming from the previous century is projected to continue in the upcoming years; thus, the climate factors will affect the epidemiological dynamics of the diarrheal propagation (Stocker et al. 2010). Therefore, a robust understanding of the future epidemics of diarrheal diseases is essential, over developing regions of the world.

Diarrheal diseases are considered to be some of the most preventable among those causing human mortality (WHO, 2016). Due to the strong association between the unsafe water-sanitation and diarrhea, the disease is considered treatable with conventional intervention such as the provision of reliable safe water provisions and improvement of water sanitation infrastructures (WHO/UNICEF 2015). However, in the developing regions like South Asia and Sub-Saharan Africa, such development of infrastructures are both time consuming and resource intensive. Especially, in the region of Bengal delta, where the vulnerability of the global warming is surmounting and population density is exploding, such improvement will take a long time to complete. Global initiatives like Millennium Development Goals (MDG) and Sustainable Development Goals (SDG) to combat infectious disease have been continuing, however, due to limited resources and lack of institutional capacities, the

complete removal of these diseases are not likely to happen in the near future (Hutton and Bartram 2008; Chowdary et al. 2009). In this context, understanding the current and future influence of environment to the disease epidemic is essential for operational initiatives and policymakers.

The seasonal occurrence of diarrheal diseases like rotavirus and cholera confirms the influence of climate and environment in their transmission cycles over the South Asia (Leckebusch and Abdussalam 2015; Prasetyo et al. 2015; Ali et al. 2016). The rotavirus diarrhea is generally prominent during the winter and cholera during the post-monsoon season (Hasan et al., 2018; Akanda et al., 2009). Though the spread of the diseases can be associated with the lack of safe drinking water, inadequate sanitation, and poor hygiene, the hydroclimatic and related environmental factors are found to be strongly co-related in the events of the diarrheal outbreak. However, such outbreaks not only depend on the mean climatic state of a season but it can also be triggered by extreme climatic events like heavy rainfall, drought, and floods (Gurarie and Seto 2009; Remais, Liang, and Spear 2008; Bandyopadhyay, Kanji, and Wang 2012; Jutla et al. 2015; Akanda et al., 2013). Recent studies attempted to evaluate the relationship between the mean state of climate with the disease epidemics, but very few studies considered climatic extremes to investigate the diseases (Hasan et. al, 2018). Thus, a robust assessment of the relationship between the diarrheal disease and climatic extremes warrants much attention not only to reduce the present-day's outbreak but also to initiate future prevention strategies to face the effects of ongoing climate change.

The climate models are widely accepted tools for projecting probable future climate around the globe (Wright et al. 2015). Global Circulation Models (GCM) are used to project large-scale global phenomenon under different climate scenarios, such as RCP scenarios (Wang et al. 2014). The GCMs usually produce coarse spatial resolution products, thus regional climate models (RCM) were introduced to generate high-resolution climate projections through downscaling techniques (Bhaskaran et al. 1996). Though the RCMs were proven to be more accurate and considered a wider range of physical parameters than GCMs, they still comprise some biases, especially in the small study areas. For the purpose of impact assessment, the bias-correction methods were later, introduced to further improve the RCM results in the regional studies (Bennett et al. 2014; Murakami et al. 2014; Macadam et al. 2016). However, adjustment of projected mean climate can be done using various methods, but the meaningful projections of climatic extremes were still challenging and handful methods to use it in the impact studies were introduced recently (Tian et al. 2007; Srivastava et al. 2015; Macadam et al. 2016). In this context, the impact study like the risk assessment of infectious diarrheal disease by climatic extremes not only needs some reliable inter-annual epidemic models, but also requires some meaningful climate extremes to drive the models. In existing literature, the impact studies that incorporated the disease risk with climatic extremes with climate extremes are rare (Teutschbein and Seibert 2012).

To project climate extremes for the impact study, there are sets of climate scenarios proposed by IPCC assessment reports (Stocker et al. 2010; Hartmann et al. 2013). The latest scenarios, that were published in IPCC 5th assessment reports, known as the RCP scenarios are considered to be the most up-to-date scenarios for climate change studies

(Kim et al. 2013). The projection of disease risk under these RCP scenarios can potentially be very useful for various stakeholders and policymaker of the developing world. Therefore, in this study, we have projected the risk of the diarrheal disease using bias-corrected climate extremes derived from high-resolution RCMs. In order to capture the uncertainty range, we have utilized five RCM projections driven by five different GCMs under latest RCP scenarios.

Firstly, we evaluated existing literature to confirm our understanding of the connections between hydro-metrological extremes with both rotavirus and cholera (Franco et al. 1997; Tanaka et al. 2007; Kang et al. 2009; Colombara et al. 2013; Prasetyo et al. 2015; Pang et al. 2016). Hasan et al, (2018) evaluated and confirmed the relationship between precipitation and temperature extremes with the rotavirus epidemics. However, indices related to relative humidity can be an influential factor for the winter season, when there is a very little amount of rainfall. Therefore, we have incorporated the relative humidity index to update the findings from Hasan et al (2018) to better quantify the relationships of rotavirus epidemic with climatic extremes. On the other hand, though cholera were assessed with various indicators, climatic extremes of precipitation and temperature were not examined in previous studies. Therefore, we have evaluated the risk of cholera epidemics with temperature and precipitation extremes and future projections.

The manuscript was arranged in the following order:

The description of obtained data and method were described in the methodology section.

The details of the climatic extremes and disease risk were explained in the method section.

The results section described the model validation of two diseases in their rising or outbreak triggering phases. The integration of climate data and disease risk were explained in the same section. The future directions were explained and discussed in the conclusion section.

Date and Methodology:

2.1. Study Area:

The Bengal Delta region of South Asia is considered to be the ancient place of origin, or native homeland, of cholera, the deadliest among the diarrheal diseases (Hu et al. 2016). The region still experiences cholera outbreak each year during summer and post-monsoon seasons (Akanda et al. 2009; Akanda and Jutla 2013). On the other hand, rotavirus diarrhea, the most common type of diarrhea also occurs every year in the same region. The region mostly comprises the area of Bangladesh, a country with 160 million population and the most densely populated country in the world. The country has a tropical monsoon climate and most threatened by ongoing global warming, perhaps more than any other place of the world. In one end, the country experiences two major diarrheal disease outbreaks and on the other hand, it also has one of the highest vulnerable people on the earth due to the intersections of high population density, poverty, and effects of climate change. Therefore, an understanding of diarrheal epidemic for the future years would be one of the vital issues for the stakeholders and policymakers of the region. We have thus selected Bangladesh as our case study region to assess the impact of the diarrheal diseases under climate change scenarios.

2.2. Data

2.2.1. Disease Data

We have collected the incidence rate for the rotavirus and cholera-related diarrhea for our analysis from 10 hospitals. The cases of rotavirus incidences over Dhaka (capital of Bangladesh) were obtained from the hospital-based surveillance system of ICDDR, B over a period from January 2003 to May 2015. The ICDDR, B Centre for Health and Population Research runs an urban hospital situated in Kamalapur, Dhaka, where more than 100,000 patients are treated for diarrhea each year. At the hospital, cholera, as well as rotavirus surveillance, are regularly conducted; stool samples are collected to determine the presence of enteric pathogens in every 50th (2%) patient attending the hospital for treatment of diarrhea. From the hospital surveillance reports, information on monthly rotavirus isolates was summarized and a time series was formulated.

The rotavirus data from other cities within Bangladesh were collected from the national surveillance campaign of the Institute of Epidemiology, Disease Control and Research (IEDCR). The cities within Bangladesh resemble similar demographic and climatic patterns. In Bangladesh, this is the only available spatial dataset with the same temporal length, to the best of our knowledge. Therefore, we have selected the surveillance data (from January 2013 to December 2016) of these cities in the analysis.

The cholera data were also collected from the hospital-based surveillance system of ICDDR, B. The data were collected from three different surveillance system of the Institute where they started during three different timeframes. The prevalence data of cholera for

the five hospitals in Dhaka, Matlab, Chatok, Matbaria, and Pirojpur were collected for 1998 to 2003. From the Health Bulletin, surveillance data for Dhaka were collected from 2003 to 2016. Under the funding of Bill and Melinda gate foundation, new surveillance of the cholera was introduced by ICDDR, B and IEDCR from 2015 which were also combined in this study. For the consistency of the data, we converted and combined all three sources of data to z-score. The detail advantages of z-score in epidemic modeling were discussed in the later parts of the methodology section.

2.2.2. Weather Data:

We have utilized two types of weather data, one for validation and other for future projections.

For the validation of the spatial diseases models, we used the long-term observed time series from existing ground stations of Bangladesh. We obtained daily maximum (TMax) and minimum temperatures (TMin), and precipitation (PR) data for Dhaka from the Bangladesh Meteorological Department (BMD) for the period 2000 to 2014. We collected climatologic records from other cities from The Global Historical Climatology Network - Daily (GHCN-Daily), version 3 from January 2013 to December 2016 (Menne et al., 2012). Homogeneity and quality control tests were conducted to ensure the removal of outliers. The tests were carried out using the RHtestsV4 software package which was developed by the joint CCI/CLIVAR/JCOMM Expert Team (ET) on Climate Change Detection and Indices (ETCCDI) (X. L. Wang & Feng, 2013).

For projecting the disease risk, we gathered RCM model-simulated data for the latest climate change scenarios. Climate data derived from the five available RCM outputs is selected for this study. The datasets were made available through COordinated Regional Climate Downscaling Experiment (CORDEX), a program that brought forth a collective effort to regional climate projections globally (Giorgi et al. 2009). The CORDEX aims to advance and coordinate the science and application of regional climate downscaling through global partnerships. The project defined some specific domains around the globe and invited communities to conduct regional downscaling in those designated domains. Through the project's data portal, several RCM results became available over South Asia (CORDEX, 2015). As domain selection could be sensitive in a regional modeling study (Bhaskaran et al. 2012), Giorgi et al. (2009) provided a detailed rationale behind domain selection and spatial resolution over CORDEX domains.

In this study, the choice of GCMs was limited due to the number of freely available RCM results. The selection of GCMs to conduct downscaling was the decision of the corresponding home institutions that simulated the RCMs for RCP scenarios (Table 1). Therefore, we utilized RCM results that are publicly available over the domain in our selected time slices and scenarios. A detailed statistics of the driven GCMs and RCMs are provided in Table 1.

Representative Concentration Pathways (RCPs) are the four global greenhouse gas and aerosol concentration (not emissions) trajectories of futures, which are different from the previous socio-economic scenarios that give rise to alternative greenhouse gas emissions

(van Vuuren et al. 2011). In this study, three RCP scenarios (historical, RCP 4.5 and RCP 8.5) for three meteorological variables from the five RCMs were utilized from 1981 through 2100.

The analysis of the extremes was conducted based on the extreme indices adopted from the CCL/CLIVAR/JCOMM Expert Team on Climate Change Detection and Indices (ETCCDI) (ETCCDI 2016). The detail list of indices can be found in Hasan et al. (2017).

2.3 Z- score:

To represent the diarrheal disease outbreak, we have incorporated the z-score metric instead of prevalence or incidence rate of a disease (Jagai et al. 2009). Both prevalence and incidence rate are population dependent. From all the disease cases, we first converted them to z-score to avoid population effects. To remove population effect, normalization of data could be another option (Kao, 2009). In the normalization process, the data are kept to a fixed range, typically (0-1). However, in disease outbreak analysis, outbreak can vary in magnitude and do not follow the normal distribution. Thus, we utilized z-score to represent the disease risk in this study. The negative scores were scaled up to positive values for meaningful outbreak representation and to implicate log transformation for multivariate modeling. However, the relative magnitude can be biased for larger skewed values; thus we assumed the -3.5 as the minimum global state of the outbreak. Hence, z-score was transformed to modified z-score by adding 3.5. Equation 1 shows the calculation of z-score for this analysis. As a mean state of the outbreak can be expressed as 0 in dual sign series, after transformation of the minimum value, we can assume that one

can be the epidemic threshold. In this study, we have attempted to quantify only the effect of climate on the diseases by any other influencing factors. Therefore, any element of the population will not represent the actual impact of the disease, and adjusted z-score would be a great way to overcome such problem. Similarly, as RCP scenarios are population independent, we have considered them in this study.

$$Z = \frac{X - \text{mean}(X)}{\text{Std}(X)} + 3.5 \quad (1)$$

Where, X is disease cases or prevalence per month.

2.4 Seasons of the outbreaks

Earlier research showed that the annual epidemics of rotavirus and cholera over the Bengal delta occur during the winter and post-monsoon season respectively (Hasan et.al 2018, Akanda et. al, 2008). As the trigger of the outbreak correlated with climatic drivers, the rising phase of both diseases were analyzed in this study. The rising phase of rotavirus and cholera epidemics are the November-December and August-September months, respectively. It should be notated that in case of Cholera, the data we used are mostly from 1998 to 2003 period. During the period, the dominant cycle of the cholera outbreak was at post-monsoon season. Thus, we have considered the post-monsoon cycle as primary outbreak cycle.

2.5 Model development

By integrating the climate extremes and z-score value of the rotavirus diarrhea and cholera, we developed two spatial models for the rising phase of the disease outbreak. We have conducted multivariate analysis with 46 temperature and precipitation extremes taken from

Hasan et al., (2018) for both diseases. Additionally, as rotavirus outbreak occurs during winter where rainfall is low compared to other times of the year, we also incorporated relative humidity indices to develop the additional model for the rising phase of rotavirus. However, relative humidity is unavailable in the RCMs results; hence, we avoided the improved RH model to conduct the future projections of the analysis.

We have selected multivariate analysis as our primary method to formulate the spatial models. However, the correlation values of multivariate analysis for top selected models are close for the different combination of the indices. Thus, we need to extend our analysis to temporal and spatial correlation analysis for individual variables to understand the influential role of each variable. Finally, we have combined the values of the temporal and spatial correlation by equation 2, to obtain a model score.

$$\text{Model Score} = \text{Cor}_{tpr} * 1 + \text{Cor}_{sp} * 1 \quad (2)$$

$$\text{Cor}_{tpr} = \text{Cor}_{pr} * 0.5 + \text{Cor}_{tmp} * 0.5 \quad (3)$$

Where, Cor_{pr} , Cor_{tmp} , Cor_{tpr} and Cor_{sp} is the correlation of precipitation index, temperature index, temporal analysis and spatial analysis, respectively. We adopted the model score from unified score proposed by Sikder et al, (2016) where they utilized several other performance matrix. In our model score, we provided equal weightage to the correlation of temporal variables. For example, for two variables, precipitation and temperature, we provided 0.5 weight to each correlation factor. For spatial analysis, we add an equal weight as temporal analysis thus provided a weightage of one. Therefore, the range of our model score would be 0 to 2, where 0 means the worse model and 2 means the best model. Based on the model score, we selected our final model from the pool of ten models for each

disease.

2.6 Bias-corrected extremes:

In this study, we have conducted bias correction on high-resolution RCM results to evaluate robust climate projections (Bennett et al. 2014). Detail of the bias-correction method was available in Hasan et al., (2017). The projections of bias-corrected extremes were further analyzed in the developed disease models under moderate RCP 4.5 and the strongest RCP 8.5 scenarios with respect to baseline climate. The changes of the z-score values from the baseline climates were presented as the future state of the diseases.

Result and Discussion:

Hasan et al., 2018 showed that the rainfall and temperature extremes could influence the rotavirus outbreak during winter. The study utilized z-scores to establish the relationship between rainfall and temperature extremes. However, the study was conducted with 1-month moving average values where the crucial indicators from the relative humidity values were absent in the study. Moreover, studies found that the relative humidity could be a potential indicator of the rotavirus outbreak. Therefore, the role of relative humidity on rotavirus needed to be explored to understand the disease epidemics more clearly. On the other hand, the relationship between climatic extremes and z-score of cholera was never done in previous studies.

Using z-score and observed meteorological information, we conducted multivariate analysis for the rising phase of both diseases. For rotavirus, we have conducted two types

of multivariate analysis, with or without RH. The R² values from the multivariate analysis were presented in Table 2, Table 3 and Table 4.

The top-ten best models for the rotavirus diarrhea that exclude the relative humidity indices show a short range of R² values (the range is 0.03) in the multivariate analysis. The temperature variable, Tn16gTx30l (concurrent climate with two months moving average) is standard in all the top models, confirms its significant role in the rotavirus propagation. The variable is also supported with Hasan et al., 2018, but Tn16gTx30l was not found due to the single moving average values. However, for precipitation indices, eight different rainfall indices namely SDII, Rx1, RR1, CR5, RR5, RR10, CR1S3, and CR1D3 show significant influence within ten models. As the difference of R² values between the models is low, we need additional information to further select a model from the top 10. Therefore, we also conducted temporal and spatial correlation of individual variables of the selected model and values were presented in Table 2. The temporal analysis of Tn16gTx30l shows a strong correlation of 0.6 where RR1 and CR5 have a high correlation coefficient of 0.47 and 0.51 respectively. However, regarding the spatial correlation for the years of 2015-2018, the CR5 shows poor relationship compare to RR1. Such strength also reflected in the combined-scores of the RR1-Tn16gTx30l model. In addition to that, Hasan et al. 2018 also found the same influence of RR1 during the same phase of the diseases. Therefore, the model can be considered as the best model for two-variable multi-variate analysis.

We also developed rotavirus diarrhea models by considering relative humidity indices as another influential factor and the R² values were shown in Table 3. Within top 10 models,

four types of temperature indices showed stronger relationship but all of them associated with the daytime temperature of the previous months. It should be noted that the models without RH show day and night time temperature range as the primary driver in the model, but that relationship is for no-lag 2-month moving average, where with RH, it is a 1-month lag with 1-month realization. For the rainfall indices, the variation between variables are quite high, but all represent small sudden rainfall amount. For the humidity indicator, the tops models are found mostly correlated with RH minimum values. Now from the combined score, we found that the CR5-Tx2932GE-RHmin performed best in the multivariate analysis. The correlation of CR5 and RHmin also confirm the significant relationship with the rotavirus outbreak phase. From an accuracy point of view, (R2 values) the model with RH performs better than the models without RH. However, the relative humidity variable is unavailable in the selected climate projections. Therefore, we selected the model without RH as our primary model for the future risk analysis.

The top-10 models of the cholera epidemic present R2 values less than 0.5, where the difference between the top and bottom model is around (0.01) (Table 4). With such short difference, any model among the tens can be considered as the best model. Regarding temperature indices, the 2-month moving average of Tx2632GE with two-month lag shows significant influence in all top-ten models. It represents that day temperature between 26 degrees to 32 degrees is a potential trigger for the post-monsoon cholera outbreak. Akanda et al (2009) found that the increased temperature in water can accelerate the growth of the bacterial host of cholera within the water; thus Tx2632GE supports such phenomenon. On the other hand, an index like RR70 represents the high amount of rainfall, which leads to water overflow resulting in a connected fecal-oral route for the bacterial cycle. Moreover,

such water networks take times to influence the outbreak and could come to the effect after two months of such situation. Therefore, two month lag of RR70 can be considered as an appropriate indicator that can trigger post-monsoon cholera outbreak(Ryan et al. 1996). From the combined score, (Table 4), it is evident that model no 9 is the best model among the top ten and it consists RR70 and Tx2632GE index as the driving variables.

Figure 1 and Figure 2 represents the spatial distribution of model and observed rotavirus over Bangladesh. The spatial pattern of the model showed agreement with observed data over the central and southwestern part of the country. However, even with relative humidity indicator, the model result in the western part of the country deviates from observe. This bias can occur not only from unknown uncertainties but also from poor coverage of observed dataset. We used six available disease station data to generate the spatial maps where the coverage in the western part is scarce compare to eastern part of the country. Thus, observed map might missing information which reflected in the developed models result.

The bias-corrected climate extremes were driven to the best cholera model for the three-time frames were presented in Figure 4. The change of risk of cholera was presented spatially over the Bengal delta. Under the RCP4.5 scenario, the change of cholera outbreak was minimum at early 21st century. However, with the progression of time, the outbreak increased toward the end of the 21st century. From the results, it is also found that the southern parts of the country will experience a higher rate of cholera than other parts of the country. With the deteriorating salinity problem, such change will create danger zone on

the southern locality.

In case of rotavirus, the spatial analysis suggests that rotavirus will decrease gradually toward the end of the century (Figure 5). Due to the decrease in RR1 and increase in winter temperature, the rotavirus will have less wetness in the soil and lower amount of cold in the winter. This will create a hindrance in the disease propagation, thus the rate of the disease will decrease in the future years.

The time series for both of the diarrheal diseases over Bangladesh were presented in Figure 6. The mean change of risks for both selected scenarios were plotted in the Figure. Similar to spatial analysis, the Cholera risk showed a gradual increase in future years during post-monsoon season. The heightened risk are more certain in RCP8.5 scenarios than 4.5 scenarios. On the other hand, the risk of rotavirus overall decrease in 21st century. The RCP8.5 shows much safer future than RCP4.5 for the disease.

Conclusion:

In summary, in this study, we conducted multivariate, temporal and spatial analyses to quantify the risk of diarrheal disease outbreaks in Bengal Delta using climatic extremes. We have utilized five bias-corrected RCM results to project the disease risk for the 21st Century. From the study, the following conclusion can be made:

For rotavirus, the multi-model analysis shows satisfactory performance using RR1 and Tn16gTx30l as driving variables. The 1-day monthly rainfall with 16°C to 30°C

temperature range, plays a critical role in triggering the outbreak. The observed spatial pattern suggests that the central region, Dhaka is the most vulnerable region among the country. The model able to capture the Dhaka outbreak, but it also over-estimated other regions of the country. The inclusion of relative humidity indices into the model, increase the performance of rotavirus outbreak prediction significantly, especially in the northeastern part of the region. However, as we do not have projected humidity data from RCM, we utilized the rainfall and temperature-driven model to project the disease risk. For the case of Cholera, the best model is driven by RR70 and Tx2632GE, which indicated the wet warming post-monsoon. In case of cholera, the projected disease risk map suggests that the southern part of the country will experience more risk of the disease in the future years. On the other hand, rotavirus outbreak is expected to decrease according to five selected RCM projections.

The projected disease risk can be utilized to conduct epidemic management and to improve vaccination strategy. A high-risk area can be given higher importance for the introduction of rotavirus vaccination. The decision maker and stakeholder can introduce new intervention strategy to improve the disease preparedness. In this study, we have introduced two types of climate variables to project the disease. Future studies should investigate the other influencing factors such as population dynamics, urbanization, change of social demography etc. Similar studies could be done for the other types of infectious diseases not only for the betterment of current population but also for the well being of the future generation.

References:

- Akanda A, Jutla A (2013) Understanding climate change impacts on global diarrhoeal disease burden. <http://outreach.stakeholderforum.org/index.php/previous-editions/cop-19/193-cop-19-day-3-climate-change-and-health/11582-understanding-climate-change-impacts-on-global-diarrhoeal-disease-burden>. Accessed 5 Jul 2016
- Akanda AS, Jutla AS, Islam S (2009) Dual peak cholera transmission in Bengal Delta: A hydroclimatological explanation. *Geophys Res Lett* 36:L19401. doi: 10.1029/2009GL039312
- Ali Z, Harastani H, Hammadi M, et al (2016) Rotavirus Genotypes and Vaccine Effectiveness from a Sentinel, Hospital-Based, Surveillance Study for Three Consecutive Rotavirus Seasons in Lebanon. *PLoS One* 11:e0161345. doi: 10.1371/journal.pone.0161345
- Bennett JC, Grose MR, Corney SP, et al (2014) Performance of an empirical bias-correction of a high-resolution climate dataset. *Int J Climatol* 34:2189–2204. doi:

10.1002/joc.3830

Bhaskaran B, Jones RG, Murphy JM, Noguer M (1996) Simulations of the Indian summer monsoon using a nested regional climate model: domain size experiments. *Clim Dyn* 12:573–587. doi: 10.1007/s003820050129

Chowdary VM, Ramakrishnan D, Srivastava YK, et al (2009) Integrated Water Resource Development Plan for Sustainable Management of Mayurakshi Watershed, India using Remote Sensing and GIS. *Water Resour Manag* 23:1581–1602. doi: DOI 10.1007/s11269-008-9342-9

Colombara D V., Cowgill KD, Faruque ASG (2013) Risk Factors for Severe Cholera among Children under Five in Rural and Urban Bangladesh, 2000-2008: A Hospital-Based Surveillance Study. *PLoS One* 8:2000–2008. doi: 10.1371/journal.pone.0054395

Franco a a, Fix a D, Prada a, et al (1997) Cholera in Lima, Peru, correlates with prior isolation of *Vibrio cholerae* from the environment. *Am J Epidemiol* 146:1067–75. doi: 10.1093/oxfordjournals.aje.a009235

Hartmann DL, Tank AMGK, Rusticucci M (2013) IPCC Fifth Assessment Report, *Climatic Change 2013: The Physical Science Basis*. IPCC AR5:31–39.

Hu D, Liu B, Feng L, et al (2016) Origins of the current seventh cholera pandemic. *Proc Natl Acad Sci U S A* 113:E7730–E7739. doi: 10.1073/pnas.1608732113

Hutton G, Bartram J (2008) Global costs of attaining the Millennium Development Goal for water supply and sanitation. *Bull World Health Organ* 86:13–19. doi: 10.2471/BLT.07.046045

Jagai JS, Castronovo DA, Monchak J, Naumova EN (2009) Seasonality of

- cryptosporidiosis: A meta-analysis approach. *Environ Res* 109:465–478. doi: 10.1016/j.envres.2009.02.008
- Kang G, Arora R, Chitambar SD, et al (2009) Multicenter, Hospital-Based Surveillance of Rotavirus Disease and Strains among Indian Children Aged \leq5 Years. *J Infect Dis* 200:S147–S153. doi: 10.1086/605031
- Kim J, Choi J, Choi C, Park S (2013) Impacts of changes in climate and land use/land cover under IPCC RCP scenarios on streamflow in the Hoeya River Basin, Korea. *Sci Total Environ* 452–453:181–195. doi: 10.1016/j.scitotenv.2013.02.005
- Leckebusch GC, Abdussalam AF (2015) Climate and socioeconomic influences on interannual variability of cholera in Nigeria. *Health Place* 34:107–117. doi: 10.1016/j.healthplace.2015.04.006
- Liu L, Johnson HL, Cousens S, et al (2012) Global, regional, and national causes of child mortality: an updated systematic analysis for 2010 with time trends since 2000. *Lancet* 379:2151–2161. doi: 10.1016/S0140-6736(12)60560-1
- Macadam I, Argüeso D, Evans JP, et al (2016) The effect of bias correction and climate model resolution on wheat simulations forced with a regional climate model ensemble. *Int J Climatol* 36:4577–4591. doi: 10.1002/joc.4653
- Murakami H, Hsu P-C, Arakawa O, Li T (2014) Influence of Model Biases on Projected Future Changes in Tropical Cyclone Frequency of Occurrence*. *J Clim* 27:2159–2181. doi: 10.1175/JCLI-D-13-00436.1
- Pang B, Du P, Zhou Z, et al (2016) The transmission and antibiotic resistance variation in a multiple drug resistance clade of *Vibrio cholerae* circulating in multiple countries in Asia. *PLoS One* 11:1–11. doi: 10.1371/journal.pone.0149742

- Prasetyo D, Ermaya Y, Martiza I, Yati S (2015) Correlation between climate variations and rotavirus diarrhea in under-five children in Bandung. *Asian Pacific J Trop Dis* 5:908–911. doi: 10.1016/S2222-1808(15)60955-0
- Ryan MJ, Ramsey ME, Brown D, et al (1996) Hospital admissions attributable to rotavirus infection in England and Wales. *J Infect Dis* 174:S12–S18.
- Srivastava PK, Islam T, Gupta M, et al (2015) WRF Dynamical Downscaling and Bias Correction Schemes for NCEP Estimated Hydro-Meteorological Variables. *Water Resour Manag* 29:2267–2284. doi: 10.1007/s11269-015-0940-z
- Stocker T, Dahe Q, Plattner G-K, et al (2010) IPCC Expert Meeting on Assessing and Combining Multi Model Climate Projections - Meeting Report.
- Tanaka G, Faruque ASG, Luby SP, et al (2007) Deaths From Rotavirus Disease in Bangladeshi Children. *Pediatr Infect Dis J* 26:1014–1018. doi: 10.1097/INF.0b013e318125721c
- Teutschbein C, Seibert J (2012) Bias correction of regional climate model simulations for hydrological climate-change impact studies: Review and evaluation of different methods. *J Hydrol* 456–457:12–29. doi: 10.1016/j.jhydrol.2012.05.052
- Tian X, Dai A, Yang D, Xie Z (2007) Effects of precipitation-bias corrections on surface hydrology over northern latitudes. *J Geophys Res Atmos*. doi: 10.1029/2007JD008420
- Wang C, Zhang L, Lee S (2014) A global perspective on CMIP5 climate model biases. *Nat Clim Chang* 4:201–205. doi: 10.1038/NCLIMATE2118
- WHO/UNICEF (2015) Progress on Sanitation and Drinking-Water: 2015 Update and MDG Assessment.

Wright AN, Schwartz MW, Hijmans RJ, Bradley Shaffer H (2015) Advances in climate models from CMIP3 to CMIP5 do not change predictions of future habitat suitability for California reptiles and amphibians. *Clim Change* 1–13. doi: 10.1007/s10584-015-1552-6

(2016) WHO | Estimated rotavirus deaths for children under 5 years of age: 2013, 215 000. In: WHO.

[http://www.who.int/immunization/monitoring_surveillance/burden/estimates/rotavirus/en/#.WMgF1AOmxgY.mendeley&title=Estimated rotavirus deaths for children under 5 years of age: 2013, 215 000](http://www.who.int/immunization/monitoring_surveillance/burden/estimates/rotavirus/en/#.WMgF1AOmxgY.mendeley&title=Estimated+rotavirus+deaths+for+children+under+5+years+of+age%3A+2013%2C+215+000). Accessed 14 Mar 2017

Figures:

Figure 1: Spatial distribution of (a) Observed and (b) Model z-score* (without relative humidity) of rotavirus outbreak at rising phase of epidemic (November-December) during the respective validation period.

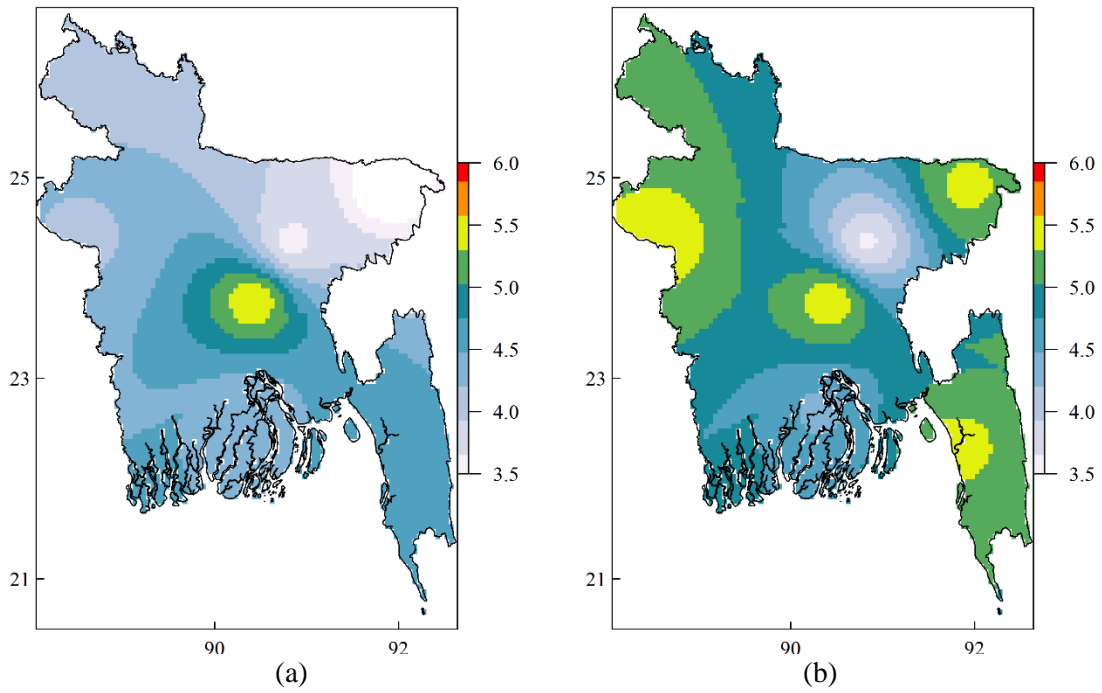


Figure 2: Spatial distribution of (a) Observed and (b) Model z-score* (including relative humidity) of rotavirus outbreak at rising phase of epidemic (November-December) during the respective validation period.

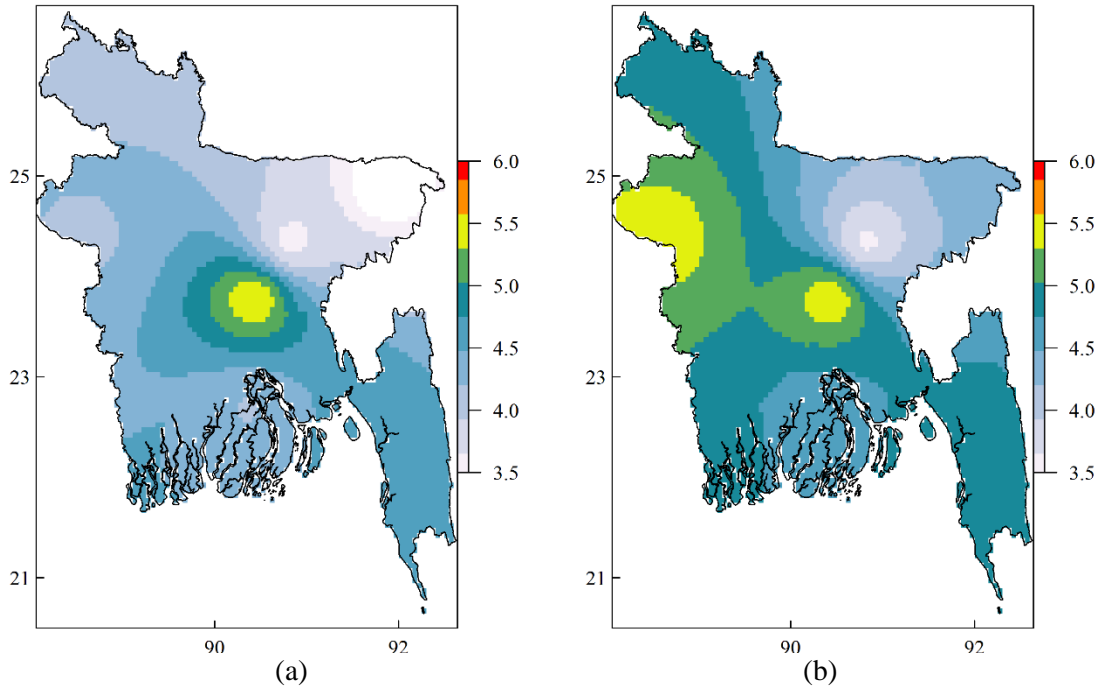


Figure 3: Spatial distribution of (a) Observed and (b) Model z-score* (including relative humidity) of cholera outbreak at rising phase of epidemic (August-September) during the respective validation period.

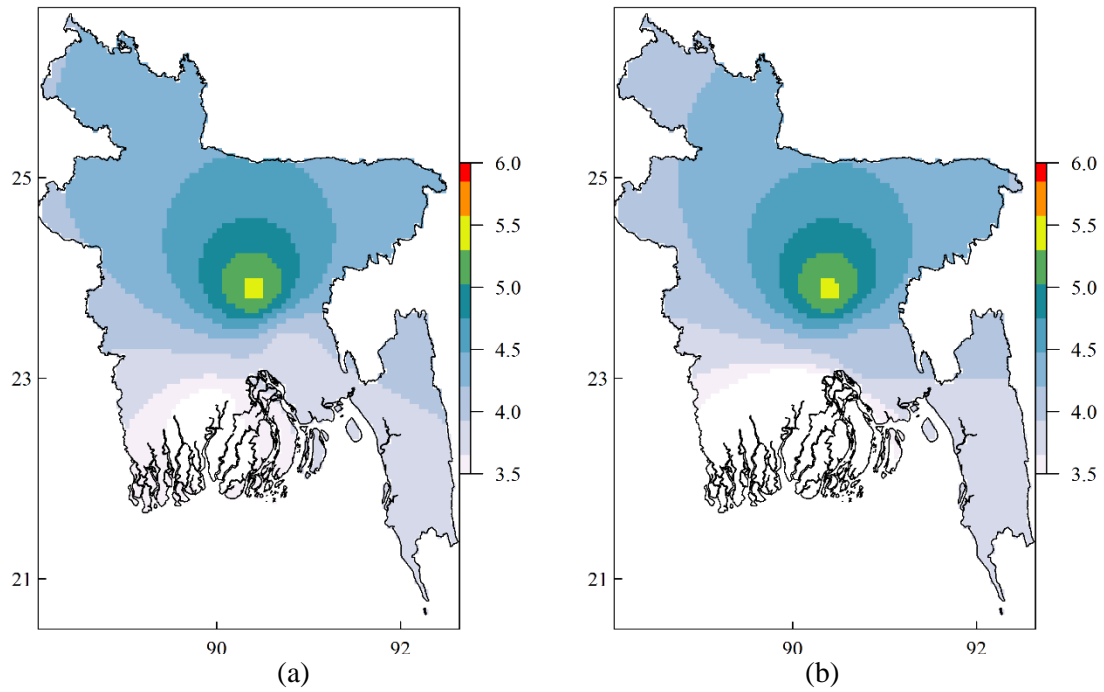


Figure 4: The changes of risk (in percentage) of cholera epidemic from baseline (1981-2005) to 2020s (2006-2040), 2040s (2041-2070) and 2080s (2071-2099) over Bangladesh.

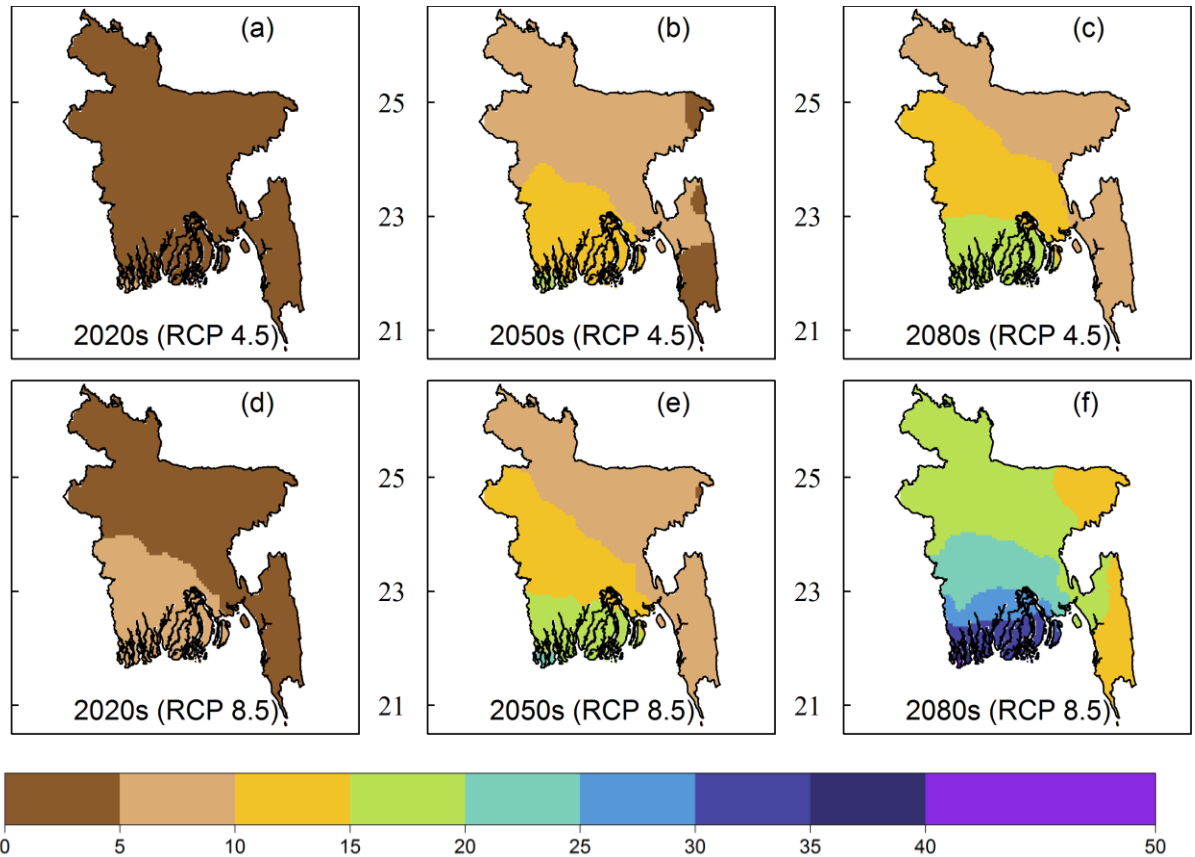


Figure 5: The changes of risk (in percentage) of rotavirus diarrhea epidemic from baseline (1981-2005) to 2020s (2006-2040), 2040s (2041-2070) and 2080s (2071-2099) over Bangladesh.

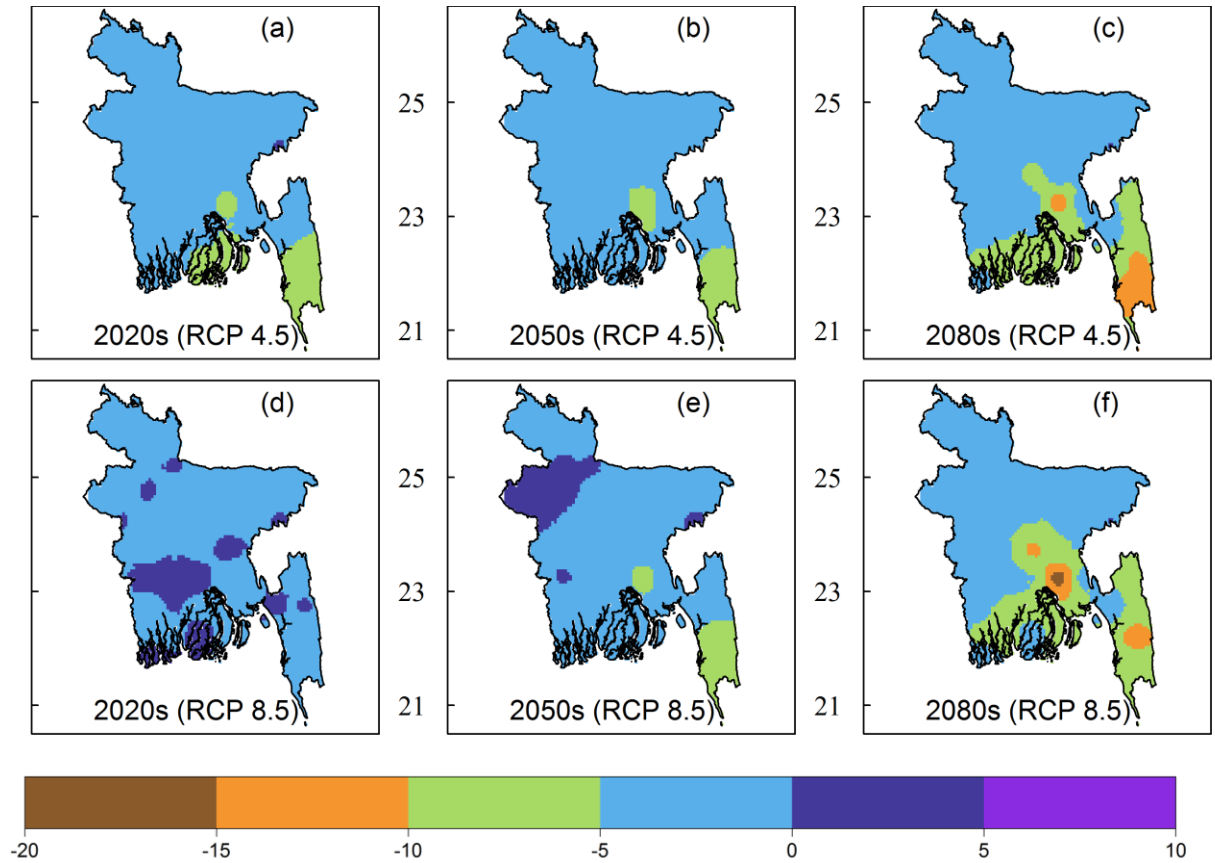
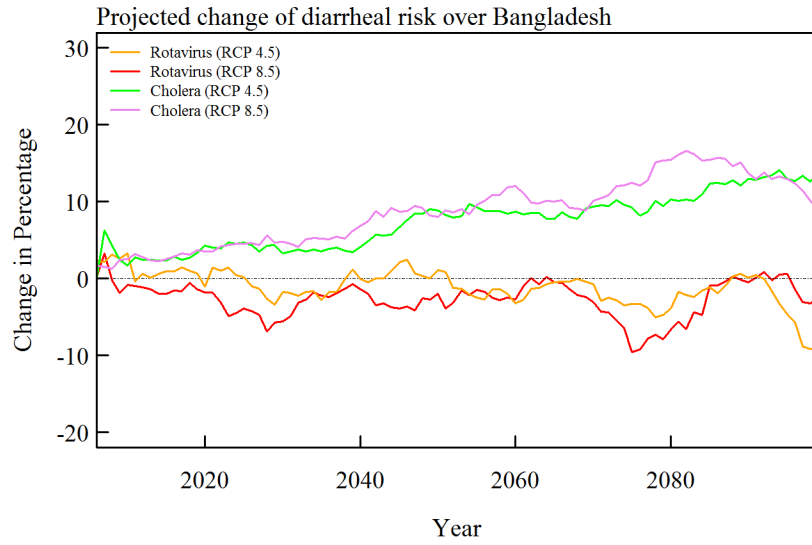


Figure 6: The changes of risk (in percentage) of diarrhea over Bangladesh from 2006 to 2100. The time series represent 10-year moving average changes.



Tables:

Table 1. Description of selected regional climate models over Bangladesh

Simulation names	Regional Climate Model	Driving GCM	Institute	Scenarios	Resolution
RCA4-EC-EARTH	Rosby Centre regional atmospheric model version 4 (RCA4) (Samuelsson et al. 2011)	European Consortium ESM (EC-EARTH)	Rosby Centre, Swedish Meteorological and Hydrological Institute (RCA4), Sweden	Historical RCP 4.5 RCP 8.5	25km
CSIRO-CNRM-CM5	Commonwealth Scientific and Industrial Research Organisation (CSIRO), Conformal-Cubic Atmospheric Model (CCAM) (Jacob and Podzun 1997)	Centre National de Recherches Météorologiques Climate Model, version 5 (CNRM-CM5)	CSIRO Marine and Atmospheric Research, Melbourne, Australia	Historical RCP 4.5 RCP 8.5	50km
CSIRO-CCSM4	Commonwealth Scientific and Industrial Research Organisation (CSIRO), Conformal-Cubic Atmospheric Model (CCAM) (Jacob and Podzun 1997)	The Community Climate System Model, version 4 (CCSM4)	CSIRO Marine and Atmospheric Research, Melbourne, Australia	Historical RCP 4.5 RCP 8.5	50km
CSIRO-MPI-ESM-LR	Commonwealth Scientific and Industrial Research Organisation (CSIRO), Conformal-Cubic Atmospheric Model (CCAM) (Jacob and Podzun 1997)	Earth system model of Max Planck Institute for Meteorology (MPI-ESM-LR)	CSIRO Marine and Atmospheric Research, Melbourne, Australia	Historical RCP 4.5 RCP 8.5	50km
REMO-MPI	The Regional Model of Max Planck Institute for Meteorology (REMO) (Teichmann et al. 2013)	Earth system model of Max Planck Institute for Meteorology (MPI-ESM-LR)	Climate Service Center, Hamburg, Germany	Historical RCP 4.5 RCP 8.5	50km

Table 2: The results from the multivariate analysis, temporal analysis and spatial analysis for Rising phase of rotavirus (without considering relative humidity).

Multivariate Analysis				Temporal Correlations				
	R2	Precipitation Indices	Temperature Indices	Lag for Precipitation Indices	Lag for Temperature Indices	Cor. of Precipitation	Cor. of Temperature	Spatial Correlation
1	0.50 0	SDII	Tn16gTx30l (2 m. av.)	1	0	-0.17	-0.62	0.21
2	0.49 5	Rx1	Tn16gTx30l (2 m. av.)	1	0	-0.05	-0.61	0.13
3	0.49 4	RR1	Tn16gTx30l (2 m. av.)	1	0	-0.47	-0.62	0.30
4	0.49 3	CR1	Tn16gTx30l (2 m. av.)	1	0	-0.28	-0.62	0.07
5	0.49 1	CR1D 3	Tn16gTx30l (2 m. av.)	1	0	-0.37	-0.62	0.11
6	0.48 8	RR5	Tn16gTx30l (2 m. av.)	1	0	-0.47	-0.62	0.16
7	0.48 7	Rx1	Tn16gTx30l (2 m. av.)	1	0	-0.07	-0.62	0.27
8	0.47 9	RR10	Tn16gTx30l (2 m. av.)	1	0	-0.44	-0.62	0.17
9	0.47 9	CR1S3	Tn16gTx30l (2 m. av.)	1	0	-0.36	-0.62	0.16
10	0.47 8	CR5	Tn16gTx30l (2 m. av.)	1	0	-0.51	-0.63	- 0.05

Table 3: The results from the multivariate analysis, temporal analysis and spatial analysis for Rising phase of rotavirus.

Model	Multivariate Analysis							Temporal Correlations			Spatial Correlation
	R2	Precipitation Indices	Temperature Indices	Relative Humidity Indices	Lag for Precipitation Indices	Lag for Temperature Indices	Lag for Relative Humidity Indices	Cor. of Precipitation	Cor. of Temperature	Cor. of Relative Humidity	
1	0.5 9	CR5	Tx90	RHmin	1	2	0	-0.45	0.37	0.45	0.34
2	0.5 7	RR5	Tx90	RHmin	1	2	0	-0.42	0.37	0.45	0.37
3	0.5 5	CR5	Tx2932G E	RHmin	1	1	0	-0.41	-0.12	0.43	0.69
4	0.5 4	CR1S 3	Tx90	RHmin	1	2	0	-0.32	0.37	0.45	0.35
5	0.5 4	CR5	Tn21gTx2 6l	RHmin	1	1	0	-0.45	-0.30	0.45	0.36
6	0.5 3	RR10	Tx90	RHmin	1	2	0	-0.40	0.37	0.45	0.41
7	0.5 2	CR5	Tx2632GE	RH607 0	1	0	0	-0.42	-0.52	-0.35	0.15
8	0.5 2	RR1	Tx90	RHmin	1	2	0	-0.41	0.37	0.45	0.27
9	0.5 2	Rx1	Tn21gTx2 6l	RHmin	1	1	0	0.01	-0.30	0.45	0.53
10	0.5 2	CR5	Tx2932GE	RH607 0	1	0	0	-0.42	-0.47	-0.35	- 0.27

Table 4: The results from the multivariate analysis, temporal analysis and spatial analysis for the rising phase of fall cholera.

Multivariate Analysis				Temporal Correlations			
R2	Precipitation Indices	Temperature Indices	Lag for Precipitation Indices	Lag for Temperature Indices	Cor. of Precipitation	Cor. of Temperature	Spatial Correlation
1	0.3 3 RR1 (1 m. av.)	Tx2632GE (2 m. av.)	2	2	-0.12	-0.23	0.9 3
2	0.3 2 CR1D3 (2 m. av.)	Tx2632GE (2 m. av.)	2	2	-0.16	-0.23	0.9 4
3	0.3 2 CR1D3 (1 m. av.)	Tx2632GE (2 m. av.)	2	2	-0.18	-0.23	0.9 4
4	0.3 2 RR1 (2 m. av.)	Tx2632GE (2 m. av.)	2	2	-0.09	-0.23	0.9 4
5	0.3 2 CR1D4 (2 m. av.)	Tx2632GE (2 m. av.)	2	2	-0.21	-0.23	0.9 4
6	0.3 2 CR1D4 (1 m. av.)	Tx2632GE (2 m. av.)	2	2	-0.22	-0.23	0.9 4
7	0.3 1 RR70 (1 m. av.)	Tx2632GE (2 m. av.)	0	2	0.55	-0.23	0.9 6
8	0.3 1 RR70 (2 m. av.)	Tx2632GE (2 m. av.)	0	2	0.35	-0.23	0.9 6
9	0.3 1 RR70 (1 m. av.)	Tx2632GE (2 m. av.)	2	2	0.27	-0.23	0.9 8
10	0.3 1 RR5 (1 m. av.)	Tx2632GE (2 m. av.)	2	2	-0.12	-0.23	0.9 2

Table 5: The combined score of the top ten models for the rotavirus and cholera diarrheal epidemic (during the rising phase).

Name of the disease	Variable considered	Combined score for the top ten models									
		1	2	3	4	5	6	7	8	9	10
Rota	Pr. + Tm. + Rh.	0.61	0.46	0.85	0.52	0.61	0.71	0.62	0.70	0.65	0.52
Rota	Pr. + Tm.	0.76	0.78	1.01	0.73	0.76	0.81	0.58	0.68	0.78	0.14
Cholera	Pr. + Tm.	0.76	0.75	0.74	0.78	0.72	0.72	1.12	0.98	1.14	0.75

APPENDIX A

CORDEX Regional Climate models

A Global Climate Model (GCM) can provide reliable prediction information on scales of around 1000 by 1000km covering what could be a vastly differing landscape (from very mountainous to flat coastal plains for example) with greatly varying potential for floods, droughts or other extreme events. Regional Climate Models (RCM) and Empirical Statistical Downscaling (ESD), applied over a limited area and driven by GCMs can provide information on much smaller scales supporting more detailed impact and adaptation assessment and planning, which is vital in many vulnerable regions of the world.

Global Climate Models (GCM) can provide us with projections of how the climate of the earth may change in the future. These results are the main motivation for the international community to take decisions on climate change mitigation. However, the impacts of a changing climate, and the adaptation strategies required to deal with them, will occur on more regional and national scales. This is where Regional Climate Downscaling (RCD) has an important role to play by providing projections with much greater detail and more accurate representation of localised extreme events.

Regional climate downscaling (RCD) techniques, including both dynamical and statistical approaches, are being increasingly used to provide higher-resolution climate information than is available directly from contemporary global climate models. The techniques available, their applications, and the community using them are broad and varied, and it is a growing area. It is important however that these techniques, and the results they produce, be applied appropriately and that their strengths and weaknesses are understood. This

requires a better evaluation and quantification of the performance of the different techniques for application to specific problems. Building on experience gained in the global modelling community, a coordinated, international effort to objectively assess and intercompare various RCD techniques will provide a means to evaluate their performance, to illustrate benefits and shortcomings of different approaches, and to provide a more solid scientific basis for impact assessments and other uses of downscaled climate information. The WCRP views regional downscaling as both an important research topic and an opportunity to engage a broader community of climate scientists in its activities. The Coordinated Regional Climate Downscaling Experiment (CORDEX) has served as a catalyst to achieve this goal.

As demonstrated at the second **International Conference on Regional Climate – CORDEX 2013** held on 4-7 November in Brussels, Belgium, and co-sponsored by **WCRP**, the **European Commission** and **IPCC**, the CORDEX concept had gained maturity and was showing strong buy-in from the science community and VIA practitioners. To meet stakeholders' expectations the **conference outcomes** were followed-up to improve the experimental framework so as to improve the CORDEX framework.

At the third **International Conference on Regional Climate – CORDEX 2016** held on 17-20 May in Stockholm, Sweden, and co-sponsored by **WCRP**, **SMHI**, **Bolin Centre**, **FORMAS**, **ECRA**, **ESA**, **EUMETSAT**, and **APN**, it was shown that CORDEX has contributed vastly to the development and production of regional climate data and information.

CORDEX Goals

1. To better understand relevant regional/local climate phenomena, their variability and changes, through downscaling.
2. To evaluate and improve regional climate downscaling models and techniques
3. To produce coordinated sets of regional downscaled projections worldwide
4. To foster communication and knowledge exchange with users of regional climate information